Universitätsklinikum Hamburg-Eppendorf

Institut für Klinische Pharmakologie und Toxikologie

Regulation of the L-Arginine-ADMA-NO pathway in coronary and pulmonary endothelial and alveolar epithelial cells during hypoxia

Dissertation zur Erlangung des Naturwissenschaftlichen Doktorgrades

am Fachbereich Biologie

der Universität Hamburg

Lena Schmidt-Hutten

Hamburg, 2023

Abgabe der Dissertation: 18.07.2023

Gutachter*innen: Prof. Dr. rer. nat. Dr. med. habil. Andreas H. Guse
PD Dr. Juliane Hannemann, PhD

Tag der Disputation: 01.12.2023

Prüfungskommission: Prof. Dr. rer. nat. Dr. med. habil. Andreas H. Guse
PD Dr. Juliane Hannemann, PhD
Prof. Dr. Julia Kehr
Prof. Dr. Wolfgang Streit

Datum Druckfreigabe der redaktionell überarbeiteten Fassung: 11.12.2023

„Das Wichtigste ist, daß man nicht aufhört zu fragen.“

- Albert Einstein

Table of Contents

List of abbreviations

Abbreviation	Name
18S	Eukaryotic 18S rRNA
ACTB	Actin beta
ADMA	Asymmetric dimethylarginine
AGXT2	Alanine glyoxylate aminotransferase 2
AKT	Protein kinase B
APS	Ammonium persulfate
B2M	Beta-2-microglobulin
BH_4	Tetrahydrobiopterin
CaM	Calcium-modulated protein, Calmodulin
CAT	Cationic amino acid transporters
cGMP	Cyclic guanosine monophosphate
CIH	Chronic intermittent hypoxia
Ct	Cycle threshold
Ct CV	Variation coefficient of Ct
DDAH	Dimethylarginine dimethylaminohydrolase
DMEM	Dulbecco's Modified Eagle's Medium
DMGV	Dimethylguanidino valeric acid
DMSO	Dimethyl sulfoxide
EDTA	Ethylenediaminetetraacetic acid
END1	Endothelin 1
ER	Endoplasmic reticulum
FAD	Flavin adenine dinucleotide
FAM	6-Carboxyfluorescein
FMN	Flavin adenine dinucleotide
GAPDH	Glyceraldehyde-3-phosphate dehydrogenase
GC	Guanylyl cyclase
GMP	Guanosine monophosphate
HCAEC	Human coronary artery endothelial cells
HEPES BSS	HEPES buffered saline solution
HIF	Hypoxia-inducible factor
HPAEC	Human pulmonary artery endothelial cells

HSP90	Heat shock protein 90
HX	Hypoxia
IP_3	Inositol triphosphate
MAPK	Mitogen-activated protein kinase
MMA	N-monomethyl arginine
NADPH	Nicotinamide adenine dinucleotide phosphate
NFDM	Non-fat dry milk
NO	Nitric oxide
NOS	NO synthase
NOSIP	Nitric oxide synthase-interacting protein
NOSTRIN	Nitric-oxide synthase trafficking inducer
NX	Normoxia
OTC	Ornithine transcarbamylase
PBS	Phosphate buffered saline
PCR	Polymerase chain reaction
PDH	Pyruvate dehydrogenase
PH	Pulmonary hypertension
PI3K	Phosphatidylinositol 3-kinases
PKG	cGMP-dependent protein kinase, protein kinase G
PLC	Phospholipase C
PPIA	Peptidylprolyl isomerase A
PRMT	Protein arginine methyltransferase
pVHL	Von Hippel–Lindau tumor suppressor protein
qRT-PCR	Quantitative real-time polymerase chain reaction
ROS	Reactive oxygen species
RPL13A	Ribosomal protein L13a
RPLP1	Ribosomal protein lateral stalk subunit P1
RT	Room temperature
SD	Standard deviation
SDHA	Succinate dehydrogenase complex flavoprotein subunit A
SDMA	Symmetric dimethylarginine
SGC	Soluble guanylyl cyclase
STAT3	Signal transducer and activator of transcription 3
TBP	TATA-box binding protein

TEMED	Tetramethylethylenediamine
TG	Target gene
TNS	Trypsin Neutralization Agent
VEGF	Vascular endothelial growth factor
VIC	2' chloro-7'-phenyl-1,4-dichloro-6-carboxyfluorescein

List of tables

List of figures

Summary

One important promoter of cardiovascular and especially pulmonary diseases is hypoxia, the insufficient supply with oxygen. It leads to hypoxic coronary vasodilation and hypoxic pulmonary vasoconstriction (HPV). Hypoxic coronary vasodilation is thought to be HIF-mediated; the mechanisms regulating HPV are less well understood. As lasting HPV might lead to vascular remodelling and the emergence of severe diseases, a deeper understanding of the mechanisms regulating HPV might help to gain insight into the emergence of those diseases and thereby provide putative therapeutic targets against hypoxia-related disorders.

The L-arginine-ADMA-NO pathway plays an important role in the regional adaption of the blood flow. A differential hypoxic regulation of this pathway within coronary and pulmonary circuit might explain hypoxic coronary vasodilation and HPV. We therefore aimed to compare gene expression, protein expression and protein activity between normoxic and hypoxic human coronary and pulmonary artery endothelial cells. We found hypoxic regulation of genes involved in the L-arginine-ADMA-NO pathway, e.g. decreased *NOS3* mRNA expression and increased *DDAH2* mRNA expression in both cell lines after exposure to hypoxia. Interestingly, *DDAH1* mRNA expression in HPAEC changed after short periods of hypoxia while it remained on normoxic level in HCAEC. However, those changes did not result in altered protein expression and ADMA concentrations remained unchanged. We further evaluated gene expression, protein expression and protein activity between normoxic and hypoxic alveolar epithelial A549 cells. Alveolar epithelial cells are the first layer of cells in contact to inhaled air, suggesting a putative role in oxygen sensing. Interestingly, we found decreased *DDAH1* mRNA expression after exposure to hypoxia accompanied by increased SDMA and ADMA concentrations, the latter one being a well-known inhibitor of NO-synthesis. Thus, we propose a cellular cross talk between pulmonary endothelial and epithelial cells responsible for the mechanism of HPV.

We further aimed to evaluate whether HIF is the responsible transcription factor regulating expression of genes involved in the L-arginine-ADMA-NO pathway within coronary and pulmonary artery endothelial as well as alveolar epithelial cell. We were able to show that hypoxic regulation of gene expression of the L-arginine-ADMA-NO pathway within those cells is not strictly HIF-dependent and that other transcription factors appear to be involved in hypoxic regulation of gene expression.

Zusammenfassung

Ein wichtiger Faktor in der Entstehung von Herzkreislauferkrankungen und besonders von Lungenerkrankungen ist Hypoxie, die unzureichende Versorgung mit Sauerstoff. Hypoxie führt zu koronarer Vasodilatation und pulmonaler Vasokonstriktion (HPV). Hypoxische koronare Vasodilatation scheint HIF-reguliert zu sein; die Mechanismen hinter der pulmonalen Vasokonstriktion sind weniger gut verstanden. Da andauernde HPV zu vaskulärem Remodelling und der Entstehung von Krankheiten führen kann, könnte ein besseres Verständnis der zugrunde liegenden Mechanismen der HPV helfen, neue Therapiemöglichkeiten gegen Hypoxie-assoziierte Erkrankungen zu finden.

Der L-Arginin-ADMA-NO Signalweg spielt eine wichtige Rolle in der regionalen Adaption des Blutflusses. Eine unterschiedliche hypoxische Regulation dieses Signalweges in Koronar- und Pulmonalkreislauf könnte eine Erklärung für hypoxische koronare Vasodilatation und HPV bieten. Unser Ziel war es daher, die Genexpression, Proteinexpression und Proteinaktivität zwischen normoxischen und hypoxischen Endothelzellen aus humanen koronaren und pulmonalen Arterien zu vergleichen. Wir konnten eine hypoxische Regulation der Genexpression von Genen des L-Arginin-ADMA-NO Signalweges zeigen und fanden beispielsweise verringerte *NOS3* mRNA-Expression und erhöhte *DDAH2* mRNA-Expression in beiden Zelllinien nach Exposition gegenüber Hypoxie. Interessanterweise war die mRNA-Expression von *DDAH1* in HPAEC nach kurzen Hypoxieperioden verringert, während sie in HCAEC auf Normoxieniveau blieb. Diese beobachteten Regulationen führten jedoch nicht zu veränderter Proteinexpression und gemessene ADMA-Konzentrationen blieben nach Hypoxieexposition unverändert. Des Weiteren haben wir Gen- und Proteinexpression sowie Proteinaktivität zwischen normoxischen und hypoxischen A549-Alveolarepithelzellen verglichen. Alveolarepithelzellen bilden die primäre Zellschicht, die in Kontakt mit der Atemluft kommt und könnten daher am Sauerstoffsensing beteiligt sein. Interessanterweise konnten wir eine verringerte *DDAH1* mRNA-Expression nach Hypoxieexposition sowie erhöhte ADMA- und SDMA-Konzentrationen nachweisen. Wir vermuten daher einen zellulären Cross-Talk zwischen pulmonalen Endothel- und Epithelzellen als zugrundeliegenden Mechanismus der HPV.

Wir haben außerdem untersucht, ob HIF als Transkriptionsfaktor an der Regulation der Genexpression von Genen des L-Arginin-ADMA-NO Signalweges in koronaren und pulmonalen arteriellen Endothelzellen und Alveolarepithelzellen beteiligt ist. Wir konnten zeigen, dass die hypoxische Regulation der Expression von Genen des L-Arginin-ADMA-NO Signalweges innerhalb dieser Zellen nicht streng HIF-abhängig ist und demnach andere Transkriptionsfaktoren an der hypoxischen Regulation der Genexpression beteiligt zu sein scheinen.

1 Introduction

1.1 The significance of hypoxia

Oxygen plays important roles in various metabolic and physiological processes; thus, it is evident that hypoxia, an insufficient supply of oxygen is a life-threatening danger. Oxygen acts as the final electron acceptor at the end of the electron transport chain [1, 2]. About 90 % of the total body O_2 consumption occurs within the mitochondria where oxygen is mainly used during oxidative phosphorylation [3], underlining its important role in energy metabolism. As cytochrome c oxidase needs oxygen as final electron acceptor, hypoxia leads to an insufficient electron transfer through the electron transport chain and therefore to the formation of reactive oxygen species (ROS). Moreover, hypoxia reversibly suppresses Na^+/K^+-ATPase activity, inhibits mRNA translation through multiple mechanisms and can induce the expression of inflammatory cytokines [1, 4, 5].

Hypoxia may result from a reduced amount of oxygen and decreased perfusion (hypoxemia), impaired oxygen delivery, or impaired cellular uptake of oxygen [6]. To avoid or overcome hypoxia, complex regulative mechanisms evolved that ensure structural and functional integrity during hypoxic periods [7]. If the arterial amount of oxygen within the coronary circuit is reduced, an increase in local blood flow occurs in order to restore oxygen supply. This effect is known as hypoxic coronary vasodilation [1, 8]. Within the lung, hypoxia leads to hypoxic pulmonary vasoconstriction (HPV) and thereby to a redistribution of deoxygenated blood from areas with poor ventilation into areas with high availability of oxygen [8, 9]. This mechanism was first described by Euler and Liljestrand in 1946 [10] and is nowadays known as Euler-Liljestrand-Mechanism. Hypoxic coronary vasodilation and hypoxic pulmonary vasoconstriction are tightly controlled by the oxygen tension. Nevertheless, what are the molecular mechanisms leading to these opposing effects in the coronary and pulmonary systems?

1.2 L-arginine – NO signalling pathway

There are various regulators of vascular perfusion, including adenosine, ATP-sensitive potassium channels, prostaglandins and nitric oxide (NO), whereby the latter has been shown to play the major role in regulating vascular perfusion [8, 11, 12].

NO is a highly lipophilic, freely diffusible messenger that has various functions. NO has been shown to decrease leukocyte and monocyte adhesion and to inhibit platelet aggregation [13-17]. It acts as direct inhibitor of the superoxide anion and is known to be released during immunological reactions and defence against pathogens [13, 18]. Disorders in the synthesis, release, or effect of NO within the vascular system are called endothelial dysfunction [14]. A disruption in formation or function of NO seems to be an important pathogenic factor in the emergence of conditions like hypertension, atherosclerosis, cancer, diabetic angiopathy, and various others [15]. However, the overproduction of NO has been shown to participate in loss of arterial resistance in septic shock [19], which clearly illustrates the importance of NO homeostasis.

NO regulates vascular tone and regional adaption of the blood flow. It negatively mediates proliferation of vascular smooth muscle cells by activating the guanylyl cyclase [13, 18]. The subsequent increase in cGMP results in activation of cGMP-dependent protein kinase (PKG) and thereby regulates calcium balance, which leads to vascular relaxation [20, 21]. Moreover, NO is capable of inducing vasodilation through the inhibition of the potent vasoconstrictor endothelin [22] and by stimulating the production of a vasodilatory prostacyclin [23]. Acetylcholine-induced vasodilation was also shown to be NO-dependent [24], underlining the versatile roles of NO in vasodilation and vasoconstriction.

As NO is a free radical, it reacts rapidly and therefore cannot be stored but needs to be synthesized de novo from L-arginine by the NO synthases [13, 18, 24]. There are three NOS isoenzymes represented by the genes *NOS1-NOS3* encoding for neuronal *NOS* (*NOS1*), inducible *NOS* (*NOS2*) and endothelial *NOS* (*NOS3*), respectively [18]. Those isoforms seem to vary in subcellular localisation and amino acid sequence. NOS1 and NOS2 are located within the cytoplasm, while NOS3 was thought to be mostly membrane-bound due to its myristylation site, although nowadays there are conflicting reports on localisation of NOS subtypes [25-27]. The NO synthases function as dimers, consisting of two identical monomers that can be divided into a C-terminal reductase domain and an N-terminal oxygenase domain. The reductase domain contains binding sites for NAPDH, FAD and FMN. The oxygenase domain can bind heme, tetrahydrobiopterin (BH_4) and the NOS substrate L-arginine [28-30]. Other important key-substrates and co-factors of NOS include iron and ROS, regulatory proteins are caveolin, calmodulin and heat shock protein 90 (HSP90) (*Figure 2*) [16, 27, 29, 31, 32].

Depending on the specific isoform, the regulation of NO synthesis occurs by different mechanisms of transcriptional and post-transcriptional regulation and by factors regulating the enzymatic activity. Moreover, ROS rapidly react with NO and thereby influence the cellular NO concentration [33]. Inducible *NOS* (*NOS2*) is induced by bacterial endotoxins and inflammatory cytokines that lead to permanent activity. This in turn leads to an elevated NO production that contributes to pathogen elimination and helps to protect organs. Once induced, NOS2 remains active until the protein is degraded. It acts independently of intracellular calcium concentration [18, 27, 34]. The constitutively expressed NOS1 and NOS3 enzymes are dynamically regulated by calcium-calmodulin (CaM), and their enzymatic activity is highly calcium dependent [18, 27, 35]. The calmodulin binding domain was shown to be located between the reductase and oxygenase domain [29]. NOS1 was further shown to be phosphorylated by e.g. calmodulin-dependent kinases, protein kinase A and protein kinase C [36, 37]. The endothelial nitric oxide synthase (NOS3) is the NOS isoform that catalyses the NO release by the endothelium under physiological conditions e.g. in response to mechanical stimulation by shear stress. It thereby regulates the homeostasis of vascular tone and vascular structure [16, 18, 38-40]. NOS3 activity is regulated by chemical as well as by mechanical factors that can alter the enzyme's production, activity and localisation within a cell [18]. Its activity can be further modulated in a calcium dependent manner or calcium-independently via vascular endothelial growth factor (VEGF) and protein kinase B (AKT) (*Figure 1*) [41]. These stimuli activate the phosphoinositide 3-kinase (PI3K) via different receptors. PI3K further phosphorylates its downstream kinase protein kinase B (AKT) that activates NOS3 [32, 42].

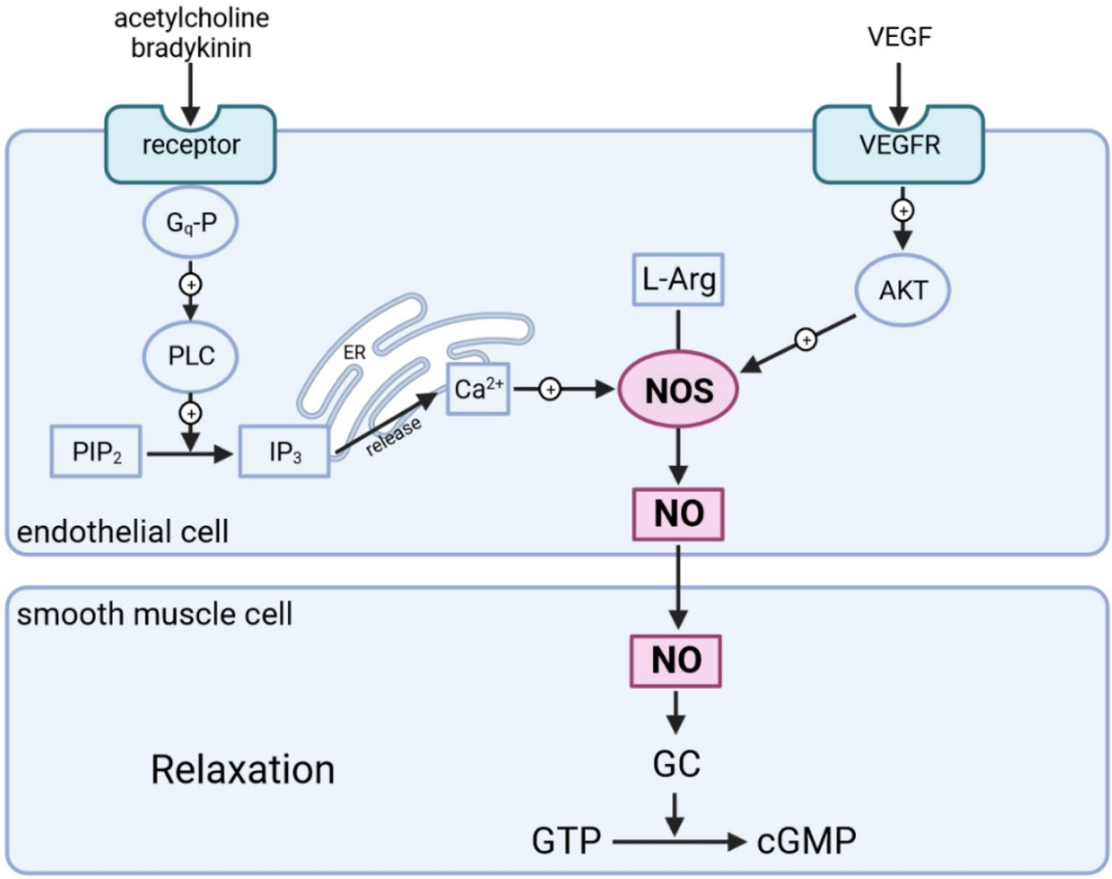

Figure 1: Calcium-dependent and calcium-independent regulation of NO synthesis. The left side shows calcium dependent stimulation of NOS, mediated by acetylcholine and bradykinin. Acetylcholine and/or bradykinin bind to a G protein (G_q-P) coupled receptor within the endothelial cell membrane, which leads to increased generation of inositol triphosphate (IP_3) by activation of phospholipase C (PLC). Increased IP_3 further leads to Ca^{2+} release from the endoplasmic reticulum (ER), which in turn increases NOS activity. The right side displays calcium-independent activation of NOS, which is stimulated by the vascular endothelial growth factor (VEGF) and protein kinase B (AKT). Increased NOS activity leads to increased NO synthesis. NO diffuses into vascular smooth muscle cells and leads to increased cGMP levels by activating the guanylyl cyclase (GC) thereby causing relaxation. Created in BioRender.com.

HSP90 acts as a physiological binding partner and regulator of NOS3 presumably by inducing a conformational change in the enzyme or by stabilizing the dimeric form. Agonists that stimulate the production of nitric oxide lead to the recruitment of HSP90 to the NOS3 complex and thereby to the activation of the protein. Those agonists include vascular endothelial growth factor (VEGF), histamine and fluid shear stress [24]. An overexpression of HSP90 increases the amount of NOS3-bound HSP90 and was shown to result in greater NOS activity [24], underlining the importance of HSP90 in NOS3 regulation.

Activation of NOS3 is achieved by binding of calcium-calmodulin (CaM), depalmitoylation, dissociation of caveolin-1 and the release of NOS3 from caveolae into the cytoplasm [43, 44]. Caveolin acts hereby as effector molecule for NOS3. The loss of caveolin results in a permanent activity of NOS3 underlining the important role of caveolin as negative regulator of NOS3 activity [16]. The resulting higher amount of NO reacts with superoxide to form reactive nitrogen species

(RNS) that interfere with proteins through tyrosine nitration. These RNS lead thereby for example to a tyrosine nitration-dependent impairment of protein kinase G (PKG) activity [16]. NOS3 dissociation from caveolae and binding of the CaM complex is achieved by receptor-mediated agonist stimulation as well as an increased amount of calcium [45]. The binding of HSP90 promotes the strong binding of CaM, the release of the inhibitory caveolin, and enhances catalytic activity by facilitating AKT-dependent phosphorylation of NOS3 [31, 32, 46]. The recruitment of NOS3 to calmodulin binding appears to be dependent on phosphorylation at Ser 617 by PKA or AKT. AKT is phosphorylated by PI3K, which is in turn activated via different receptors by physiological stimuli as VEGF or laminar shear stress (*Figure 2*) [32, 47, 48]. AKT can phosphorylate NOS3 on Ser 1179 and activate the enzyme, thereby leading to NO production. This phosphorylation of NOS3 by AKT is sufficient to regulate NO production at resting levels of calcium [31, 45].

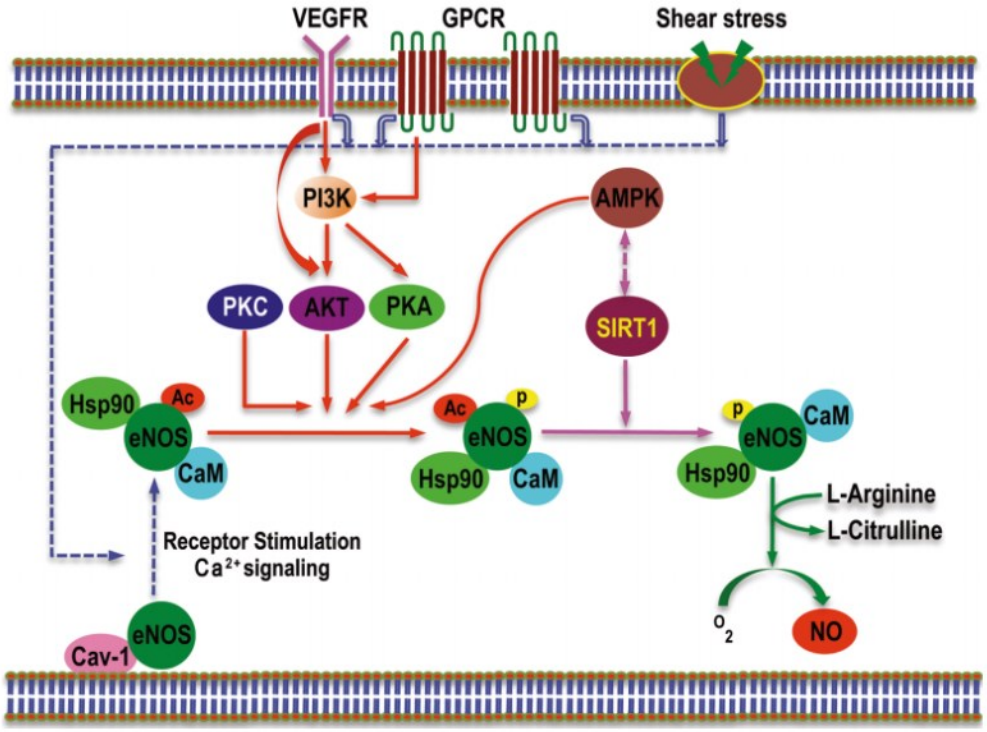

Figure 2: Co-factors, binding partners and phosphorylation of NOS3. NOS3 is associated with caveolin-1 and thereby to the membrane. The increase of free intracellular calcium or receptor-mediated agonist stimulation lead to NOS3 dissociation from caveolae and binding to the calcium–calmodulin (CaM) complex. The recruitment of HSP90 facilitates this binding to CaM. NOS3 is further phosphorylated (mediated by protein-kinases, PK, red arrows) and deacetylated (mediated by SIRT1, pink arrows). Depending on the phosphorylation site, NOS activity increases or decreases. Phosphorylation at Ser1177 by PKA, AKT (protein kinase B), PKC, and adenosine monophosphate kinase (AMPK) lead to an increased activity, while phosphorylation at Ser116 and Thr495 inhibit NOS3 activity. Active NOS3 catalyses the synthesis of NO, using L-arginine as substrate and nitrogen donor (green arrows). From: [32].

1.3 Asymmetric dimethylarginine (ADMA)

One important mechanism in the regulation of NOS activity is the inhibition of NOS3 by methylarginines, mainly asymmetric dimethylarginine (ADMA). ADMA is a dimethylated derivate of L-arginine that acts as competitive inhibitor of NOS and competes for catalytic substrate conversion [49]. Symmetric dimethylarginine (SDMA) on the other hand is not a direct inhibitor of NOS activity, but it was shown to reduce availability of L-arginine, probably by competing for transport by the cationic amino acid transporters (CAT) [50], as also shown for ADMA. However, the IC_{50} values are above the estimated endogenous ADMA and SDMA concentrations, indicating that this mechanism does not occur under physiological condition [51].

ADMA and its stereoisomer SDMA are released into the cytoplasm during physiological protein turnover via the degradation of methylated proteins [52, 53]. The posttranslational protein methylation is catalysed by protein arginine methyltransferases (PRMTs) which utilize S-adenosylmethionine as a methyl group donor [54]. During protein methylation, one or two methyl groups are added in different ways (depending on the PRMT type) to a nitrogen of the guanidine group of arginine residues. PRMTs thereby regulate protein function, activity, subcellular localisation and interactions with binding partners [55, 56]. So far, eleven PRMTs are characterised. In humans, PRMTs are classified into type I and type II PRMTs, depending on their specific catalytic activity. Both types of enzymes first catalyse the formation of monomethyl arginine (MMA) as an intermediate. In a following step, type I enzymes (PRMT1, PRMT2, PRMT3, CARM1/PRMT4, PRMT6 and PRMT8) lead to the formation of asymmetric dimethyl arginine (ADMA), whereas the type II enzymes (PRMT5 and PRMT9) produce symmetric dimethyl arginine (SDMA) [55, 57, 58]. Each PRMT is responsible for a specific substrate-dependent protein methylation and has a distinct subcellular localisation [55]. PRMT1 contributes to about 85% of cellular PRMT activity [59] and represents the major asymmetric arginine methyl transferase. As NO deficiency was shown to promote cardiovascular diseases, a dysregulation of PRMT1 activity is thereby likely to participate in their emergence [54, 56].

Reduced availability of nitric oxide (NO) in patients suffering from pulmonary hypertension (PH) is one of the most important alterations and further associated with increased plasma concentrations of ADMA [57, 60-62]. The concentration of ADMA in pulmonary disorders and pre-eclampsia [63] was shown to be elevated and can be seen as a predictive marker of morbidity and mortality in cardiovascular diseases [49, 52, 64]. Experimental evidence support the role of ADMA in the emergence of cardiovascular diseases: The supplementation of endothelial cells with ADMA was shown to cause a reduction in NO synthesis and elevated production of superoxide together with monocyte adhesion to endothelial cells [65]. The inhibition of NOS by ADMA could in turn be

prevented by addition of L-arginine [66] as also seen by dietary L-arginine in cholesterol-fed rabbits, where L-arginine supplementation led to reduced progression of atherosclerosis [67].

ADMA does not only affect NOS activity but was shown to induce the activation of signal transducer and activator of transcription 3 (STAT3) and stabilisation of hypoxia inducible factor 1A (HIF1A), thereby altering normal cellular functions (e.g., NO production, cell proliferation/Ca^{2+} concentration, production of pro-inflammatory mediators, and expression of NOS3, DDAH1, and ICAM-1) [60]. ADMA also enhances production of ROS significantly by uncoupling NOS3 and thereby reducing NO production [60].

1.4 ADMA degradation

Enzymes of the dimethylarginine dimethylaminohydrolase (DDAH) family metabolize the competitive NOS inhibitor ADMA to L-citrulline and dimethylamine and thereby play a key function in maintaining NO homeostasis [17, 56]. Alanine-glyoxylate aminotransferase 2 (AGXT2) was also shown to participate in ADMA and SDMA metabolism by transaminating the dimethylated arginines into asymmetric dimethylguanidinovaleric acid or symmetric dimethylguanidinovaleric acid, respectively [17]. However, this mechanism was only observed when AGXT2 was experimentally overexpressed [68]. Another mechanism of ADMA clearance is the export via cationic amino acid transporters (CAT) [69]. As about 70 % of ADMA is thought to be metabolized by the two members of the DDAH family, namely DDAH1 and DDAH2, this appears to be the major degradation route [17, 70].

DDAH1 appears to play the main role in ADMA metabolism, the role of DDAH2 remains unclear [17, 71]. Recent experiments in rats generated a siRNA-mediated *DDAH2* knockdown and showed impaired acetylcholine-dependent vasodilatation, indicating a putative regulation by DDAH2 [71]. The localisation of the two DDAH isoforms remains controversial [61, 62, 72], although DDAH1 seems to be the major isoform in kidneys and liver and DDAH2 appears to be the main isoform expressed within the vasculature [73]**.**

The crystal structure of purified bovine DDAH1 showed a single inhibitory zinc ion bound to the active site cysteine (Cys273) of the holoenzyme. The removal of zinc by either imidazole or phosphate resulted in increased DDAH activity [74]. As about 95 % of total DDAH1 purified protein was shown to exist as the zinc-bound form, DDAH1 appears to exist predominantly in its inhibited conformation [75]. To date, there is no evidence of specific cofactors that are required for DDAH enzymatic activity [73]. DDAH1 protein expression can be activated by estradiol [76], insulin [77] and vitamin E [78], while TNF-α [79]; glucose [80] and erythropoietin [74] inhibit DDAH activity [17].

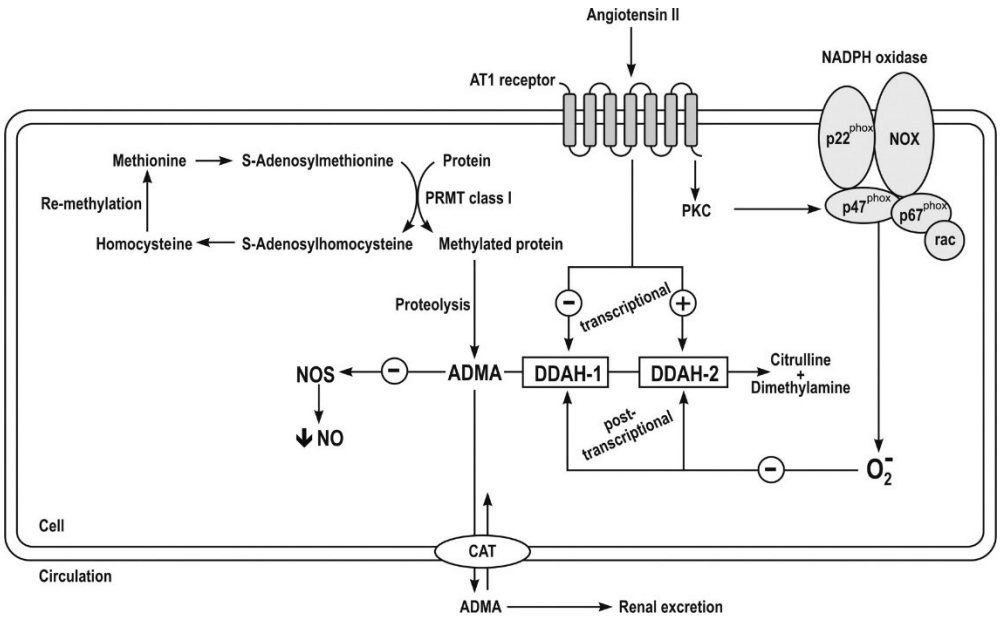

Figure 3: ADMA metabolism. Physiological protein turnover of methylated proteins leads to release of ADMA, which in turn inhibits NOS synthases and leads to reduction in NO production. About 70 % of ADMA are degraded by DDAH1 and DDAH2 to L-citrulline and dimethylamine. Small amounts of ADMA escape degradation and leaves the cell via cationic amino acid transporters (CAT). Transcriptional regulation of DDAH involves angiotensin, post-transcriptional regulation occurs via ROS. From: [73].

In humans, single-nucleotide polymorphisms in genes encoding for DDAH1 and DDAH2 have been shown to be associated with elevated blood ADMA concentrations [81], underlining the importance of DDAHs in ADMA metabolism. Experimental evidence of several studies targeting DDAH in cell culture as well as in animal models underline the important role of DDAH in ADMA clearance and NO homeostasis. Leiper and colleagues showed that heterozygous deletion of *DDAH1* in mice increased ADMA concentrations in plasma, brain, and lung by 20 % [82]. By pharmacologically inhibiting DDAH in vascular endothelial cells, Ghebremariam and colleagues were able to achieve reduced ADMA degradation, resulting in reduced NO production [83]**.** In other studies, the overexpression of *DDAH* in endothelial cells increased NOS activity and NO production. *DDAH1* and *DDAH2* overexpression in transgenic mice led to reduced ADMA plasma concentration and higher NOS activity together with elevated NO concentration and was shown to protect against ADMA-induced endothelial dysfunction [84, 85]. Increased NO production in endothelial cells was also achieved by treatment with the combined PDE-3/4 inhibitor tolafentrine. These cAMP phosphodiesterase inhibitors appear to induce DDAH2 expression in a cAMP-dependent manner and thereby result in decreased ADMA concentrations [86]**.** NO in turn can directly inhibit DDAH, which is thought to provide a homeostatic mechanism inhibiting further NO synthesis if NO concentration is already increased. This reversible inhibition occurs through S-nitrosylation of the active site cysteine residue of DDAH (Cys273 in bovine DDAH1, Cys274 in human DDAH1, Cys249 in

human DDAH2). This inhibitory activity is typically associated with increased *NOS2* expression and therefore elevated NO synthesis but does not occur under basal conditions [87]. Disorders in DDAH activity lead to an increased concentration of ADMA and thus to a reduction of endothelial NO production and thereby promote the emergence of diseases [62, 88]. DDAH1 for example was shown to be associated with coronary heart disease [89] and endothelial dysfunction in pulmonary hypertension [60]. Hypoxia-induced impairment of DDAH1 activity/expression in human pulmonary endothelial cells is responsible for ADMA accumulation during endothelial dysfunction [60]. This clarifies the crucial role of DDAH in ADMA degradation and NO homeostasis and the complex interplay of proteins involved in the L-arginine-ADMA-NO pathway. However, the mechanisms controlling gene expression in chronic hypoxia remain to be elucidated.

1.5 Oxygen sensing and cellular adaption to low amounts of oxygen

To react to changes in oxygen availability, cells obviously need a mechanism for oxygen sensing. There are various putative mechanisms regulating the response to decreased oxygen supply, underlining the importance of oxygen to ensure cellular function. Cellular responses to hypoxia include the release of neurotransmitters by the glomus cells of the carotid body, the release of erythropoietin, and the release of vascular growth factors [90]. But how is an altered amount of oxygen detected?

It was suggested that changes in the available amount of oxygen can be sensed by heme-based proteins, O_2-sensitive ion channels, AMP kinase, NADPH oxidase and mitochondria [1, 90, 91], although the underlying mechanisms are not fully understood. It is known that cysteine residues on the haemoglobin β-chain react with NO to form a nitroso-adduct, whereby the affinity of haemoglobin for NO is similar to that for O_2. Erythrocytes may thereby act as O_2 sensors to control regional blood flow [1]. Ion channels are able to adjust their conductance in response to an altered level of O_2, but it remains unclear whether they are responsive themselves or whether these changes occur as a secondary response activated by a separate O_2 sensor [8, 90]. Hypoxia was shown to increase the AMP:ATP ratio, activating AMP-activated protein kinases (AMPK) via phosphorylation. This in turn modulates cellular metabolism e.g. via an increase in intracellular Ca^{2+} concentration [1, 91]. A decreased O_2 tension was shown to reduce the capacity of cytochrome c oxidase to metabolize NO. This alters the redox state of more proximal complexes in the electron transport chain, which may allow the cytochrome c oxidase to function as mitochondrial oxygen sensor and to signal by generating ROS [1, 90, 92].

One of the most important oxygen sensors and regulators of adaption to varying oxygen supply is hypoxia-inducible factor (HIF). Just recently, the investigation of the role of HIF was awarded with

a Nobel Prize [93]. HIF is a transcription factor that is involved in a variety of key physiological and pathophysiological processes, like angiogenesis, energy metabolism, cell proliferation, pulmonary hypertension and cancer [94]. HIF is composed of one of three different α-subunits (HIF1A – HIF3A) and a β-subunit [8, 95]. HIF1 - composed of HIF1A and HIF1B-subunit - plays a major role in the cellular adaption to low amounts of oxygen [6, 94]. This heterodimer induces expression of multiple genes that promote adaptation to hypoxia and survival. The HIF1B-subunit (also known as Aryl-Hydrocarbon-Receptor Nuclear Translocator (ARNT)) is constitutively expressed, while the α-subunit expression is tightly regulated by local oxygen tension via prolyl hydroxylase (PHD) [8, 94-96]. In normoxia, PHDs hydroxylate HIF1A at two proline residues. Hydroxylated HIF1A can be recognized by the von-Hippel-Lindau Protein (pVHL), which ubiquitinates the alpha subunit leading to HIF1A degradation by the proteasome [97, 98]. The Factor Inhibiting HIF (FIH) suppresses HIF1 transcriptional activity in an oxygen-dependent manner, thereby preventing co-activator recruitment in normoxia (*Figure 4*) [95]. Other known target genes are erythropoietin, endothelin, and VEGF, which play a role in various signalling pathways regulating oxygen supply [94]. HIF1 promotes the expression of NOS2 and thereby increases NO production [1, 99].

Gene expression under systemic hypoxia appears to be regulated by the transcription factor HIF. However, the regulative mechanism controlling gene expression in pulmonary hypoxia remains elusive.

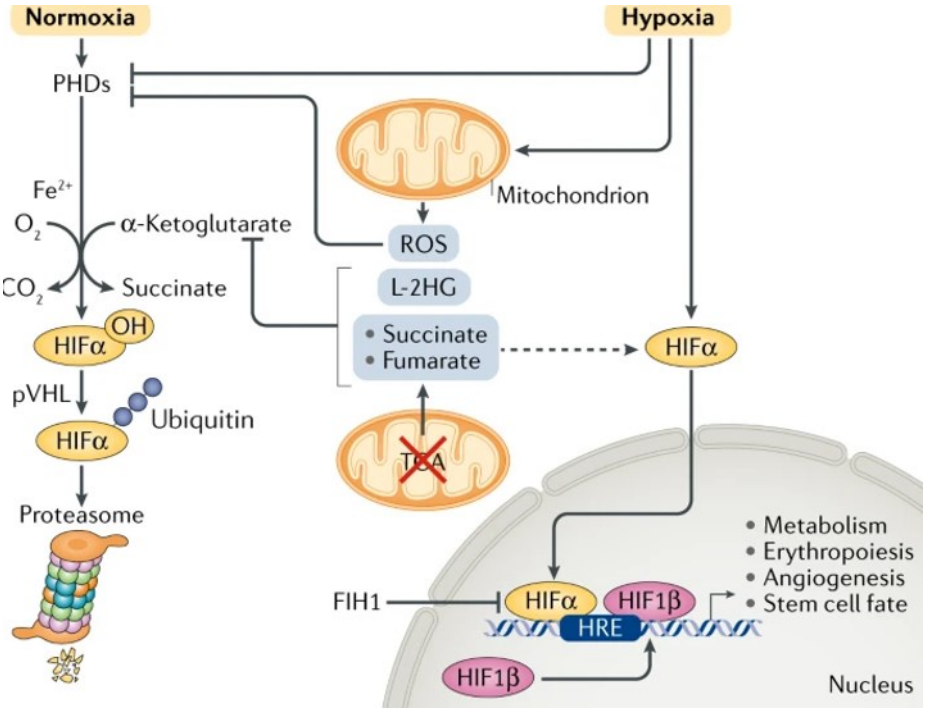

Figure 4: The transcription factor HIF. In normoxia, PHDs hydroxylate HIFA at two proline residues. The von-Hippel-Lindau Protein (pVHL) can then recognize HIFA and polyubiquitinate the subunit. The ubiquitinated subunit gets then proteosomally degraded. The Factor Inhibiting HIF (FIH) suppresses HIF1 transcriptional activity in an oxygen-dependent manner, thereby preventing co-activator recruitment in normoxia. Under hypoxia, PHDs are inhibited, leading to a HIFA stabilisation. The stabilised alpha-subunit can translocate into the nucleus and bind to the constitutively expressed HIF1B, resulting in activity of the HIF-transcription factor. From: [100].

1.6 Aim of work

Cardiovascular diseases are the leading cause of death in Germany as well as worldwide. With a proportion of about 40 % of all deaths and severe individual sequelae they still represent a great burden to humankind [101, 102]. Hypoxia is one important promoter of cardiovascular diseases. If humans are exposed to chronic pulmonary hypoxia, e.g. in high altitude or during respiratory disease, pathologic consequences like higher pulmonary blood pressure and higher shear at the vascular endothelium, acute altitude sickness and acute pulmonary oedema may develop [103]. Vascular endothelial cells express NOS3 and play thereby a crucial role in regulating NO homeostasis, which is necessary for vasodilation [104]. To date, there is strong evidence for the important role of DDAH in ADMA degradation and NO homeostasis. A disruption in NO homeostasis by impaired DDAH activity is therefore likely to be responsible for the emergence of cardiovascular disorders. However, the regulatory mechanisms of NO homeostasis are complex *(Figure 5)* and hypoxic regulation is not fully understood.

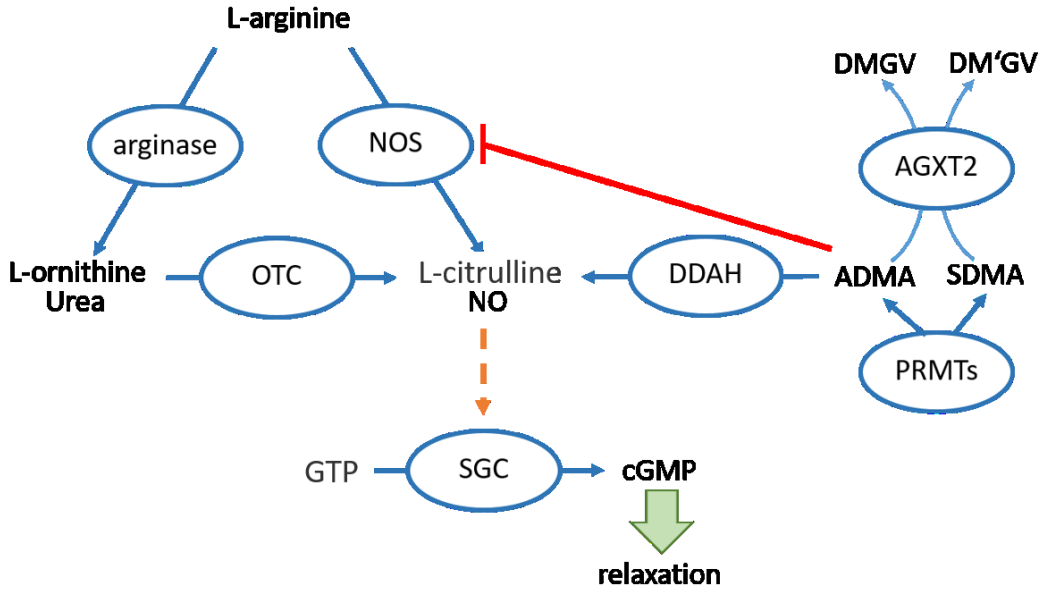

Figure 5: L-arginine-ADMA-NO metabolism: Enzymes of the NOS family generate NO and L-citrulline out of L-arginine. A large amount of L-arginine is metabolized by arginase and excreted via the urea cycle, limiting substrate availability for NOS. NOS is inhibited by ADMA, a metabolite that is released during physiological turnover of methylated proteins. Therefore, PRMTs play a role in NO-homeostasis, as well as DDAHs, the two isoforms of ADMA metabolizing enzymes. Degradation by AGXT2 depicts another ADMA metabolizing mechanism. ADMA: asymmetric dimethylarginine, AGXT2: alanine-glyoxylate aminotransferase 2, ASL: argininosuccinate lyase, ASS: argininosuccinate synthase, DDAH: dimethylarginine dimethylaminohydrolase, DMGV: dimethylguanidino valeric acid, GMP: guanosine monophosphate, OTC: ornithine transcarbamylase, PRMTs: protein arginine methyltransferases, SDMS: symmetric dimethylarginine. SGC: soluble guanylyl cyclase.

In patients suffering from cardiovascular diseases, an elevated ADMA concentration was shown to be predictive for morbidity and mortality [49, 52, 64]. Reduced availability of NO in patients with pulmonary hypertension is one of the most important alterations and further associated with increased plasma concentration of ADMA [57, 60-62, 105].

Preliminary work of our group gave insights into effects of chronic hypoxia and chronic intermittent hypoxia (CIH) on the regulation of the L-arginine-ADMA-NO pathway. The group of Hannemann and colleagues showed that ADMA concentration is increased in CIH and chronic hypobaric hypoxia, suggesting a predictive role in the emergence of PAH [106-109]. Furthermore, it has been shown that elevated serum concentrations of ADMA and SDMA can aid in identifying COVID-19 patients at high risk of in-hospital mortality [110]. Hannemann et al. could also show multiple associations of genes of the L-arginine-ADMA-NO pathway with high-altitude pulmonary hypertension [110], underlining the importance of this pathway in the development of pulmonary diseases. A deeper understanding of the molecular mechanisms responsible for the hypoxic regulation of the L-arginine-ADMA-NO pathway could provide valuable insights into potential new therapeutic targets for the treatment of pulmonary disorders in the future.

The aims of this thesis were:

1. To compare normoxic and hypoxic expression of genes involved in the L-arginine-ADMA-NO pathway in endothelial cells of systemic (HCAEC) and pulmonary circulation (HPAEC) and alveolar epithelial cells (A549). The specific questions were:
    - Are there differences in gene expression between normoxia and hypoxia in HCAEC, HPAEC and/or A549 cells?
    - Are there differences in hypoxic gene expression between HCAEC, HPAEC and A549 cells?

2. To compare normoxic and hypoxic expression and activity of proteins involved in the L-arginine-ADMA-NO pathway endothelial cells of systemic (HCAEC) and pulmonary circulation (HPAEC) and alveolar epithelial cells (A549). The specific questions were:
    - Are there differences in protein expression and activity between normoxia and hypoxia in each cell line?
    - Are there differences in hypoxic protein expression and activity between the cell lines?

3. To evaluate HIF as a putative transcription factor regulating *DDAH1*, *DDAH2* and *NOS3* expression in HCAEC, HPAEC and A549.

2 Materials

2.1 Equipment and devices

Electronic devices and equipment used in this work are presented in the following table (*Table 1*).

Table 1: List of electronic devices and equipment.

Device	Model	Company
Analytical scale	CP225D	Sartorius AG (Göttingen, DE)
Benchtop centrifuge	MC6	SARSTEDT AG & Co. KG (Nümbrecht, DE)
Block heater	Thermomixer compact Thermomixer comfort	Eppendorf AG (Hamburg, DE)
Centrifuges	5415 D 5415 R 5424 R	Eppendorf AG (Hamburg, DE)
Centrifuge for conical tubes	Rotina 35 R	Andreas Hettich GmbH & Co. KG (Tuttlingen, DE)
Centrifuge for 96-Well plates	RVC 2-25	Martin Christ Gefriertrocknungsanlagen GmbH (Osterode am Harz, DE)
Freezer -20°C		
Freezer -80°C		
Gel caster and tray (agarose gel electrophoresis)	(Wide) Mini Sub-Cell GT	Bio-Rad Laboratories, Inc. (Hercules, US)
Gel caster and tray (SDS-PAGE)	Mini Trans-Blot® Cell	Bio-Rad Laboratories, Inc. (Hercules, US)
Horizontal electrophoresis cell	(Wide) Mini-Sub Cell GT, Mini SubTM DNA Cell	Bio-Rad Laboratories, Inc. (Hercules, US)
Horizontal plate shaker	Titramax 101	Heidolph Instruments GmbH & Co. KG (Schwabach, DE)
Incubator	MCO-18AC-PE HERACELL VIOS 160i	PHCbi; PHC Holdings Corporation (Tokyo, JP) Heracell, Thermo Fisher Scientific, Inc. (Waltham, US)
LC-MS/MS Column 2.1x50 mm	Acquity UPLC® BEH C18 1.7 µm 186002350	Waters Corporation (Milford, US)
LC-MS/MS: Column Manager	Acquity UPLC® 186015043	Waters Corporation (Milford, US)
LC-MS/MS: Quarternary Solvent Manager	Acquity UPLC® H class plus 186015080	Waters Corporation (Milford, US)
LC-MS/MS: Sample Manager FTN-H	Acquity UPLC® H class plus 186015085	Waters Corporation (Milford, US)
LC-MS/MS: Triple Quadrupole	Xevo TQ-S cronos	Waters Corporation (Milford, US)

Magnetic stirrer	MR Hei-Tec, IKAMAG REO	Heidolph Instruments GmbH & Co. KG (Schwabach, DE), Janke & Kunkel KG IKA-WERK (Staufen, DE)
Micro spectrophotometer	N60	Implen (München, DE)
Microwave	Micromat 15 G715MA	AEG; Electrolux Hausgeräte GmbH (Nürnberg, DE)
Molecular Imager	ChemiDoc XRS+	Bio-Rad Laboratories, Inc. (Hercules, US)
PCR-Mastercycler	epgradient	Eppendorf AG (Hamburg, DE)
pH meter	FiveEasy	Mettler-Toledo, LLC (Columbus, US)
Pipette controller	PIPETBOY acu 2	INTEGRA Biosciences AG (Zizers, CH)
Platform shaker	Duomax 1030	Heidolph Instruments GmbH & Co. KG (Schwabach, DE)
Power supply, agarose gels	Biometra® Standard Power pack P25	Analytik Jena AG (Jena, DE)
Power supply, SDS-PAGE	PowerPac™ Basic	Bio-Rad Laboratories, Inc. (Hercules, US)
Real-time PCR cycler	QuantStudioTM 5	Thermo Fisher Scientific, Inc. (Waltham, US)
Roller shaker	RM5 V-30	Ingenieurbüro CAT, M. Zipperer GmbH (Ballrechten-Dottingen, DE)
Scale	BP 3100 S	Sartorius AG (Göttingen, DE)
Ultra-Pure water system	Milli-Q Plus	Millipore GmbH (Schwalbach, DE)
Ultrasonification water bath	RK 100	BANDELIN electronic GmbH & Co. KG (Berlin, DE)
Vacuum pump	BVC control	VACUUBRAND GmbH & Co. KG (Wertheim, DE)
Water bath	1003	Memmert GmbH & Co. KG (Schwabach, DE)

2.2 General Buffer and antibodies

The reagents and solutions used in this thesis for SDS-Gel electrophoresis, Western blot and gel electrophoresis are listed in *Table 2*.

Table 2: List of reagents and solutions for SDS-gel electrophoresis, Western blot and gel electrophoresis.

Solution	Composition	
10 % ammonium persulfate (APS)	10 % (w/v) in ddH2O	100 mg APS ad 1000 µl ddH2O
Blocking solution	5 % (w/v) non-fat dry milk TBS-T	1 g non-fat dry milk powder 20 ml TBS-T
4x buffer running gel (Lower Tris-Buffer)	1.5 M Tris-HCl 0.4 % SDS (w/v) pH 8.8	18.17 g Tris-Base (MW 121.14 g/mol) in 60 ml ddH2O pH 8.8 with 6N HCl +2 ml 20 % SDS ad 100 ml ddH2O
4x buffer stacking gel (Upper Tris-Buffer)	0.5 M Tris-HCl 0.4 % SDS (w/v) pH 6.8	6.06 g Tris-Base (MW 121.1 g/mol) In 60 ml ddH2O pH 6.8-6.87 with HCl if necessary + 2 ml 20 % SDS ad 100 ml ddH2O
ddH2O/glycerol	50 % ddH2O 50 % Glycerol	50 ml ddH2O 50 ml Glycerol
EDTA 0.5 M		9.035 g EDTA + 40 ml ddH2O pH 8.0 with 2 M NaOH ad 50 ml ddH2O
Ponceau S solution	0.1 % Ponceau S (w/v) 5 % acetic acid (v/v)	1 g Ponceau S 5 ml acetic acid ad 100 ml ddH2O
1x running buffer	25 mM Tris-Base 192 mM Glycine 1 % SDS pH 8.3	100 ml 10x Tris-Glycine buffer ad 1000 ml ddH2O + 5 ml 20 % SDS
6x sample buffer	187.5 mM Tris-HCl, pH 6.8 60 % Glycerol 6 % SDS (v/v) 0,01 % Bromophenol Blue(w/v) 15 % β-Mercaptoethanol	6.25 ml 1.5 M Tris-HCl Stock + 30 ml Glycerol + 3 g SDS + 0.003 g Bromophenol Blue ad 42.5 ml ddH2O; Add β-Mercaptoethanol always directly before use!
20 % Sodiumdodecylsulfate (SDS)	20 % (w/v) in ddH2O	20 g SDS ad 100 ml ddH2O
5x TBE buffer		54 g Tris-Base (MW: 121.14 g/mol) 27.5 g boric acid 20 ml EDTA (0.5 M, pH8) ad 1000 ml ddH2O

10x TBS	0.2 M Tris, pH 7.5 1.4 M NaCl	48.4 g Tris-Base (MW: 121.14 g/mol) 163.6 g NaCl (MW: 58.44 g/mol) 1.5 l ddH2O pH 7.5 with HCl ad 2 l ddH2O
1x TBS-T	20 mM Tris, pH 7.5 140 mM NaCl 0.1 % Tween-20	50 ml 10x TBS 0.5 ml Tween-20 ad 500 ml ddH2O
1x transfer buffer	25 mM Tris-Base 192 mM Glycine 20 % methanol (v/v)	100 ml 10x Tris-Glycine buffer 200 ml methanol ad 1000 ml ddH2O
10x Tris-Glycine buffer	250 mM Tris-Base 1.92 M Glycine pH 8.3	30.3 g Tris-Base (MW 121.14 g/mol) 144.1 g Glycine (MW 75.07 g /mol) ad 1000 ml ddH2O

Antibodies used for protein detection via Western blot are listed below (*Table 3*).

Table 3: List and description of antibodies.

Antibody	Supplier	Description
DDAH1(ab180599)	Abcam Cambridge, UK)	Rabbit monoclonal [EPR13922] to DDAH1
DDAH2 (ab184166)	Abcam (Cambridge, UK)	Rabbit monoclonal [EPR15508(B)] to DDAH2
HIF1A (PA1-16601)	Thermo Fisher Scientific, Inc. (Waltham, US)	Rabbit polyclonal, Immunogen: fusion protein containing amino acids 432-528 of human HIF-1alpha
HIF2A (PA1-16510)	Thermo Fisher Scientific, Inc. (Waltham, US)	Rabbit polyclonal, Immunogen: A peptide derived from the C-terminus of mouse/human HIF-2 alpha protein.
NOS3 (ab76198)	Abcam (Cambridge, UK)	Mouse monoclonal [M221] to eNOS
TUBB (ab6046)	Abcam (Cambridge, UK)	Rabbit polyclonal to beta Tubulin - Loading Control

2.3 Kits

The kits used in this thesis are listed in *Table 4*.

Table 4: List of kits.

Kit	Order Number	Supplier
High-Capacity cDNA Reverse Transcription Kit	4368814	Applied Biosystems™, Thermo Fisher Scientific, Inc. (Waltham, US)
PureLink® RNA Mini Kit	12183018A	Invitrogen, Thermo Fisher Scientific, Inc. (Waltham, US)
TRIzol™ Plus RNA Purification Kit	A33254	Invitrogen, Thermo Fisher Scientific, Inc. (Waltham, US)
Mycoplasma PCR Detection Kit	Ab289834	Abcam (Cambridge, UK)
ECL™ Prime Western-Blot-System	GERPN2232	Cytiva, Global Life Sciences Solutions (Marlborough, US)

2.4 HIF inhibitors and HIF stabiliser

Table 5 lists the used compounds for HIF inhibition and HIF stabilisation and their respective stock solution in DMSO.

Table 5: List of HIF inhibitors and HIF stabiliser and respective stock solutions.

Name	Order Number	Supplier	Function	Molecular Weight	Stock solution
PT2399	HY-108697	MedChemExpress (Monomouth Junction, US)	HIF2A antagonist	419,32	20 mM in DMSO
KC7F2	HY-18777	MedChemExpress (Monomouth Junction, US)	HIF1A translation inhibitor	570,38	20 mM in DMSO
DMOG	400091	Merck kGaA (Darmstadt, DE)	PHD-inhibitor/HIF-stabiliser	175,14	200 mM in DMSO

2.5 Cell lines and cell culture solutions

Cell lines, cell culture media and cell culture solutions used in this thesis are listed in *Table 6*.

Table 6: List of cell lines and cell culture solutions.

Cell line/Product	Order Number	Supplier
EA.hy926 cells	CRL-2922	ATCC (Manassas, US)
A549 lung carcinoma, human cell line	CCL-185™	ATCC (Manassas, US)
Human Coronary Artery Endothelial Cells (HCAEC) (cryopreserved)	C-12221	PromoCell (Heidelberg, DE)
Human Pulmonary Artery Endothelial Cells (HPAEC) (proliferating)	C-12241	PromoCell (Heidelberg, DE)
DetachKit	C-41220	PromoCell (Heidelberg, DE)
Freezing Medium Cryo-SFM	C-29912	PromoCell (Heidelberg, DE)
Endothelial Cell Growth Medium	C-22010	PromoCell (Heidelberg, DE)
Endothelial Cell Growth Medium MV	C-22020	PromoCell (Heidelberg, DE)
Dulbecco's Phosphate Buffered Saline (DPBS)	14190144	Gibco, Thermo Fisher Scientific, Inc. (Waltham, US)
Dulbecco's Modified Eagle Medium (DMEM)	21885025	Gibco, Thermo Fisher Scientific, Inc. (Waltham, US)
Trypsin-EDTA	T2610-100ML	Sigma-Aldrich (St. Louis, US)
Fetal Bovine Serum (FBS)	FBS-11A	Capricorn (Ebsdorfergrund, DE)
Penicillin/Streptomycin (Pen/Strep)	P4333-100ML	Sigma-Aldrich (St. Louis, US)
Dimethylsulfoxide (DMSO)	D2650-5X5ML	Sigma-Aldrich (St. Louis, US)

2.6 Software

The following table (*Table 7*) lists the software and programs used for this thesis.

Table 7: Software and Programs.

Software	Manufacturer
ACQUITY UPLC® H class Console version 1.69	Waters Corporation (Milford, US)
BioRender	BioRender
EndNote X9	Clarivate Analytics (London, UK)
GraphPad Prism 8.4.3	GraphPad Software (San Diego, US)
ImageLab 5.2.1	Bio-Rad Laboratories, Inc. (Hercules, US)
MassLynx V4.2 SCN1001	Waters Corporation (Milford, US)
QuantStudioTM Design & Analysis Software v1.4.3	Thermo Fisher Scientific, Inc. (Waltham, US)
SkanIt™ Software for Microplate Readers	Thermo Fisher Scientific, Inc. (Waltham, US)

3 Methods

3.1 Cell culture

For all cell culture methods, rules of sterile working were strictly followed. All cell culture work was performed in a sterile bench with laminar airflow. If not otherwise specified, A549 cells and EA.hy926 cells were cultured according to *Table 8* in Dulbecco's Modified Eagle Medium (DMEM) supplemented with 10 % (v/v) fetal bovine serum (FBS) and 1 % (v/v) penicillin-streptomycin in a humidified atmosphere composed of 21 % O_2 and 5 % CO_2 for A549 and 21 % O_2 and 7 % CO_2 for EA.hy926. HPAEC were cultured in Endothelial Cell Growth Medium and HCAEC were cultured in Endothelial Cell Growth Medium MV according to the supplier's instructions. Both primary cell lines were cultured in a humidified atmosphere containing 21 % O_2 and 5 % CO_2 (*Table 8*).

Table 8: Cell culture conditions for different cell lines.

Cell line	Incubation normoxia	Incubation hypoxia	Medium
EA.hy926 cells	37 °C, 21 % O_2 and 7 % CO_2	37 °C, 1 % O_2 and 7 % CO_2	DMEM + 10 % FBS + 1 % penicillin-streptomycin
A549 cells	37 °C, 21 % O_2 and 5 % CO_2	37 °C, 1 % O_2 and 5 % CO_2	DMEM + 10 % FBS + 1 % penicillin-streptomycin
HCAEC	37 °C, 21 % O_2 and 5 % CO_2	37 °C, 1 % O_2 and 5 % CO_2	Endothelial Cell Growth Medium MV
HPAEC	37 °C, 21 % O_2 and 5 % CO_2	37 °C, 1 % O_2 and 5 % CO_2	Endothelial Cell Growth Medium

3.1.1 Thawing of cryoconserved cells

Thawing of immortalized cells. The culture medium was equilibrated at room temperature and 10 ml were transferred into a T75 cell culture flask (TC-flask T75 Stand. Vent., Sarstedt, Nümbrecht, DE) and pre-incubated at 37 °C for 30 min. Frozen immortalized cells in cryo-vials in 1 ml DMEM medium containing 10 % Dimethylsulfoxide (DMSO) were taken out of the liquid nitrogen container and kept on dry ice until use. The lid of the cryo-vial was opened a quarter turn under a laminar flow to release pressure. The lid was tightened again before the cells were thawed in a 37 °C water bath for 2 minutes until only somewhat frozen cells remained. The cryo-vial was disinfected using 70 % ethanol, opened under the laminar flow and cells were transferred into a 50 ml centrifuge tube containing 10 ml cell culture medium. The suspension was centrifuged for 3 minutes at 120 x g at room temperature. The supernatant was discarded, cells were resuspended in 1 ml medium and transferred into the prepared T75 flask with pre-incubated medium. Cells were kept in humidified

atmosphere according to *Table 8* for 16-24 hours. After cells had attached to bottom of the cell culture flask, the medium was changed.

Thawing of primary human cells. Thawing of primary human cells was performed according to the manufacturer's instructions [111]. Briefly, T75 flasks containing 10 ml medium were pre-warmed for 30 min in an incubator (*Table 8*). The vial containing cryopreserved cells was removed from the liquid nitrogen container and kept on dry ice. Under a laminar flow, pressure was relieved by opening the vial's cap a quarter turn. The reclosed cryovial was thawed in a 37 °C water bath for 2 minutes. Afterwards the cryovial was sanitized with 70 % ethanol before opening it under the laminar flow to transfer the cells into the flasks containing pre-warmed medium. The flasks were kept in an incubator according to *Table 8*. The medium was changed after 16-24 hours.

3.1.2 Subculturing of stable, adherent cell lines and primary human cells

Subculturing of immortalized cells. Immortalized cell lines were cultured in 10 cm dishes (TC-dish 100 standard, Sarstedt) in DMEM according to *Table 8*. For subculturing, phosphate buffered saline (PBS), trypsin and the cell culture medium were equilibrated at room temperature for 30 min. The used medium was aspirated and discarded. Cells were washed carefully two times with 10 ml PBS. 1 ml trypsin per dish was added and cells were kept in an incubator at 37 °C for 3-4 minutes until cells started to detach. Cells were further detached by softly tapping against the dish. Trypsination reaction of the cells was stopped by adding 10 ml medium. The cells were suspended and transferred into a 50 ml centrifuge tube, before pelleting in a centrifuge at room temperature and 120 x g for 3 min. The supernatant was discarded. As A549 cells had a population doubling time of about 22-24 hours, they were split 1:4 for 24 h incubation, 1:8 for 48 h incubation and 1:10 for 72 h incubation in order to reach confluence after the respective incubation time. Therefore, the cell pellet of one cell culture dish was resuspended in 4 ml, 8 ml or 10 ml medium. 10 ml medium were added into each new 10 cm cell culture dish, 1 ml cell suspension was added, and cells were incubated as described in *Table 8*.

Subculturing of primary human cells. Primary Human Coronary Artery Endothelial Cells (HCAEC) and Primary Human Pulmonary Artery Endothelial Cells (HPAEC) were cultured in 10 cm dishes (TC-dish 100 standard, Sarstedt) with 10 ml Endothelial Cell Growth Medium MV or Endothelial Cell Growth Medium, respectively (*Table 8*). Subculturing of primary cell lines was performed when reaching 70-80 % confluence according to the manufacturer's instructions using a DetachKit consisting of HEPES Buffered Saline Solution (HEPES BSS), Trypsin/Ethylenediaminetetraacetic acid (EDTA) (0.04 %/0.03 %) and Trypsin Neutralization Agent (TNS). Shortly, the DetachKit was pre-conditioned at room temperature for 30 min. Medium was aspirated from the cultured cells

and discarded. Cells were washed with 5 ml Hepes BSS per dish. 5 ml trypsin/EDTA were added and detachment was observed microscopically. As soon as cells started to detach, they were further detached by gently tapping against the cell culture dish. By adding 5 ml of trypsin neutralization solution, the trypsination reaction was stopped. Cell suspension was transferred into a 50 ml centrifuge tube and cells were pelleted for 3 min at 220 x g at room temperature. Supernatant was discarded and cells were resuspended in medium according to their growth. The primary cell lines had a population doubling time of about 24-48 h, depending on their passage. According to their growth and confluence, cells were split between 1:2 and 1:6 in order to reach confluence after the respective incubation time.

3.1.3 Cryoconservation of immortalized, adherent cell lines and primary human cells

Cryoconservation of immortalized cells. One day before cryoconservation of immortalized, adherent cells, a cryo container was filled with isopropanol and kept overnight at 4 °C. On the day of cryoconservation, when confluence reached at least 80 %, PBS and trypsin were pre-conditioned at room temperature, cryomedium (DMEM + 10 % (v/v) FBS + 1 % (v/v) penicillin-streptomycin + 10 % DMSO) was kept on ice. The medium was removed from the cells and discarded. Cells were washes twice with 10 ml PBS. 1 ml trypsin per 10 cm cell culture dish was added and cells were incubated 3-4 min at 37 °C until cells started to detach. Cells were further detached by gently tapping against the cell culture dish. Trypsination reaction was stopped by adding 10 ml medium. Cells were pelleted at 120 x g at room temperature for 3 min. The supernatant was discarded, and cells were resuspended in 5 ml room-temperated medium before pelleting at 120 x g for 3 min again. The supernatant was discarded, and cells were resuspended in 1 ml cold cryomedium. The suspension was directly transferred into pre-cooled cryovials and kept on ice until all samples were processed. Then, cryovials were stored in the cryo container, kept at -20 °C for 2 h and overnight at -80 °C. Cryovials were transferred into liquid nitrogen long-term storage container the next day.

Cryoconservation of primary cells. Cryoconservation of primary cells in 10 cm cell culture dishes was performed at 70-80 % confluence. The solutions of the DetachKit were pre-conditioned at room temperature; Freezing Medium Cryo-SFM was kept on ice. The medium was removed and discarded. Cells were washed with 5 ml Hepes BSS per dish. 5 ml trypsin/EDTA were added, and detachment was observed microscopically. As soon as cells started to detach, they were further detached by gently tapping against the cell culture dish. By adding 5 ml of trypsin neutralization solution, the trypsination reaction was stopped. Cell suspension was transferred into a 50 ml centrifuge tube and cells were pelleted for 3 min at 220 x g at room temperature. The supernatant was discarded, and cells were resuspended in 1 ml Freezing Medium Cryo-SFM. The suspension was

directly transferred into pre-cooled cryovials and kept on ice until all samples were processed. Then, cryovials were stored in the cryo container, kept at -20 °C for 2 h and overnight at -80 °C. Cryovials were transferred into a liquid nitrogen container the next day for long-term storage.

3.1.4 Mycoplasma PCR

To ensure mycoplasma-free cell culture work and to avoid contamination, mycoplasma polymerase chain reaction (PCR) tests followed by agarose gel electrophoresis were performed regularly using a Mycoplasma PCR Detection Kit (Abcam). The protocol was performed in duplicate samples according to the manufacturer's instructions. Briefly, conditioned cell culture medium of cells incubated for 48-72 h without disturbance was collected. All reagents of the kit and samples were brought to room temperature 30 min prior to the assay. The respective sample, positive control and negative control were mixed in PCR tubes on ice as described in *Table 9* and briefly centrifuged. A standard PCR protocol was performed according to *Table 10* before analysing the amplification products by agarose gel electrophoresis. For agarose gel electrophoresis, a 1 % DNA gel was prepared by solving 0.7 g agarose in 7 ml 5x TBE (*Table 2*) and 63 ml H_2O in a microwave for 60 sec. The solution was poured in the agarose gel electrophoresis chamber where polymerization took about 30 min. After polymerization, the electrophoresis chamber was filled with 0.5x TBE buffer. 10 µl sample were mixed with 1 µl Midori Green Direct (Nippon Genetics Europe GmbH, Düren, DE) and applied to the gel pockets. 5 µl Generuler 1 kB DNA Ladder (Thermo Fisher Scientific) were mixed with 1 µl Midori Green Direct and applied to the first pocket. The DNA gel was run at 65 V for 90 min before visualizing bands in the ChemiDoc XRS+ molecular imaging system using ImageLab 5.2.1 software (Bio-Rad Laboratories, Inc., Hercules, US) and settings for ethidium bromide-stained gels according to the manufacturer's instructions of the used dye.

Table 9: Pipetting scheme for mycoplasma PCRs.

	Test samples	Positive control	Negative control
ExpressTaq 2x PCR MasterMix	12.5 µl	12.5 µl	12.5 µl
MycoplasmaPCR Primer Mix	1 µl	1 µl	1 µl
Test sample	2.5 µl	-	-
Mycoplasma Positive Control	-	2.5 µl	-
Nuclease-free water	9 µl	9 µl	11.5 µl
Final volume	25 µl	25 µl	25 µl

Table 10: Mycoplasma PCR settings.

Step	Temperature	Duration	Cycle(s)
Enzyme Activation	95°C	3 min	1
Denaturation	95°C	15 sec	40
Annealing	55°C	15 sec	
Extension	72°C	15 sec	
Final Extension	72°C	1 min	1
Holding	4°C	-	-

3.2 Incubation at hypoxia and normoxia

Incubation of immortalized cells. Immortalized cells were incubated according to *Table 8* in hypoxia (HX, 1 % O_2) and normoxia (NX, 21 % O_2). Medium was pre-incubated 24 h prior to medium change in normoxia or hypoxia to adapt to the respective atmosphere and changed every 24 h. Cells were seeded 24 h before incubation start in order to settle and attach. To start the incubation, medium was replaced with pre-incubated medium. After incubation for 24 h or 72 h, respectively, cells reached a confluence of 70-80 %.

Incubation of primary cells. HCAEC and HPAEC in passage 6-7 were used for incubation under hypoxic (1 % O_2) and normoxic conditions (21 % O_2) and incubated according to *Table 8*. Medium was pre-incubated for 24 h in normoxia or hypoxia to adapt to the respective atmosphere and changed every 24 hours. Cells were seeded 24 h before incubation start in order to settle and attach. To start the incubation, medium was replaced by pre-incubated medium. After incubation for 24 h or 72 h, respectively, cells reached a confluence of 60-70 %.

3.3 Incubation with HIF inhibitors and stabiliser

To investigate the role of HIF in hypoxic regulation of genes involved in the ADMA-NO pathway, cells were grown in the presence of different HIF inhibitors or a HIF stabiliser, respectively. Cells with HIF inhibitors were incubated in HX trying to prevent the hypoxic effect on putative HIF target genes, cells with the HIF stabiliser in NX aiming to mimic the hypoxic effect on putative HIF target genes.

Test for optimal concentration. In order to find optimal concentrations of HIF inhibitors and the HIF stabilisers balancing between the maximal inhibitory/stabilising effect and minimal cytotoxicity, pilot experiments were performed with EA.hy926 cells. Therefore, EA.hy926 cells incubated with different concentrations of the respective reagents. According to *Table 11*, stock solutions in DMSO and dilutions of inhibitors and stabiliser in DMEM were prepared. Cells were incubated for 72 h and handled as described in *3.1*. Medium containing the respective concentrations of inhibitor/stabiliser was changed every 24 h, whereby the inhibitors and stabiliser were diluted and added to the fresh medium directly before medium change. Cell viability and growth were monitored daily by microscopic observation and compared to cells grown under normoxic conditions without inhibitors or stabiliser (NX control).

Table 11: Tested concentrations of HIF inhibitors and HIF stabiliser in EA.hy926.

Name	Function	IC_{50}	Molecular Weight	Stock solution	Tested concentrations
PT2399	HIF2A inhibitor	0.2 µM [112]	419,32	20 mM in DMSO 0,005 g/(0,02 mol/L*419,32 g/mol) = 0,596 ml	2 µM 0.3 µM 0.2 µM 0.1 µM 0.02 µM
KC7F2	HIF1A translation inhibitor	20 µM [113]	570,38	20 mM in DMSO 0,01 g/(0,02 mol/L*570,38 g/mol) = 0,877 ml	100 µM 30 µM 20 µM 10 µM 2 µM
DMOG	PHD inhibitor/ HIF stabiliser	1 mM [114]	175,14	200 mM in DMSO 0,05 g/(0,2 mol/L*175,14 g/mol) = 1,427 ml	1.5 mM 1 mM 0.5 mM 0.1 mM

For incubation of primary cells and A549 with HIF inhibitors and the HIF stabiliser, concentrations were adjusted. HCAEC, HPAEC and A549 cells were incubated as described in *3.2* for 72 h in duplicates with the concentrations listed in *Table 12*. Cells incubated at NX, HX and with DMSO (0.5 %) served as controls. After incubation for 72 h, cells were washed with cold PBS, detached from the cell culture dish with a cell scraper and resuspended in 1 ml TRIzol™ before transferring into pre-cooled micro reaction tubes.

Table 12: Tested concentrations of HIF inhibitors and HIF stabiliser in A549, HPAEC and HCAEC.

Name	Stock solution	Tested concentrations			Optimal concentration
		HCAEC	HPAEC	A549	
PT2399	20 mM in DMSO	10 µM 5 µM 2 µM 0.2 µM	10 µM 5 µM 2 µM	20 µM 10 µM 2 µM	10 µM
KC7F2	20 mM in DMSO	15 µM 10 µM 5 µM 2 µM	10 µM 5 µM 2 µM	10 µM 2 µM 1 µM	2 µM
DMOG	200 mM in DMSO	1 mM, 0.5 mM, 0.1 mM			0.5 mM

Incubation with optimal concentrations. Cells were incubated (n=4 biological replicates for primary cells and n=8 replicates for A549) as described in *3.2* for 24 h and 72 h in NX or HX with the final concentration of the respective compound (*Table 12*). NX DMSO samples and HX DMSO samples with a final concentration of 0.1 % DMSO, as well as NX and HX controls without solvent served as controls. Medium was changed every 24 h and compounds were diluted in fresh medium directly before medium change. After incubation, cells were washed with cold PBS, detached from the cell culture dish with a cell scraper and resuspended in 1 ml TRIzol™ before transferring into pre-cooled micro reaction tubes.

3.4 RNA Isolation

RNA isolation was performed using the PureLink™ RNA Mini Kit (Thermo Fisher Scientific) according to the instructions. Briefly, medium was aspirated, and cells were washed with 10 ml cold PBS. Using a cell-scraper, cells were removed from the bottom of the cell culture dish. The cells were resuspended in 1 ml cold TRIzol™ and transferred into 2 ml pre-cooled reaction tubes. The tubes were kept on ice until all samples were processed. Samples were stored at -80 °C until further use or directly processed.

When frozen, cells in TRIzol™ were thawed on ice for further processing. Samples were incubated for 5 minutes at room temperature to dissociate nucleoprotein complexes. 200 µl chloroform were added, the suspension was vortexed for 20-30 sec, incubated 5 min on ice and afterwards centrifuged for 15 min at 4 °C and 12,000 x g. The aqueous upper phase (about 600 µl) was transferred into RNase free tubes. An equal amount of 70 % ethanol was added, the liquids were thoroughly mixed by repeatedly inverting the tube and a maximum of 700 µl was transferred onto a column. The column was centrifuged for 15 sec at 12,000 x g at 4 °C. The flow through was discarded. These steps were repeated until the total sample was processed. Afterwards, the column was washed once with 300 µl Wash Buffer 1 and transferred into a new collection tube. For digestion of genomic DNA, PureLink DNase was dissolved according to the manufacturer's instructions in 550 µl RNase-free water to a final concentration of 3 U/µl and a DNAse mix containing 8 µl 10x DNase I Reaction Buffer, 10 µl dissolved PureLink DNase and 62 µl RNase-free water per column was prepared. The DNAse mix was added to the columns and incubated for 15 min at room temperature. Subsequently, the column was washed once again with 300 µl Wash Buffer 1, placed in a new collection tube, and washed twice with 500 µl Wash Buffer 2; each washing step was followed by a centrifugation for 30 sec at 12,000 x g at room temperature. After the last washing step, the column was placed in a clean RNase-free elution tube, incubated with 50 µl RNase free water for 1 min and centrifuged for 1 min at 12,000 x g at room temperature. The column was transferred onto a fresh tube, incubated again with 20 µl RNase free water for 1 min and centrifuged for 1 min at 12,000 x g at room temperature. The concentrations of both eluates were measured at a wavelength of 260 nm using the N60 NanoPhotometer® (Implen, Munich, Germany). To verify a high quality of RNA-isolates, agarose gel electrophoresis was performed. Therefore, a 1 % agarose gel was prepared by dissolving 0.7 g agarose in 7 ml 5x TBE (*Table 2*) and 63 ml H_2O in a microwave for 60 seconds. The solution was poured in the agarose gel electrophoresis chamber where polymerization took about 30 min. After polymerization, the electrophoresis chamber was filled with 0.5x TBE buffer. 5 µl Generuler 1 kB DNA Ladder (Thermo Fisher Scientific) were mixed with 1 µl Midori Green Direct and applied to the first pocket. 100 ng of total RNA were diluted with

ddH_2O to a final volume of 10 µl. 1 µl Midori Green Direct (Nippon Genetics Europe) dye was added and samples were loaded on the gel. The gel was run for 1.5 h at 65 V before visualizing the 18s and 28s rRNA bands in the ChemiDoc XRS+ molecular imaging system using ImageLab 5.2.1 software (Bio-Rad Laboratories, Inc., Hercules, US) and settings for ethidium bromide-stained gels according to the manufacturer's instructions of the used dye. The RNA eluates were stored at -80 °C until further use.

3.5 cDNA synthesis

cDNA synthesis was performed using a MultiScribe High Capacity cDNA Reverse Transcriptase Kit (Thermo Fisher Scientific) according to the instructions.

A total amount of 2 µg template-RNA was diluted with nuclease free water to a volume of 14.2 µl. If the RNA concentration was insufficient, a maximum of 14.2 µl was used and the utilized amount of RNA was calculated. 5.8 µl of prepared MasterMix (2 µl 10x RT Buffer, 0.8 µl 25x dNTP Mix, 2 µl 10x RT Random Primers and 1 µl MultiScribe Reverse Transcriptase) were added to the template-RNA, the suspension was mixed by carefully pipetting three times up and down and reverse transcription was performed in a PCR cycler (10 min 25 °C, 120 min 37 °C and 5 min 85 °C). Afterwards, the samples were kept in the PCR cycler at 4 °C for as short as possible and stored at -80 °C until further use.

3.6 Quantitative real-time PCR

Reference gene quantitative real-time PCR. The expression levels of nine putative reference genes was investigated for each cell line by quantitative real-time PCR (qRT-PCR) using 6-Carboxyfluorescein-labelled (FAM-labelled) TaqMan® real-time PCR assays (*Table 13*, Applied Biosystems™, Thermo Fisher Scientific, US) in order to find the most stable housekeeping gene under hypoxic and normoxic conditions. For each gene, a separate 96-well plate was used. The 2x TaqMan™ Universal PCR-Mastermix (Applied Biosystems™) and the respective 20x TaqMan® assay were mixed according to *Table 14* and 5.5 µl of this suspension were transferred into the wells of a 96-well plate (MicroAmp® Optical Well Reaction Plate, Thermo Fisher Scientific). The cDNA was diluted to a concentration of 4 ng/µl. Per well, 4.5 µl were used corresponding a total amount of 18 ng cDNA per reaction. The suspension was mixed by carefully pipetting three times up and down and the plate was centrifuged for 30 sec. The assays were run directly after preparation using QuantStudio5 real-time PCR system (Thermo Fisher Scientific) according to the settings in *Table 15*.

Table 13: FAM-labelled TaqMan™ Assays used for reference gene qRT-PCR.

Gene symbol	Gene name	Assay ID
18S	Eukaryotic 18S rRNA	Hs03003631_g1
ACTB	actin beta	Hs01060665_g1
B2M	beta-2-microglobulin	Hs00187842_m1
GAPDH	glyceraldehyde-3-phosphate dehydrogenase	Hs00266705_g1
PPIA	peptidylprolyl isomerase A	Hs04194521_s1
RPLP13A	ribosomal protein L13a	Hs04194366_g1
RPLP1	ribosomal protein lateral stalk subunit P1	Hs01653088_g1
SDHA	succinate dehydrogenase complex flavoprotein subunit A	Hs00188166_m1
TBP	TATA-box binding protein	Hs00427620_m1

Table 14: Pipetting scheme for reference gene qRT-PCR and multiplex target-gene qRT-PCR. TG = target gene, RG = reference gene.

	Mastermix			**Dilution cDNA**	**Volume cDNA**	**Total amount cDNA**
	TaqMan™ Mastermix	FAM-labelled TG	VIC-labelled RG			
Reference gene qRT-PCR	5 µl	0.5 µl	-	4 ng/µl	4.5 µl	18 ng
Target gene qRT-PCR	5 µl	0.5 µl	0.5 µl	5 ng/µl	4 µl	20 ng

Target gene quantitative real-time PCR. Using a multiplex qRT-PCR, relative mRNA expression levels of cells kept under hypoxia compared to normoxia were evaluated using FAM-labelled target genes and 2'-chloro-7'-phenyl-1,4-dichloro-6-carboxyfluorescein-labelled (VIC-labelled) reference gene in the same reactions. A master mix was prepared according to *Table 14* and pipetted into the wells of a 96-well plate (MicroAmp® Optical Well Reaction Plate, Thermo Fisher Scientific). The generated cDNA was diluted to a final concentration of 5 ng/µl. Per well, 4 µl were used equating a total amount of 20 ng cDNA. The suspension was mixed by carefully pipetting three times up and down before the plate was centrifuged for 30 sec. The assays were run directly after preparation using QuantStudio5 real-time PCR system (Thermo Fisher Scientific) according to the settings in *Table 15*.

Table 15: Settings for quantitative real-time PCR with TaqMan assays.

Step	Temperature	Time	Cycles
UNG-Incubation	50°C	2 min	hold
Polymerase activation	95°C	10 min	hold
Denaturation	95°C	15 sec	40 x
Annealing/Extension	60°C	1 min	

3.7 Cell lysis

Depending on the experiment, cells were lysed using different methods.

Solution-based lysis. For sodium dodecyl sulphate–polyacrylamide gel electrophoresis (SDS-Page), cells were incubated as described in *3.2*. Medium was aspirated and discarded. Cells were washed once with 10 ml cold PBS and then detached from the bottom of the cell culture dish using a cell scraper, before transferring them into pre-cooled reaction tubes. Cells were either stored at -80 °C until further use or directly lysed. For lysis, cell suspension was mixed 1:1 with lysis buffer (1 tablet of cOmplete™, EDTA-free Protease Inhibitor Cocktail, Roche, dissolved in 5 ml ddH2o by vortexing 5 min, 10 µl Triton X-100) and incubated 30 min on ice. Afterwards, the suspension was centrifuged 10 min at 12.000 x g at 4 °C. The protein-containing supernatant was transferred into a fresh reaction tube. Protein concentration was determined by measuring the absorbance at 280 nm using a NanoPhotometer® N60 (Implen Inc., Westlake Village, US).

Physical disruption. For liquid chromatography–mass spectrometry (LC-MS/MS) analysis, cells were incubated as described in *3.2*. Medium was aspirated and discarded. Cells were washed with PBS once and then collected using a cell scraper, before transferring them into pre-cooled reaction tubes. Cells were either stored at -80 °C until further use or directly lysed. Cells were lysed by three repeated freeze-thaw cycles in liquid nitrogen before incubating in an ultrasound-bath with ice-water for 5 min. Afterwards, two more freeze-thaw cycles were performed before incubating again in an ultrasound-bath with ice-water for 5 min. The suspension was centrifuged 10 min at 12.000 x g at 4 °C. The supernatant containing the proteins was transferred into a fresh reaction tube. Protein concentration was assessed by measuring the absorbance at 280 nm using a NanoPhotometer® N60 (Implen Inc.).

3.8 SDS-Polyacrylamide gel electrophoresis

For SDS-PAGE, cells were incubated and lysed as described in *3.7* using a solution-based lysis.

SDS-PAGE gel preparation. SDS-polyacrylamide gels were prepared according to *Table 16*. Shortly, ddH_2O, 40 % acrylamide and separating buffer were mixed according to the desired gel-percentage and stirred for 15 min using a magnetic stirrer for degasification. Then, 40 µl 10 % ammonium persulfate (APS) and 10 µl tetramethylethylenediamine (TEMED) were added, while further stirring. The mixture was rapidly pipetted between the two glass plates and overlaid with isopropanol. The gel polymerized for 30 min before removing the isopropanol and pouring the stacking gel (*Table 17*). After additional 30 min of polymerization, the gel was either directly used or stored over night at 4 °C wrapped in wet towels and cling film.

Table 16: Composition running gel for SDS-PAGE.

	Gel percentage		
	15 %	**10 %**	**8 %**
ddH_2O/Glycerol (1:1)	3.75 ml	5 ml	5.5 ml
Acrylamide (40 %)	3.75 ml	2.5 ml	2.0 ml
4x buffer running gel (Lower Tris-Buffer)	2.5 ml	2.5 ml	2.5 ml
10 % APS	40 µl	40 µl	40 µl
TEMED	10 µl	10 µl	10 µl

Table 17: Composition stacking gel for SDS-PAGE.

	4 %
ddH_2O	1.95 ml
Acrylamide (40 %)	300 µl
4x buffer stacking gel (Upper Tris-Buffer)	750 µl
10 % APS	15 µl
TEMED	5 µl

Sample processing and SDS-PAGE. To prepare the separation of proteins according to their molecular weight, the handcast SDS-gels were placed in the electrophoresis cell. The inner buffer chamber was filled with running buffer (*Table 2*). The combs were removed carefully, and the gel pockets were gently washed with running buffer. For NOS3, HIF1A and HIF2A Western blots, 5 µl PageRuler™ Plus Prestained Protein Ladder (ThermoFisher, 26619) were applied to the first gel pocket. For DDAH1 and DDAH2 Western blots 5 µl PageRuler™ Prestained Protein Ladder (ThermoFisher, 26616) were applied to the first slot of each gel as size standard. Depending on the target protein, protein suspension was diluted to 25 µl using ddH_2O to the desired concentrations (*Table 18*). 5 µl 6x loading buffer (*Table 2*) were added and proteins were denatured by heat shocking at 95 °C for 5 min and directly put on ice afterwards. Cellular debris was pelleted by centrifugation at 10,000 x g at 4 °C for 10 min, before loading the protein-containing supernatant on the gel. Gel electrophoresis was performed at a constant voltage of 100 V for 3-5 h, whereby protein migration was monitored by observing the stained size standard.

3.9 Western blot

For protein analysis, Western blots were performed by either semi-dry or wet tank blotting. After the SDS-PAGE, the gel was removed from the glass plates and equilibrated in transfer buffer (*Table 2*). for 15-20 min, together with WhatMann™ filter paper and nitrocellulose membrane (both GE Health Care Life Sciences, US) with the respective pore size (*Table 18*). A transfer sandwich was built as seen in *Figure 6.*

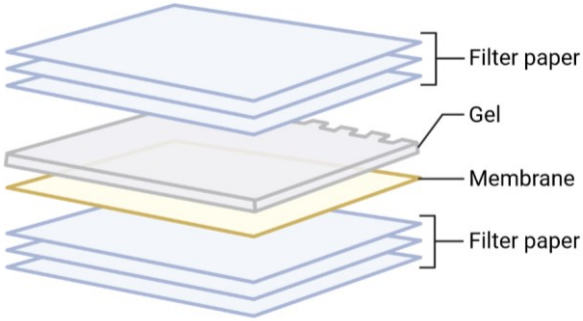

Figure 6: Composition of the transfer sandwich for protein transfer via Western blotting. After SDS-PAGE, the gel was removed from glass plates and equilibrated in transfer buffer together with WhatMann™ filter paper and a nitrocellulose membrane. A transfer sandwich consisting of three filter papers, overlaid by the nitrocellulose membrane, the SDS-PAGE gel and three more filter papers was built for protein transfer using Western blot wet tank blotting. Created with BioRender.com.

The wet tank blotting chamber was filled with cold (4 °C) transfer buffer (*Table 2*) and a cooling pack and placed in a box containing ice to hold a low temperature and avoid overheating of proteins.

Proteins were blotted onto the membrane at a constant current of 300 mA for 50-60 min in a wet tank blotting chamber, according to molecular weight (Table 18). The semi-dry blot of HCAEC proteins was performed at 1.0 A for 20 min (NOS3 WB) or 0.3 A for 30 min (DDAH1 and DDAH2).

After blotting, the transfer sandwich was opened carefully, and the transfer was verified by checking the size standard. All the following steps were performed at room temperature (RT) unless otherwise specified. The membrane was equilibrated in ddH_2O for 5 min before staining with Ponceau S solution (*Table 2*) for 10 min on a rocking plate. Afterwards, the membrane was shortly washed in ddH_2O three times to remove background staining. The protein transfer was documented photographically, and the membranes were cut into three pieces separating the size standard, the house keeping control or the target protein, respectively. The membrane pieces were then de-stained for 10 min in 1x TBS-T on the rocking plate, before blocking non-specific antibody binding sites in 5 % non-fat dry milk (NFDM) in 1x TBS-T for 1 h on roller shaker, except of HIF1A, which was blocked for 3 h. Afterwards, the membrane pieces were washed two times for 5 min in 1x TBS-T and incubated with the desired primary antibody over night at 4 °C. Primary antibodies were diluted in 5 % NFDM in 1x TBS-T in the respective dilutions listed in *Table 18*. After incubation with the primary antibody, the membrane pieces were washed three times for 10 min at RT in 1x TBS-T. Membranes were then incubated with the appropriate (*Table 18*) horseradish peroxidase-conjugated secondary antibody in 5 % NFDM in 1x TBS-T in a dilution indicated in *Table 18* for 1 h at RT. Excess, unbound antibody was removed by washing three times with 1x TBS-T followed by washing once with 1x TBS, each time for 10 min. Imaging was performed using the ChemiDoc XRS+ and Image Lab software (Bio-Rad Laboratories, Inc., Hercules, US). The membrane pieces were placed in the ChemiDoc detection chamber. Protein bands were visualized using chemo luminescence: 500 µl solution A (luminol solution) and 500 µl solution B (peroxide solution) of the Amersham™ ECL™ Prime Western-Blot-System were mixed in a brown micro reaction tube and directly applied onto the membrane. Data acquisition was performed for target protein and loading control separately, using various exposure times until saturated pixels were observed.

Table 18: Antibody dilutions and Western blot settings.

Antibody	Dilution in 5% NFDM TBS-T	Secondary Antibody	Expected size/ predicted molecular weight	SDS-Gel percentage	Total amount of applied protein	Nitrocellulose-membrane	Transfer Wet Tank	Transfer SemiDry
NOS3 (ab76198)	1:500	Anti-mouse 1:10,000	133 kDa	8 % or 10 %	50 µg	0,45 µM	300 mA const., 1 h	1 A const. 20 min
DDAH1 (ab180599)	1:10,000	Goat-α-Rabbit 1:10,000	37 kDa	15 %	60-75 µg	0,2 µM	300 mA const., 50 min	300 mA const. 30 min
DDAH2 (ab184166)	1:1,000	Goat-α-Rabbit 1:10,000	30 kDa	15 %	60-75 µg	0,2 µM	300 mA const., 50 min	300 mA const. 30 min
HIF1A (PA1-16601)	1:1,000	Goat-α-Rabbit 1:10,000	116 kDa	8 %	50 µg	0,45 µM	300 mA const., 1 h	-
HIF2A (PA1-16510)	1:1,000	Goat-α-Rabbit 1:10,000	120 kDa	8 %	50 µg	0,45 µM	300 mA const., 1 h	-
Reference gene: TUBB (ab6046)	1:5,000	Goat-α-Rabbit 1:10,000	55 kDa	-		-	-	-

3.10 Metabolite measurement using LC-MS/MS

ADMA and SDMA concentrations were measured using LC-MS/MS. Three solutions containing defined amounts of isotope labelled analytes (*Table 19,* here called calibration solution) in dialysed plasma were prepared and stored at -20 °C. The measured concentrations of these solutions were used to generate a standard curve and a line equation. Internal standard solution was applied to each sample in order to compensate metabolite loss due to sample processing. The internal standard solution containing 2 µmol/L $^{2}H_{7}$-ADMA and 2 µmol/L $^{2}H_{6}$-SDMA in 96 % methanol was prepared and stored at 4 °C until use. Two controls containing a known concentration of metabolites were prepared and stored at -20 °C. These controls were applied as quality controls to each plate to ensure reproducibility of measurements and consistent quality over different plates.

Table 19: Standard solutions for LC-MS/MS.

	Internal standard (IS) solution		**Calibration solution (in dialysed plasma)**			**Control**	
Metabolite	IS	Concentration	Cal. 1	Cal. 2	Cal. 3	Con. 1	Con. 2
ADMA	$^{2}H_{7}$-ADMA	2 µM	0.5 µM	1 µM	2 µM	Human plasma	Human plasma + 1 µM ADMA
SDMA	$^{2}H_{6}$-SDMA	2 µM	0.5 µM	1 µM	2 µM	Human plasma	Human plasma + 1 µM SDMA

Sample processing. Cells were lysed as described in *3.7* and protein concentrations were measured using a NanoPhotometer® N60. The internal standard solution was equilibrated to room temperature immediately before use. A 0.22 µM MultiScreen 96-well filter plate (Millipore, MSGVN2250) was placed over a 96-well polypropylene plate (Greiner). Per well, 100 µl of the methanolic internal standard solution was applied to the filter plate. 25 µl of calibration solution (*Table 19*), sample, or quality control (*Table 19*) were added to each well before the plates were incubated at RT for 15 min on an orbital shaker at 400 to 500 rpm. Calibration solution and quality control were applied in triplicates, samples in duplicates. The polypropylene plate overlaid by the MultiScreen filter plate containing the solutions was centrifuged for 10 min at 4 °C and 3,000 rpm in a plate centrifuge. Afterwards, the polypropylene plate containing the eluent was kept under a hood on a heating block at 75 °C for about 30 min until the solution was completely evaporated. The plate was removed from the heating block and after shortly cooling down 100 µl of a 1 N butanoic hydrochloric acid were added per well. The plate was sealed with a covering mat (Sarstedt) and incubated on a heating block at 65 °C for 30 min. The covering mat was hereby

weighted to prevent opening of the coverage. After cooling down to RT the plate was centrifuged at RT for 1 min at 2,000 rpm. Afterwards, the covering mat was removed and the butanoic hydrochloric acid was evaporated by incubating again on a heating block at 75 °C for 60 min. When cooled down to RT, the plate was covered with a mat again and stored at -20 °C over night. The next day, the plate was brought to RT, 110 µl sample buffer was pipetted to each well and the plate was covered with a covering mat once more before incubating at RT for 60 min on an orbital shaker at 400-500 rpm. Using a 8-channel pipette, 100 µl of each well were transferred in a new 96-well filter plate (0.45 µM MultiScreen, MSHVN4550, Millipore), that was placed over a new 96-well polypropylene plate. The plates were centrifuged at 4 °C at 3,000 rpm for 10 min. The polypropylene plate containing the eluent was afterwards sealed with a covering mat and directly measured in a LC-MS.

Liquid chromatography. 10 µl of the processed samples were injected to the chromatography unit at 10 °C via the auto sampler. The column temperature was set to 10 °C, the flow rates of pumps was set to 0.4 ml/min. An ACQUITY UPLC BEH C18 column (Waters Corporation, US) was used for chromatography. 0.1 % formic acid in LC-MS-H_2O (Solvent A) and 0.1 % formic acid in acetonitrile (Solvent B) were used as solvent gradient. At the starting point of each measurement the ratio of the two solvents were 95 % solvent A and 5 % solvent B. During the measurement this ratio changed to 30 % solvent A and 70 % solvent B. Total measuring time was 2.8 min per sample.

Table 20. Specifications of used column for liquid chromatography.

Specification	
Chemistry	C18
Separation Mode	Reverse Phase
Particle Substrate	Hybrid
Particle Shape	Spherical
Particle Size	1.7 µM
Pore Size	130 Å
Inner Diameter	2.1 mm
Length	50 mm

Mass spectrometry. Following the liquid chromatography, the liquid flow was directed into the triple quadrupole mass spectrometer. Analytes were ionised in the ion source via positive electron spray ionisation (ESI^+). Nitrogen (500 °C, 650 L/h) was used as carrier gas for API (atmospheric pressure ionization) to evaporate the liquids. Inside the mass analyser, analytes were separated according to their mass-to-charge-ratio (first quadrupole) and fragmented by collision with argon thereafter (second quadrupole). Using mass transitions listed in *Table 21* metabolites were detected. Cone energy was set to 18 V, collision energy to 16 V to achieve these fragmentations of ADMA and SDMA. The resulting fragments were selected and detected (third quadruple).

Table 21: Mass transitions of metabolites.

Metabolite	Parent (m/z)	Daughter (m/z)	Cone energy (V)	Collision energy (V)
$^2H_7$-ADMA	266.28	221.21	18	14
ADMA	259.29	214.18	18	16
$^2H_6$-SDMA	265.22	231.17	18	16
SDMA	259.22	228.17	18	16

3.11 Evaluation of reference gene expression by quantitative real-time PCR

Mean Ct-values. Mean cycle threshold (Ct)-values of each putative reference gene and their respective standard deviation (SD) collectively of all cell lines (HCAEC, HPAEC, A549) and conditions (NX, 24 h HX, 72 h HX) were calculated in order to assess the expression profile of the nine candidate reference genes.

Coefficient of variation. The expression stability of the candidate reference genes was then analysed calculating the coefficient of variation of Ct values by dividing standard deviation of Cts by average Ct for each cell line separately as well as for all samples together.

Pairwise ΔCt comparison. Using a pairwise ΔCt comparison according to Silver et al. [115], mean SDs of gene expression were calculated within each cell line and for all cell lines together. This method calculates the ΔCt-values pairwise for each possible combination of two candidate reference genes. The mean SD is hereby used to assess the expression stability of the putative reference genes. The results of this analysis were ranked from low to high mean SD.

NormFinder. Additionally, relative quantities of all candidate genes were calculated by dividing the minimum Ct of a putative reference gene by each individual Ct-value of the same gene. The NormFinder Add-In for Excel uses these relative quantities to analyse the stability of candidate genes among different conditions. It ranks these candidate genes according to their stability value and can be used with or without differentiating between biological groups. The NormFinder algorithm considers both, overall expression variation as well as variation in gene expression between the biological subgroups for the putative reference genes [116]. The analysis was performed for each cell line separately, as well as for all cell lines taken together. Each condition (NX, 24 h HX, 72 h HX) was defined as a different biological group by using sample group identifiers. When comparing all three cell lines, the cell lines were also separated in different biological groups, resulting in a total of nine biological groups (HPAEC NX, HPAEC 24 h HX, HPAEC 72 h HX, HCAEC NX, HCAEC 24 h HX, HCAEC 72 h HX, A549 NX, A549 24 h HX, A549 72 h HX).

Mean ranking. After performing all of the analyses listed above, a mean rank for each putative reference gene was calculated to summarize the results of the analyses.

3.12 Quantification of mRNA expression by quantitative real-time PCR

Relative mRNA expression was calculated using the $2^{-\Delta\Delta Ct}$-method as described by Livak and Schmittgen [117]. Therefore, the mean Ct of technical replicates and the mean Ct of biological replicates were calculated separately for each condition for the target gene (Ct Target) and the reference gene (Ct internal control). In a next step, ΔCt-values were calculated by subtracting the mean Ct internal control from the mean Ct Target and the ΔΔCt was generated by subtracting the ΔCt of the Calibrator (NX) from ΔCt of each Experimental Condition (24 h HX, 48 h HX and 72 h HX). By calculating $2^{-\Delta\Delta Ct}$ the relative mRNA expression of target genes normalized to the reference gene was calculated and relative expression of the calibrator (NX) was set to 1.

3.13 Quantification of protein expression

To relatively quantify levels of target protein under various conditions, densitometric quantification was performed. Images of Western blots were chosen close to but below the saturation point. The files for reference and target protein were opened in Image Lab software, version 5.2.1 and assigned to the respective channels in “Normalization” method. TUBB images were selected for normalization channel with housekeeping protein bands for normalization. Lanes and bands were set manually, and the lane background was subtracted with 70 mm disk size for profile consistency. The software calculated volume intensities for each band based on the detected chemiluminescent signal. Quantification was performed by normalizing the housekeeping protein bands to the

normoxic control and multiplying the target volumes with the normalizing factor. The normalized volume intensities were then used to calculate the relative protein expression in hypoxia compared to normoxic control. NX expression was set to 1.

3.14 Quantification of metabolites

After measuring the plate in the LC-MS, the MassLynx data were analysed. The tailing of peaks was controlled and if necessary manually reintegrated. The software then calculated peak areas of each metabolite in sample and internal standard and normalized peak areas of samples to peak areas of internal standards with the known concentrations of metabolites. The resulting data were exported to Excel. The mean of the two technical replicates per sample was calculated. The protein concentration of the samples was then used to calculate the amount of metabolite per mg protein in order to compensate differences in cell confluence.

3.15 Statistical Analysis

All statistical analyses were performed using Graphpad PRISM 8.4.3. As the sample number for all experiments was relatively low, Gaussian distribution of the results was not given. Therefore, a non-parametric Mann-Whitney-U test was performed. All column charts show the mean of the samples of a respective condition, whiskers represent standard deviation (SD). Confidence level of the two-tailed t-test was set to 95 %, resulting in a definition of statistical significance for p-values smaller 0.05.

4 Results

4.1 Incubation in NX and HX

4.1.1 Reference gene qRT-PCRs

In order to find the steadiest gene in hypoxia and normoxia, the expression levels of nine putative reference genes were assessed by qRT-PCR as described in *3.11*.

4.1.1.1 Expression profiles of reference genes in normoxic and hypoxic HCAEC, HPAEC and A549 cells

Ct values were obtained for every putative reference gene and every investigated condition (NX, 24 h HX, 72 h HX) in the three different cell types, and variation in gene expression was assessed. *18S* was the most abundant gene in all cell lines with a mean Ct value of 7.783 ± 0.371; the lowest expression levels throughout all cell types were observed for *TBP* (26.270 ± 0.430), *PPIA* (25.920 ± 0.363) and *SDHA* (25.260 ± 0.747). Furthermore, some genes, e.g. *B2M* and *SDHA* showed a relatively wide transcription range (SD 0.764 and 0.748, respectively). Ct values for all experiments are shown as boxplots in *Figure 7.*

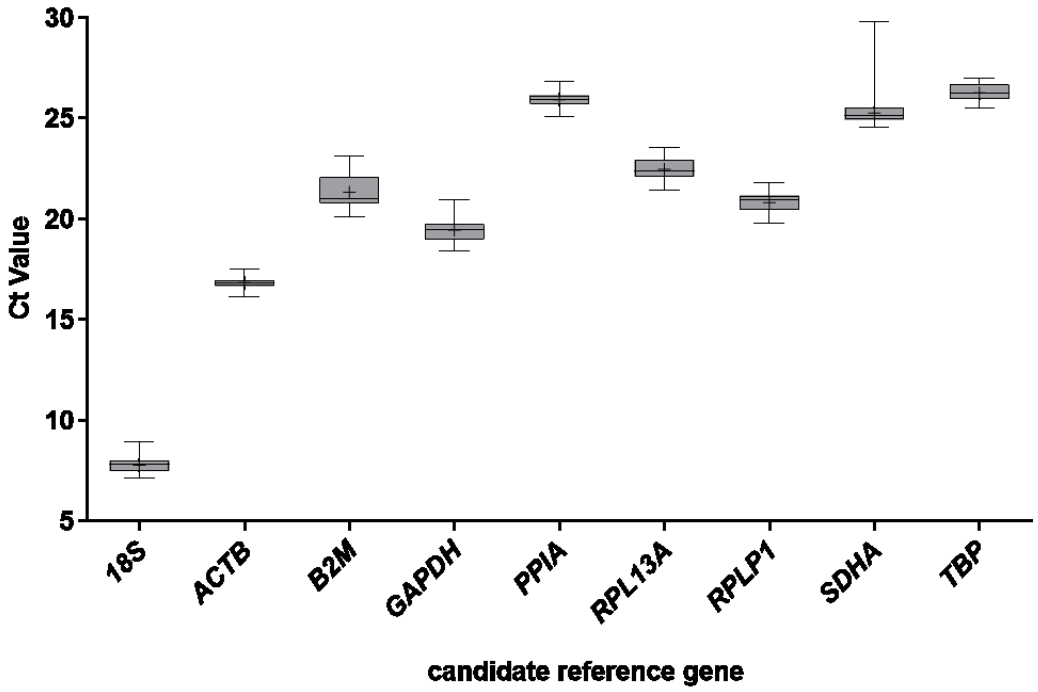

Figure 7: Cycle threshold (Ct) values of the 9 candidate reference genes used in this study. Mean Ct values of all putative reference genes were calculated. Box plots represent the interquartile range (IQR, 25th–75th). Horizontal lines and plus sign represent the median and mean, respectively. Whiskers indicate the minimum and maximum values.

4.1.1.2 Expression stability of reference genes in normoxic and hypoxic HCAEC, HPAEC and A549 cells

Ct CV. Subsequently, Ct coefficients of variation (Ct CV, in %) were calculated for each putative reference gene in the different cell lines (*Table 22*). A number of often-used reference genes such as *18S* and *B2M* showed high variation between normoxia and hypoxia, with different levels of variation between the different cell lines. *18S* showed the highest Ct CV calculated for each cell line separately (4.73 % in HCAEC, 3.46 % in HPAEC and 4.72 % in A549) as well as calculated for all cell lines together (4.72 %). In A549, all calculated Ct CVs were similar, except for *18S* with by far the highest Ct CV. *SDHA* whose Ct CV was the second highest in HCAEC (4.19 %) showed the lowest Ct CV for HPAEC (0.71 %). When comparing all cell lines together, Ct CV of *SDHA* was the third highest (2.93 %) after *18S* (4.72 %) and B2M (3.55 %). Other putative reference genes such as *TBP*, *PPIA*, *RPLP1* and *RPL13A* showed relatively low Ct CV, calculated for each cell line separately as well as for all cell lines together. In HCAEC, the lowest Ct CVs were calculated for *TBP* (1.13 %), *PPIA* (1.19 %) and *RPL13A* (1.27 %). In HPAEC, *SDHA* (0.71 %), *ACTB* (0.77 %) and *B2M* (0.81 %) showed the lowest Ct CVs. Lowest Ct CVs in A549 were calculated for *RPL13A* (1.14 %), *SDHA* (1.20 %) and *RPLP1* (1.41 %). When calculating Ct CV for all cell lines together, *PPIA* (1.39 %) showed the lowest Ct CV, followed by *TBP* (1.62 %) and *ACTB* (1.72 %).

Table 22: Coefficient of variation. The coefficient of variation of the putative reference genes was calculated separately for each cell line as well as for all samples together. RG= Candidate reference gene.

RG	HCAEC	HPAEC	A549	All
18S	4.73 %	3.46 %	4.05 %	4.72 %
ACTB	1.81 %	0.77 %	1.64 %	1.72 %
B2M	1.70 %	0.81 %	1.79 %	3.55 %
GAPDH	1.98 %	1.03 %	1.42 %	2.78 %
PPIA	1.19 %	1.05 %	1.85 %	1.39 %
RPL13A	1.27 %	1.20 %	1.14 %	2.33 %
RPLP1	1.43 %	1.37 %	1.41 %	2.27 %
SDHA	4.19 %	0.71 %	1.20 %	2.93 %
TBP	1.13 %	0.99 %	1.46 %	1.62 %

Pairwise ΔCt comparison. The results of the pairwise ΔCt comparison were ranked from low to high mean SD and are shown in *Table 23*. *B2M* showed a relatively low mean SD compared to other candidate genes in A549 and HPAEC (mean SD 0.285 and 0.209) and a high variation in HCAEC (mean SD 0.372). *B2M* was listed at the lowest rank when comparing all cell lines together using this method. Compared to other SD values, the expression of *SDHA* in HCAEC (mean SD 0.976) varied greatly. In HPAEC, *SDHA* also had the highest mean SD (0.372), in A549 it was listed on rank 7 (mean SD 0.306). *GAPDH* also showed a high standard deviation in A549 and HCAEC after pairwise ΔCt comparison (SD 0.379, 0,460, respectively), while it had a relatively low mean SD in HPAEC (0.226). *RPL13A* was listed at rank 8 in HPAEC with a mean SD of 0.340, however it showed the lowest mean SD in A549 (0.265). When comparing all cell lines together, the lowest mean SDs were observed for *TBP*, *PPIA* and *18S* (0.461, 0.480 and 0.499, respectively). *GAPDH*, *SDHA* and *B2M* showed the highest mean SDs (0.617, 0.763 and 0.865, respectively).

Table 23: Ranking of mean SD values of pairwise comparison of ΔCt values of putative reference genes. Mean SD values were calculated using the pairwise ΔCt comparison and ranked from low SDs to high SDs. The analysis was performed for each cell line separately as well as for all cell lines together.

Rank	HCAEC	mean SD	HPAEC	mean SD	A549	mean SD	All Samples	mean SD
1	*TBP*	0.305	*PPIA*	0.196	*RPL13A*	0.265	*TBP*	0.461
2	*RPLP1*	0.310	*B2M*	0.209	*ACTB*	0.276	*PPIA*	0.480
3	*PPIA*	0.341	*18S*	0.218	*B2M*	0.285	*18S*	0.499
4	*RPL13A*	0.347	*ACTB*	0.218	*TBP*	0.290	*RPLP1*	0.526
5	*ACTB*	0.352	*RPLP1*	0.226	*RPLP1*	0.290	*RPL13A*	0.536
6	*18S*	0.368	*GAPDH*	0.226	*18S*	0.298	*ACTB*	0.556
7	*B2M*	0.375	*TBP*	0.239	*SDHA*	0.306	*GAPDH*	0.617
8	*GAPDH*	0.460	*RPL13A*	0.340	*PPIA*	0.348	*SDHA*	0.763
9	*SDHA*	0.976	*SDHA*	0.372	*GAPDH*	0.379	*B2M*	0.865

NormFinder analysis. To complement the variation analysis, NormFinder Excel add-in was used to analyse gene expression stability. An overview of the ranking based on the Ct CV and NormFinder results in the different cell lines is given in *Table 24*, the individual stability values are visualized in *Figure 8*. In HPAEC, the three top ranking genes (*PPIA*, *18S* and *ACTB*) showed very similar stability values of 0.060, 0.065 and 0.069, respectively. In HCAEC, the top ranking gene (*RPLP1*, stability value 0.053) was more distant from genes on position two and three (*PPIA* and *ACTB*), which in turn showed a very similar gene expression stability (stability values 0.071 and 0.082, respectively. In A549 cells, the two top ranking genes (*ACTB*, 0.085 and *RPL13A*, 0.089) showed similar gene expression stability, followed by *RPLP1* with a slightly higher expression variation (0.106). Comparing the stability values of candidate genes between the three cell lines, HCAEC, HPAEC and A549 showed similar expression stability for several genes, especially for *RPL13A* (*Figure 8*). *GAPDH*, *PPIA* and *SDHA* on the other hand showed a striking variance in their stability values calculated by the NormFinder algorithm. The variation analysis of putative reference genes was also performed collectively for all cell lines together. An overview of the ranking based on the Ct CV and NormFinder results is also given in *Table 24*. The NormFinder Algorithm calculated the stability values shown in *Figure 8* (data shown in light grey). The three candidate reference genes with lowest stability value calculated for all cell lines together are *RPL13A*, *18S* and *ACTB* (stability values 0.098, 0.108, 0.111, respectively).

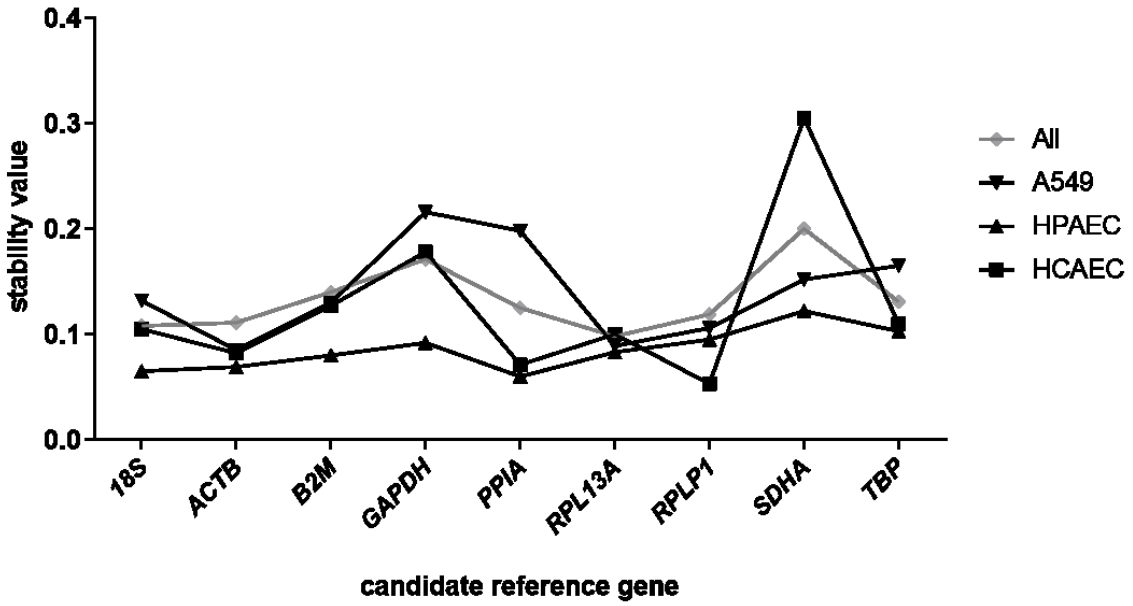

Figure 8: Stability values calculated by the NormFinder Algorithm. Stability values were calculated for each cell line separately (black), differentiating between three biological groups (NX, 24h HX, 72h HX), respectively. Using relative quantities the algorithm calculates intra- and intergroup variation, resulting in lower stability values for candidate genes with higher stability in gene expression. The stability values for all cell lines analysed together are shown in grey.

Table 24: Ranked results of Ct CV and NormFinder analysis. Results of Ct CV and NormFinder Analysis were ranked from number 1-9 with 1 as the lowest coefficient of variation and stability value for each cell line separately and for all cell lines together.

	HCAEC		HPAEC		A549		All	
Ranking	**Ct CV**	**Norm Finder**	**Ct CV**	**Norm Finder**	**Ct CV**	**Norm Finder**	**Ct CV**	**Norm Finder**
1	*TBP*	*RPLP1*	*SDHA*	*PPIA*	*RPL13A*	*ACTB*	*PPIA*	*RPL13A*
2	*PPIA*	*PPIA*	*ACTB*	*18S*	*SDHA*	*RPL13A*	*TBP*	*18S*
3	*RPL13A*	*ACTB*	*B2M*	*ACTB*	*RPLP1*	*RPLP1*	*ACTB*	*ACTB*
4	*RPLP1*	*RPL13A*	*TBP*	*B2M*	*GAPDH*	*B2M*	*RPLP1*	*RPLP1*
5	*B2M*	*18S*	*GAPDH*	*RPL13A*	*TBP*	*18S*	*RPL13A*	*PPIA*
6	*ACTB*	*TBP*	*PPIA*	*GAPDH*	*ACTB*	*SDHA*	*GAPDH*	*TBP*
7	*GAPDH*	*B2M*	*RPL13A*	*RPLP1*	*B2M*	*TBP*	*SDHA*	*B2M*
8	*SDHA*	*GAPDH*	*RPLP1*	*TBP*	*PPIA*	*PPIA*	*B2M*	*GAPDH*
9	*18S*	*SDHA*	*18S*	*SDHA*	*18S*	*GAPDH*	*18S*	*SDHA*

Each method resulted in different gene rankings, however they often define the same candidate RGs as most stable and least stable genes. In A549 cells, based on Ct CV and NormFinder analysis the best reference gene is *RPL13A* (rank 2 and 1, respectively), followed by *RPLP1* and *ACTB*. In HCAEC, *PPIA* and *RPLP1* are both ranked on top of the list, followed by *RPL13A* and *TBP*. The reference gene with the most stable expression in hypoxia and normoxia in HPAEC cells is *ACTB*, followed by *PPIA* and *B2M*. When comparing all cell lines, the three most frequently top ranked genes are *ACTB*, *PPIA* and *RPL13A*.

Mean ranking. We further calculated the mean rank (*Table 25*) of the putative reference genes based on all three analyses (ΔCt, Ct CV and NormFinder). In HCAEC, *PPIA* and *RPLP1* were both listed top of the list (mean rank 2.33), *GAPDH* and *SDHA* scored poorly (mean rank 7.67 and 8.67, respectively). In HPAEC, *PPIA* scored also well (2.67, rank 1), followed by *ACTB* and *B2M* (both mean rank 3.00). *RPL13A* and *RPLP1* were both listed at the bottom of the list with a mean rank of 6.67. In A549 on the other hand, *PPIA* which was ranked at the top for primary cells was ranked at the bottom (mean rank 8.00) after *GAPDH* (7.33). The top ranking reference gene in A549 was *RPL13A* (mean rank 1.33). The top reference genes according to the mean of all analyses calculated for all cell lines together are *PPIA*, *TBP* and *RPL13A* (mean rank 2.67, 3.00 and 3.67, respectively). *B2M* and *SDHA* were ranked at the bottom of the list (both mean rank 8.00). Based upon all experiments performed in order to identify the most suitable reference gene for our experimental setting, all further mRNA expression analyses were performed with normalisation to *RPL13A*.

Table 25: Mean rank of putative reference genes. After performing three different analyses, namely ΔCt, Ct CV and NormFinder, mean ranks for the candidate reference genes for each cell line separately as well as for all cell lines together were calculated to summarize the results of the different analyses.

	HCAEC		HPAEC		A549		All	
Ranking	**Gene**	**Mean Rank**	**Gene**	**Mean Rank**	**Gene**	**Mean Rank**	**Gene**	**Mean Rank**
1	*PPIA*	*2.33*	*PPIA*	*2.67*	*RPL13A*	*1.33*	*PPIA*	*2.67*
2	*RPLP1*	*2.33*	*ACTB*	*3.00*	*ACTB*	*3.00*	*TBP*	*3.00*
3	*TBP*	*2.67*	*B2M*	*3.00*	*RPLP1*	*3.67*	*RPL13A*	*3.67*
4	*RPL13A*	*3.67*	*18S*	*4.67*	*B2M*	*4.67*	*ACTB*	*4.00*
5	*ACTB*	*4.67*	*GAPDH*	*5.67*	*SDHA*	*5.00*	*RPLP1*	*4.00*
6	*B2M*	*6.33*	*SDHA*	*6.33*	*TBP*	*5.33*	*18S*	*4.67*
7	*18S*	*6.67*	*TBP*	*6.33*	*18S*	*6.67*	*GAPDH*	*7.00*
8	*GAPDH*	*7.67*	*RPL13A*	*6.67*	*GAPDH*	*7.33*	*B2M*	*8.00*
9	*SDHA*	*8.67*	*RPLP1*	*6.67*	*PPIA*	*8.00*	*SDHA*	*8.00*

4.1.1.3 Effects of reference gene selection on relative *VEGFA* gene expression in hypoxic HCAEC, HPAEC and A549 cells

To evaluate the effect of the reference gene used for normalization on calculating the relative mRNA expression, *VEGFA* mRNA expression was normalized to the chosen reference gene *RPL13A* as well as to the two lowest ranked putative reference genes according to mean rank of all analyses in all cell lines together (*B2M* and *SDHA*). As shown in *Figure 9* the chosen reference gene had a major impact on the calculated relative mRNA expression of *VEGFA*. While in HCAEC the reference gene choice did not affect relative *VEGFA* mRNA expression, it was highly affected in HPAEC and A549. In HPAEC, calculated relative *VEGFA* mRNA expression differed significantly when normalizing to *RPL13A* or *SDHA* (2.141 ± 0.419 compared to 2.737 ± 0.247 and 2.385 ± 0.380 compared to 2.744 ± 0.359 after 24 h HX and 72 h HX, respectively). The difference between relative mRNA expression was even greater when comparing *VEGFA* mRNA expression normalized to *B2M* and *SDHA* ($p = 0.002$ after both 24 h and 72 h HX). In A549 *VEGFA* mRNA expression after 72 h HX normalized to *SDHA* also differed significantly to *VEGFA* mRNA expression normalized to *RPL13A* (3.033 ± 0.352 and 1.952 ± 0.144, respectively).

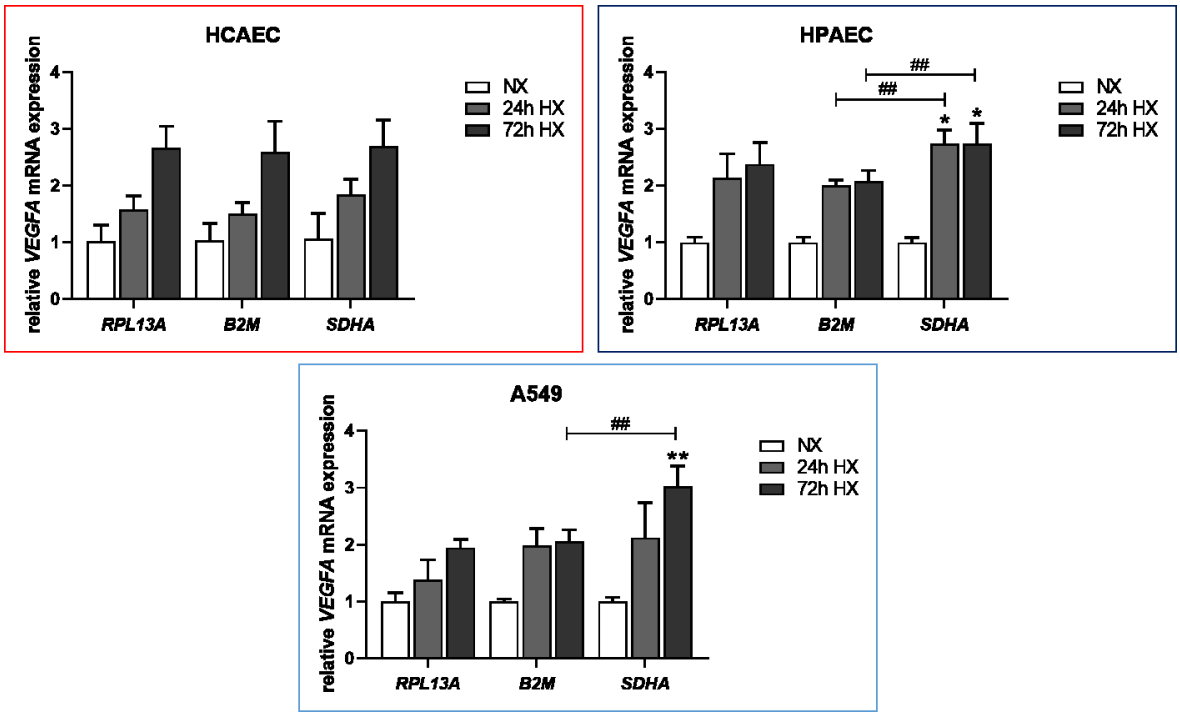

Figure 9: Relative mRNA expression of VEGFA normalized to respective reference genes in HCAEC, HPAEC and A549. Relative *VEGFA* mRNA expression in HCAEC (red), HPAEC (dark blue) and A549 (light blue) incubated in HX and NX was calculated using the ΔΔCt method. Relative mRNA expression in normoxia was set to 1 for each tested reference gene. White bars represent respective NX controls, dark grey bars from left to right the mRNA expression after 24 H HX an 72 h HX, respectively. Bars represent mean ± SD. N=5, *= p≤0.1 compared to same condition in *RPL13A*; **= p≤0.01 compared to same condition in *RPL13A*, ## = p≤0.01 compared to same condition in *B2M*. Non-parametric Mann-Whitney U-test.

4.1.2 mRNA expression in human coronary and pulmonary artery endothelial cells

The relative mRNA expression of *VEGFA* normalized to *RPL13A* in HCAEC and HPAEC after incubation in HX compared to NX are shown in *Figure 10.* A significant increase in the *VEGFA* mRNA expression after exposure to HX was observed in both cell lines. The expression level in HPAEC was not affected by the duration of HX (2.197 ± 0.361, 2.467 ± 0.362, 2.336 ± 0.178 after 24 h, 48 h and 72 h of HX, respectively), whereas the expression level in HCAEC increased further with longer lasting exposure to HX (1.408 ± 0.210, 2.137 ± 0.170, 2.497 ± 0.225 after 24 h, 48 h and 72 h of HX, respectively).

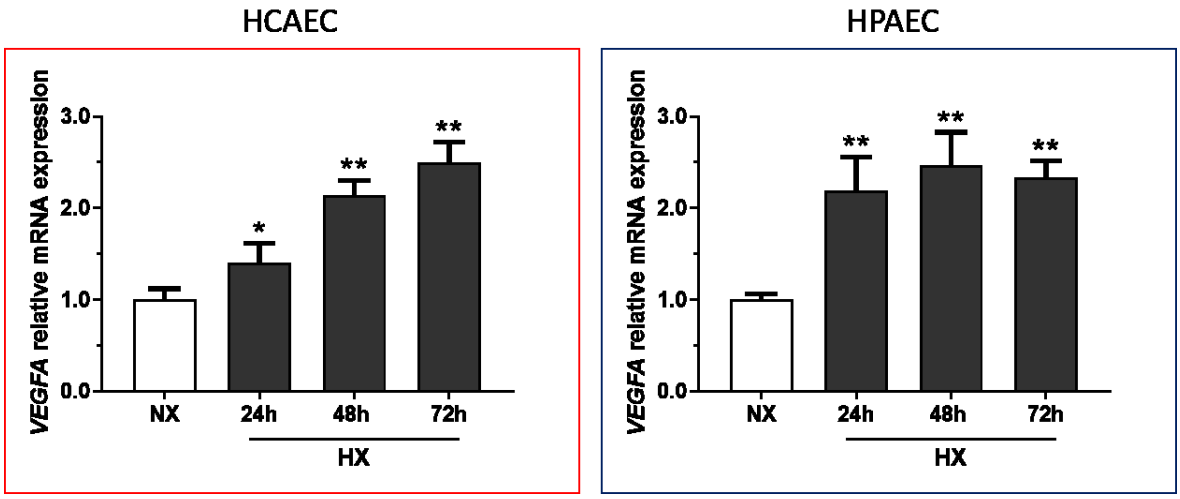

Figure 10: Relative mRNA expression of VEGFA after exposure to NX and 24 h, 48 h and 72 h of HX. HCAEC and HPAEC were incubated in NX and 24h, 48h and 72h of HX. Relative mRNA expression was assessed using qRT-PCR and normalized to *RPL13A*. Expression in control (NX) was set to 1. Bars represent mean ± SD. N=5, *= p≤0.1; **= p≤0.01, Non-parametric Mann-Whitney U-test.

The relative mRNA expression of *NOS3*, *DDAH1* and *DDAH2* are shown in *Figure 11.*

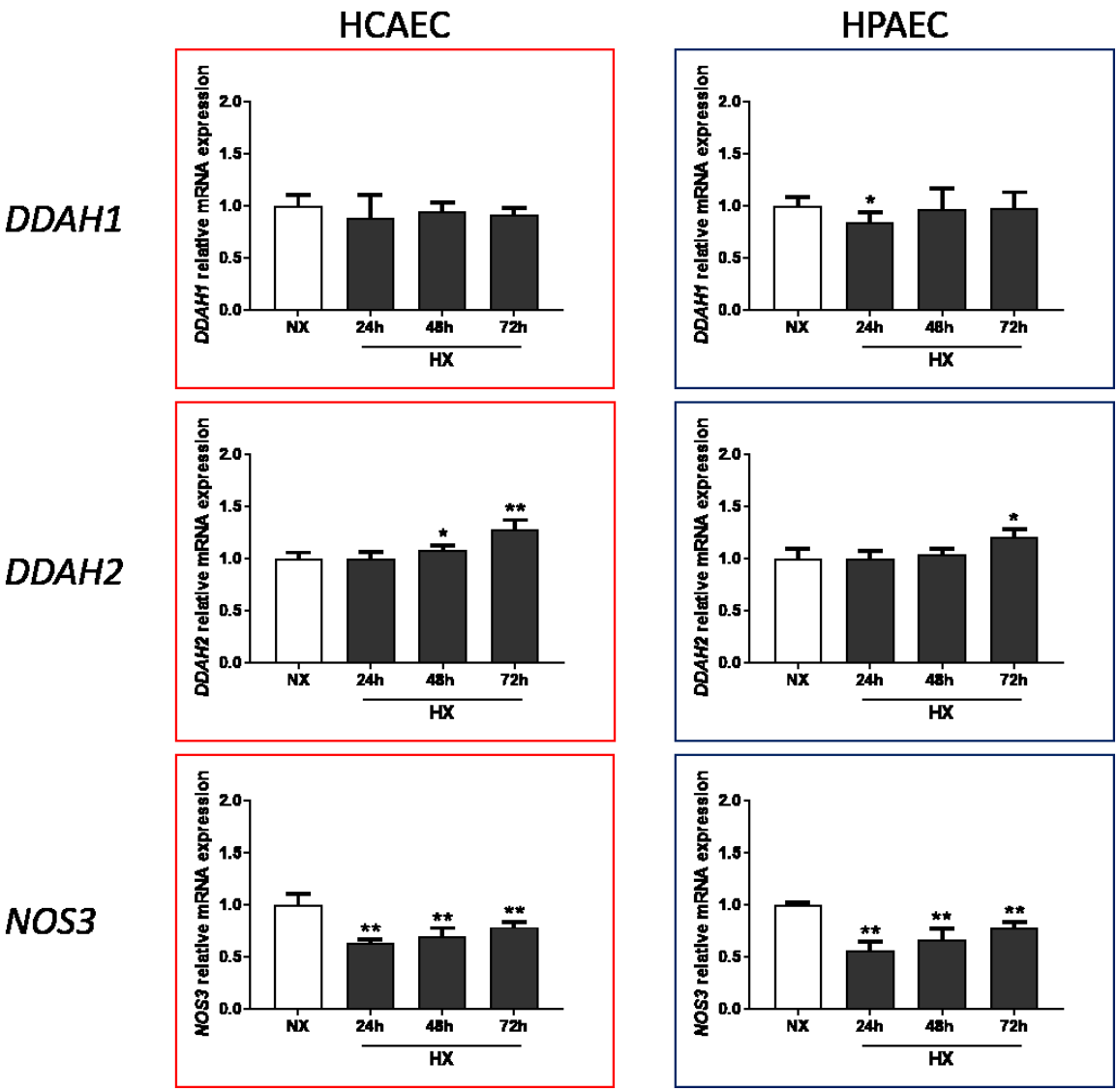

Figure 11: Comparison of relative mRNA expression of genes of the ADMA-NO pathway in HPAEC and HCAEC after exposure to NX and 24 h, 48 h and 72 h HX. HPAEC and HCAEC were incubated in NX and 24 h, 48 h and 72 h of HX. Relative mRNA expression was assessed using qRT-PCR and normalized to *RPL13A*. Expression in control (NX) was set to 1. Bars represent mean ± SD. N=5, *= p≤0.1; **= p≤0.01, Non-parametric Mann-Whitney U-test.

The expression of *DDAH1* in HCAEC was not affected by HX, whereas the expression in HPAEC decreased after 24h HX (0.844 ± 0.099). The mRNA expression of *DDAH2* was increased in both cell lines (1.211 ± 0.069 and 1.287 ± 0.084 in HPAEC and HCAEC, respectively) after 72h HX, while *NOS3* mRNA expression decreased after exposure to HX (0.567 ± 0.0786 and 0.639 ± 0.031 in HPAEC and HCAEC after 24h HX, respectively).

The expression levels of *PRMT*s (*Figure 12* for HCAEC, *Figure 13* for HPAEC), did not show any differences in hypoxic regulation between the two cell lines, neither did the expression levels of *ARG1*, *ARG2, END1* nor *HIF1A* (Figure 14 for HCAEC, *Figure 15* for HPAEC).

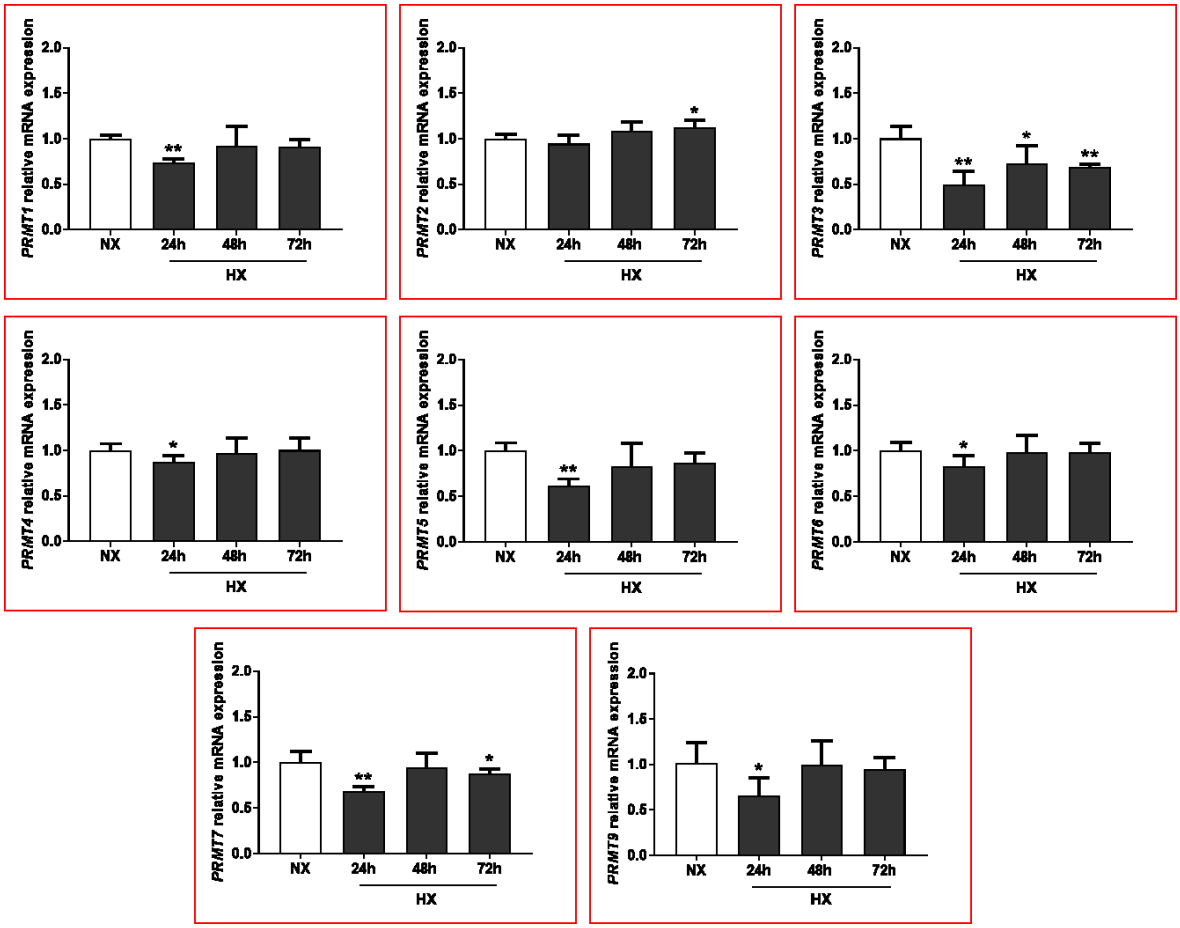

Figure 12: Relative PRMT mRNA expression in HCAEC after exposure to NX and 24 h, 48 h and 72 h HX. HCAEC were incubated in NX and 24 h, 48 h and 72 h of HX. Relative mRNA expression was assessed using qRT-PCR and normalized to *RPL13A*. Expression in control (NX) was set to 1. Bars represent mean ± SD. N=5, *= p≤0.1; **= p≤0.01, Non-parametric Mann-Whitney U-test.

In HCAEC, *PRMT1*, *PRMT4*, *PRMT5*, *PRMT6* and *PRMT9* expression decreased after 24 h HX (0.735 ± 0.043, 0.879 ± 0.064, 0.621 ± 0.072, 0.829 ± 0.121 and 0.687 ± 0.051, respectively) and increased after longer exposure to HX to approximately NX expression level. As also seen in HPAEC, *PRMT2* was the only *PRMT* whose relative mRNA expression increased after 72 h HX (1.130 ± 0.073). *PRMT3* and *PRMT7* expression decreased after exposure to HX (0.500 ± 0.141 and 0.687 ± 0.051 after 24 h HX), but interestingly *PRMT7* expression did not change after 48 h HX compared to NX expression.

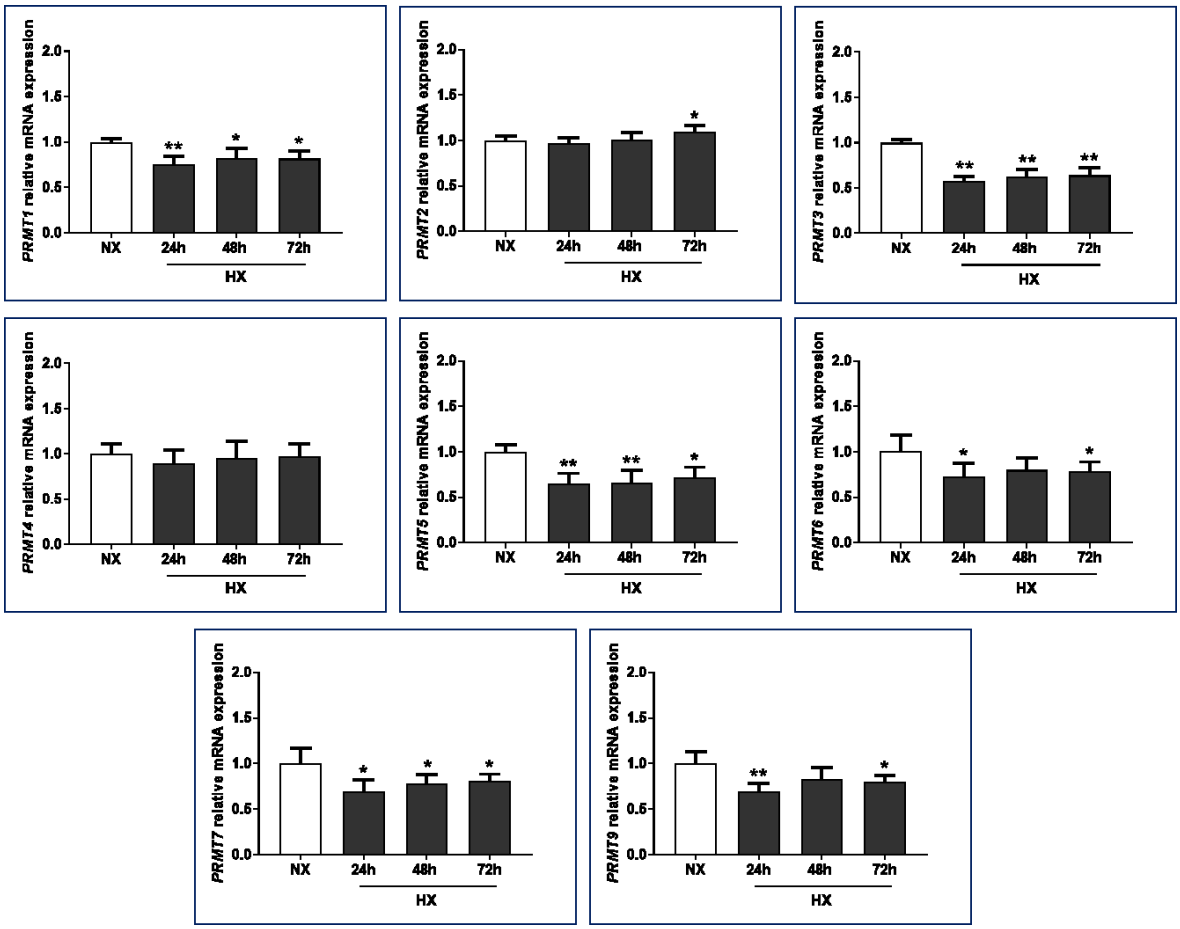

Figure 13: Relative PRMT mRNA expression in HPAEC after exposure to NX and 24 h, 48 h and 72 h HX. HPAEC were incubated in NX and 24 h, 48 h and 72 h of HX. Relative mRNA expression was assessed using qRT-PCR and normalized to *RPL13A*. Expression in control (NX) was set to 1. Bars represent mean ± SD. N=5, *= p≤0.1; **= p≤0.01, Non-parametric Mann-Whitney U-test.

In HPAEC, *PRMT1*, *PRMT3*, *PRMT5* and *PRMT7* expression decreased after exposure to HX (0.760 ± 0.081, 0.578 ± 0.053, 0.650 ± 0.114, 0.692 ± 0.133 after 24 h exposure to HX, respectively). The duration of HX did not affect the level of decrease of these *PRMTs*, except for *PRMT1* and *PRMT5*, whose expression was less decreased after 72 h HX compared to 24 h HX. *PRMT2* was the only *PRMT* whose relative mRNA expression increased after 72 h HX (1.095 ± 0.067). *PRMT6* and *PRMT9* mRNA expression decreased after 24 h and 72 h HX, an effect that could not be observed after 48 h HX. *PRMT4* expression was not affected by exposure to HX, which appeared to be the only difference compared to *PRMT* expression in HCAEC, where HX lead to a decrease in *PRMT4* expression after 24 h.

In HCAEC, *ARG2* expression decreased significantly (0.649 ± 0.045 after 24 h of HX, *Figure 14*), whereas *END1* expression was not affected by exposure to HX. There was no detectable *ARG1* and *PRMT8* expression (data not shown). *HIF1A* expression decreased after exposure to 24 h HX (0.609 ± 0.217 compared to NX) but increased to NX level after longer lasting hypoxia.

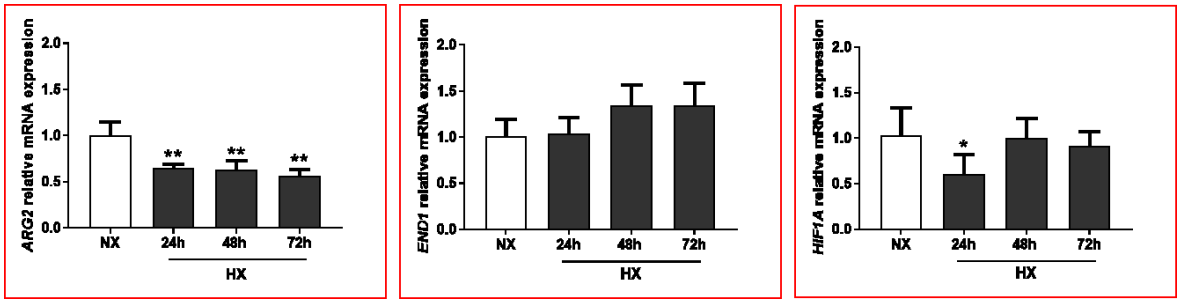

Figure 14: Relative mRNA expression of ARG2, END1 and HIF1A in HCAEC. HCAEC were incubated in NX and 24 h, 48 h and 72 h of HX. Relative mRNA expression was assessed using qRT-PCR and normalized to *RPL13A*. Expression in control (NX) was set to 1. Bars represent mean ± SD. N=5, *= p≤0.1; **= p≤0.01, Non-parametric Mann-Whitney U-test.

After exposure to hypoxia, *ARG2* expression in HPAEC decreased significantly (*Figure 15*, 0.642 ± 0.162, 0.600 ± 0.068, 0.592 ± 0.0745 after 24 h, 48 h and 72 h of hypoxia, respectively) whereas *END1* expression was not affected. There was no detectable *ARG1* and *PRMT8* expression (data not shown). The same tendencies were also observed in HCAEC. The regulation of *HIF1A* on the other hand differed between the two primary endothelial cell lines; it was significantly decreased after 24 h, 48 h and 72 h of HX in HPAEC (0.638 ± 0.091, 0.746 ± 0.099, 0.773 ± 0.041, after 24 h, 48 h and 72 h of HX, respectively), whereas its expression in HCAEC was only significantly decreased after 24 h of HX.

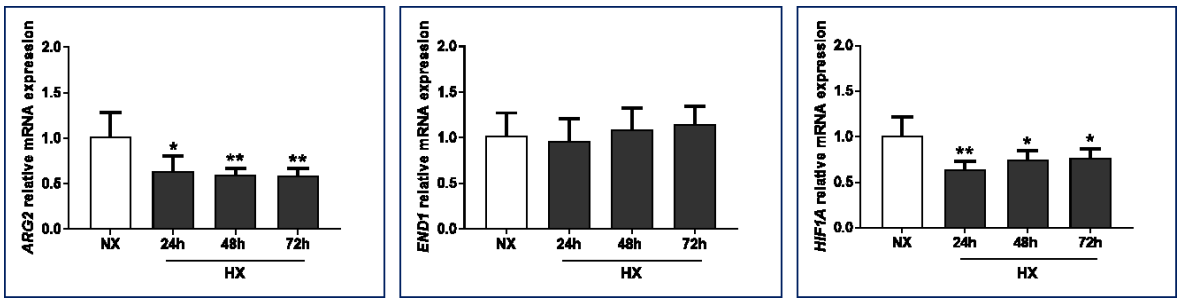

Figure 15: Relative mRNA expression of ARG2, END1 and HIF1A in HPAEC. HPAEC were incubated in NX and 24 h, 48 h and 72 h of HX. Relative mRNA expression was assessed using qRT-PCR and normalized to *RPL13A*. Expression in control (NX) was set to 1. Bars represent mean ± SD. N=5, *= p≤0.1; **= p≤0.01, Non-parametric Mann-Whitney U-test.

4.1.3 Protein expression in human coronary and pulmonary artery endothelial cells

Representative Western blots for DDAH1, DAH2 and NOS3 in HCAEC and HPAEC are shown in Figure 16. In DDAH1 and DDAH2 Western blots, the upper band (55 kDa) represented the TUBB control, the lower band the respective target protein. In NOS3 Western blots, the upper band (130 kDa) was NOS3 protein, the lower band the TUBB control. Ladders and sizes can be seen on the left lane of each blot. Blotting in a wet tank blotting chamber (as performed with HPAEC) resulted in more even and clearer bands.

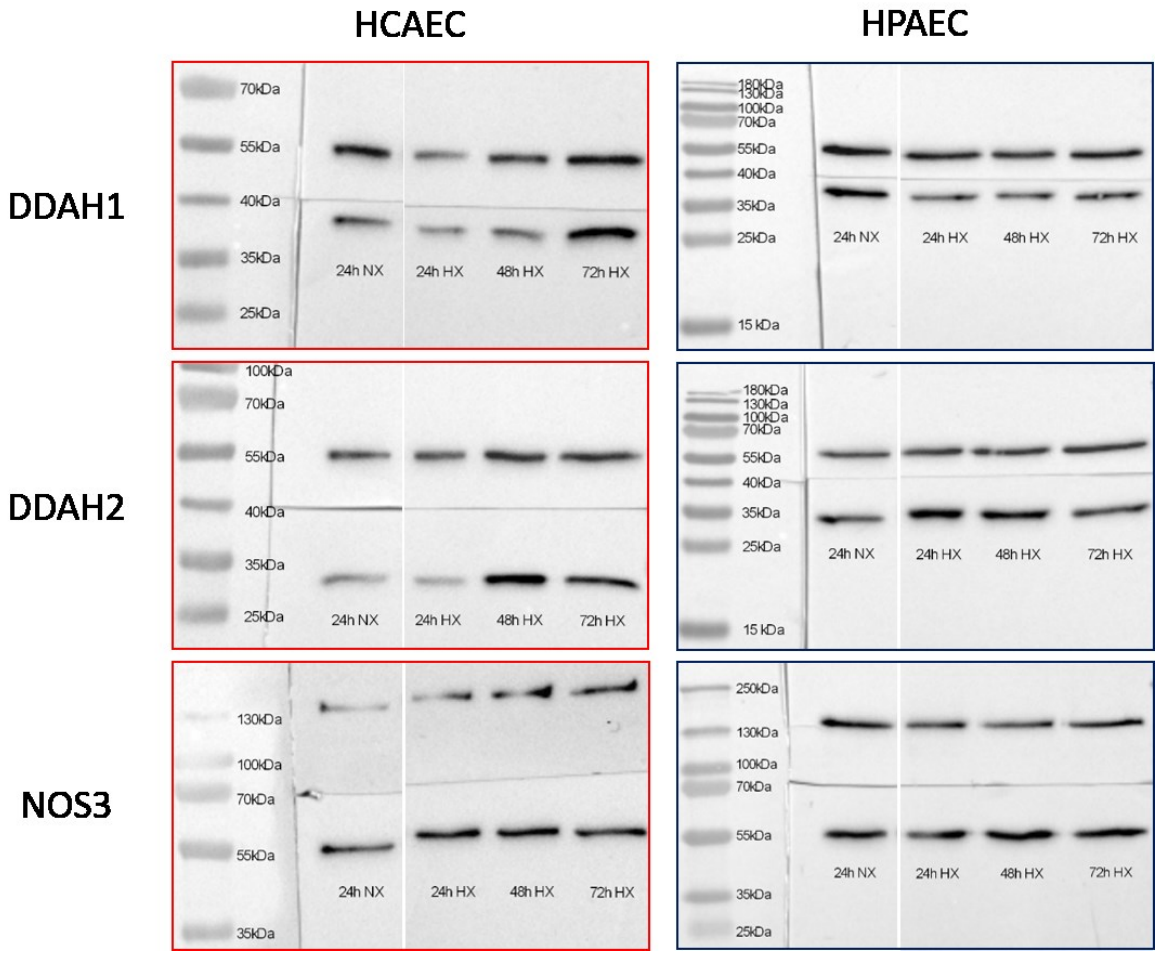

Figure 16: Representative Western Blots of DDAH1, DDAH2 and NOS3. HCAEC Western blots were performed using a semi-dry blotting chamber, HPAEC in a Wet Tank Blotting chamber. Left lane contains prestained ladder, in order to verify correct size of detected proteins. DDAH1 and DDAH2 Blots: upper band (ca. 55 kDa) represents TUBB as housekeeping control, lower band the respective target (37 kDa and 30 kDa for DDAH1 and DDAH2, respectively). For NOS3 Western blots, upper band represents the target protein, lower band the housekeeping control TUBB. A colorimetric picture showing the ladder was merged with chemi-luminescent pictures of the targets.

Quantification of protein expression was performed as described in *3.13*. As seen in *Figure 17*, HX did not alter protein expression in HPAEC compared to NX. Neither NOS3 nor DDAH1 or DDAH2 protein expression were affected by hypoxia. In HCAEC on the other hand, NOS3 expression was significantly increased after exposure to 48 h and 72 h of HX (2.246 ± 1.346 and 1.792 ± 0.748). DDAH1 and DDAH2 protein expression were not influenced by exposure to HX, as also seen in HPAEC.

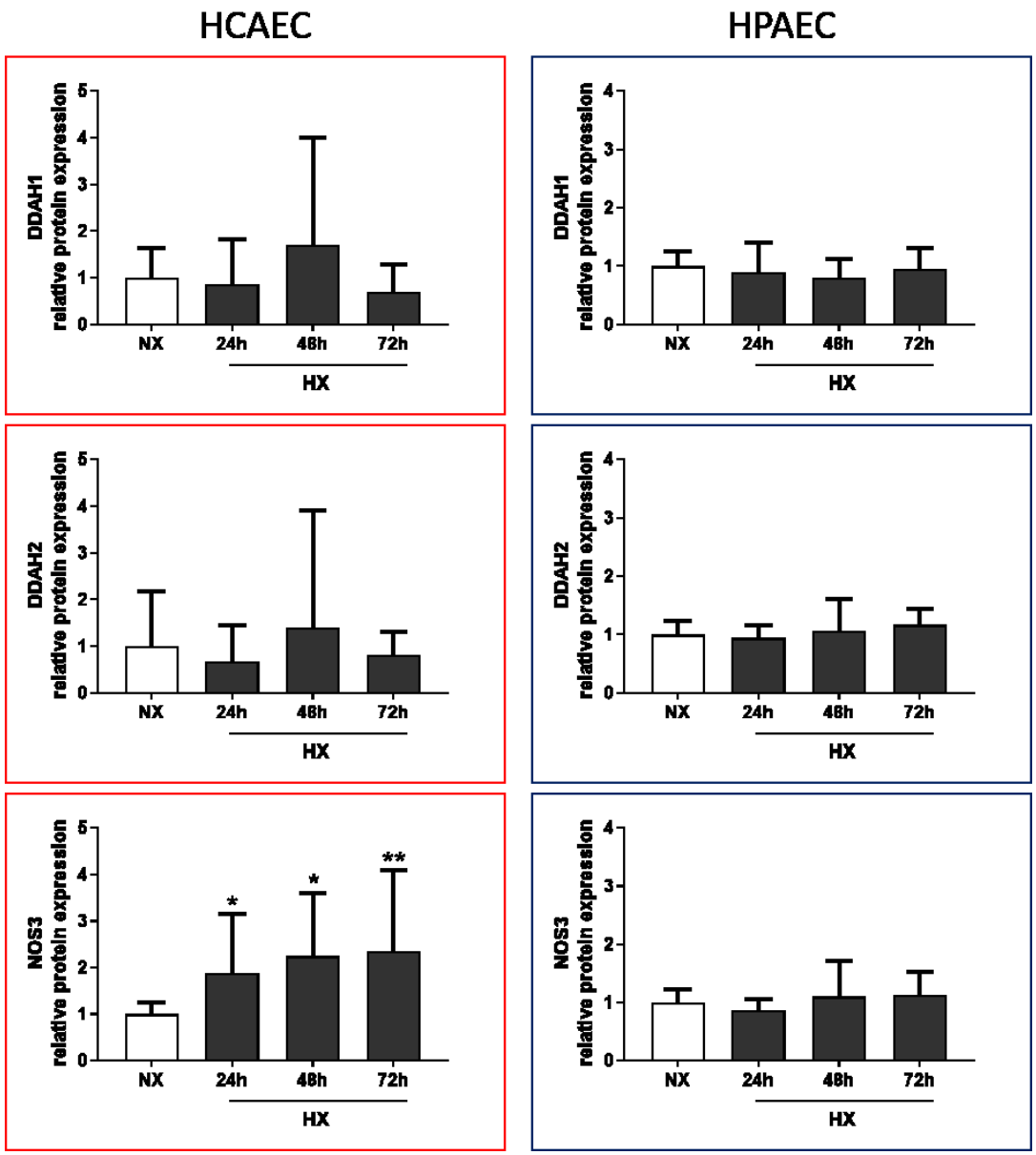

Figure 17: Relative protein expression in HCAEC and HPAEC in HX compared to NX. SDS-PAGE followed by Western blot were performed for a densiometric quantification of the respective proteins. Volume intensities of target proteins of each sample was normalized to volume intensities of its respective TUBB control. NX protein expression was set to 1. Bars represent mean ± SD. N=6, *= p≤0.1; **= p≤0.01, Non-parametric Mann-Whitney U-test.

4.1.4 Metabolite profile of human coronary and pulmonary artery endothelial cells

ADMA and SDMA concentrations were analysed using LC-MS/MS in order to gain insight into NOS3 and DDAH1 and DDAH2 protein activity. As shown in *Figure 18* the amount of SDMA in HCAEC cells increased after exposure to 48 h and 72 h of hypoxia compared to NX (0.015 ± 0.002 µM/g protein and 0.014 ± 0.002 µM/g protein after 48 h and 72 h HX, compared to 0.009 ± 0.002 µM/g protein after exposure to NX). ADMA concentration in HCAEC was not affected by exposure to HX. In HPAEC cell pellet as well as in supernatant medium, HX did not effect SDMA nor ADMA concentration.

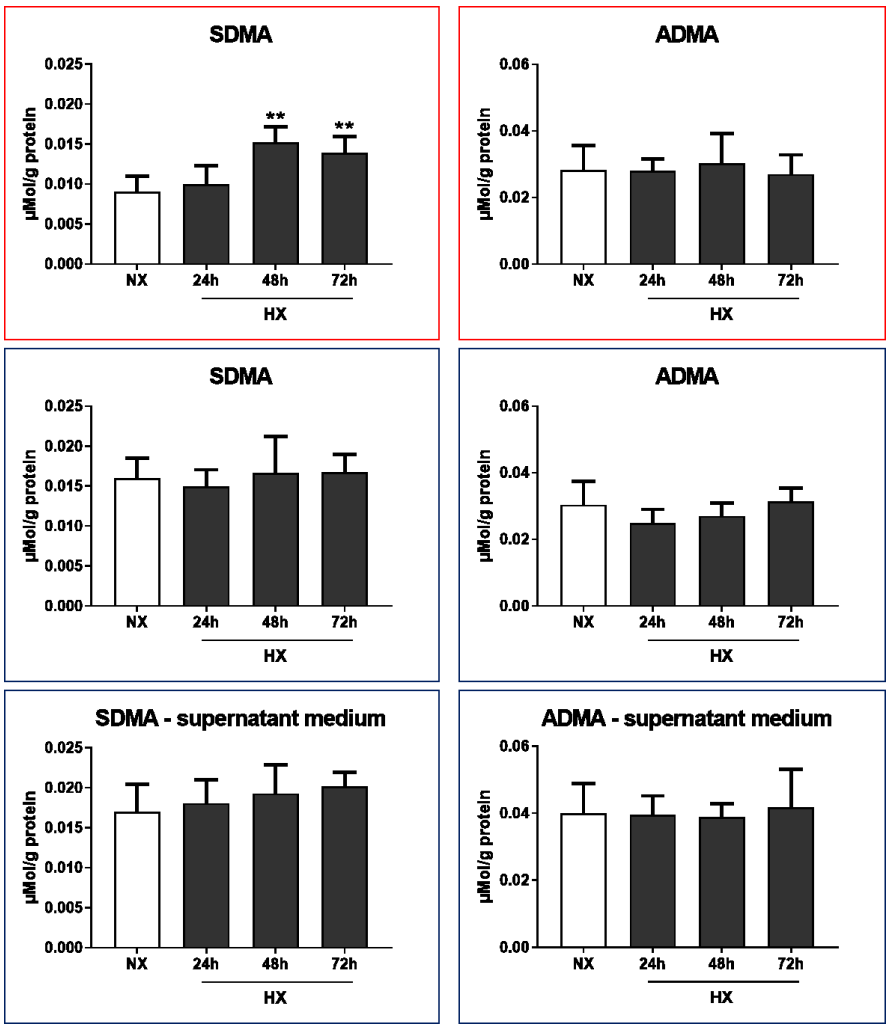

Figure 18: Metabolite profile in HCAEC and HPAEC cells after exposure to NX and HX. Medium was collected, cells were harvested and lysed, and protein concentration was measured. SDMA and ADMA concentrations per g protein were measured using LC-MS/MS. Bars represent mean ± SD. N=6, supernatant medium N=5, *= p≤0.1; **= p≤0.01, Non-parametric Mann-Whitney U-test.

4.1.5 mRNA expression in A549 alveolar epithelial cells

The relative mRNA expression levels for *VEGFA, NOS2, DDAH1* and *DDAH2* after incubation in HX and NX are shown in *Figure 19*. After exposure to 48 h and 72 h HX, *VEGFA* mRNA expression increased significantly (1.916 ± 0.164 and 1.941 ± 0.127, respectively), as also observed in endothelial cells. In A549, no *NOS3* activity was detected (data not shown), but *NOS2* mRNA decreased after exposure to HX (0.403 ± 0.061, 0.561 ± 0.057 and 0.051 ± 0.016 after 24 h, 48 h and 72 h HX, respectively). *DDAH1* expression decreased after 24 h of HX (0.523 ± 0.191), as it was also observed in HPAEC. The expression level after prolonged HX (42h and 72h) increased to NX level. *DDAH2* mRNA expression did not show any differences compared to NX expression after exposure to HX, in contrast to its significantly increased expression in endothelial cells after 72 h HX.

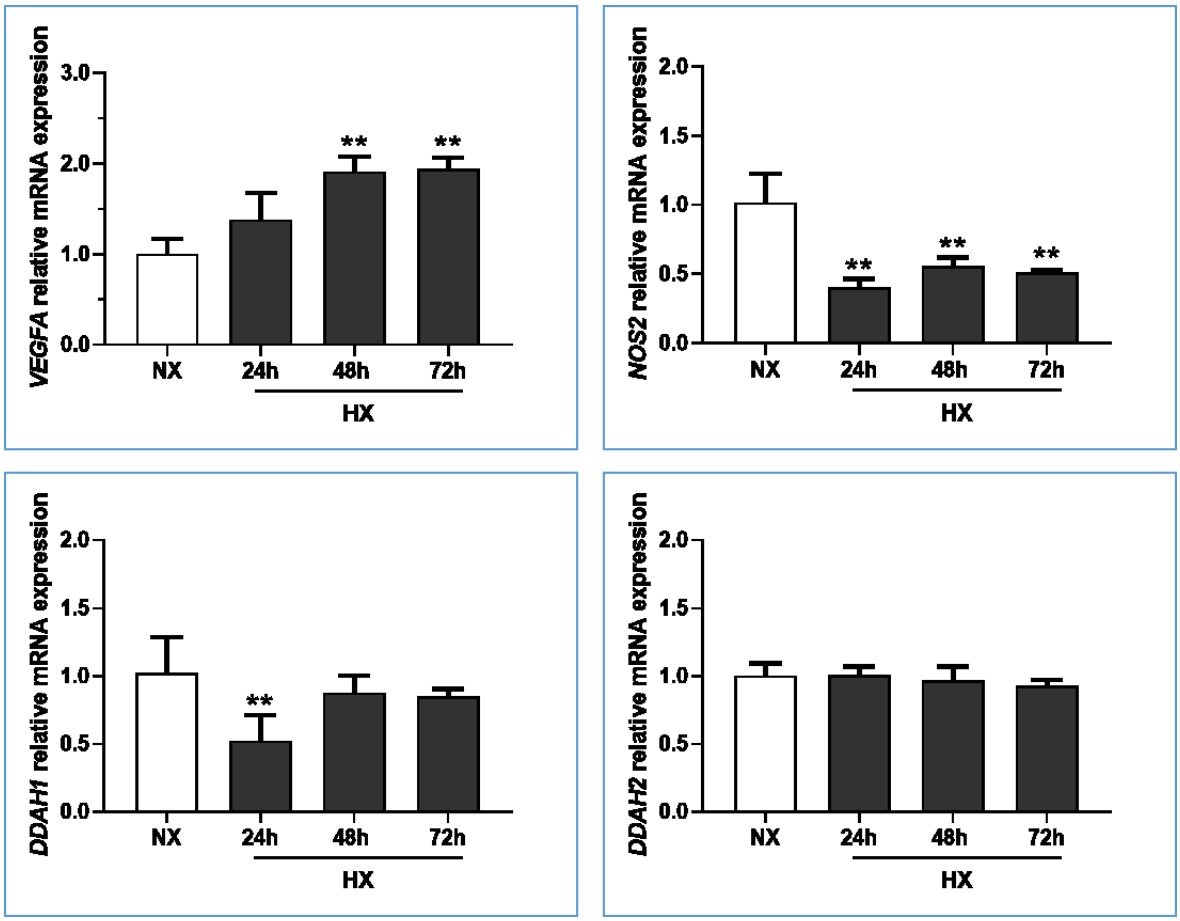

Figure 19: Relative mRNA expression of genes of the ADMA-NO pathway. A549 were incubated in NX and 24 h, 48 h and 72 h of HX. Relative mRNA expression was assessed using qRT-PCR and normalised to RPL13A. Expression in control (NX) was set to 1. Bars represent mean ± SD. N=5, *= p≤0.1; **= p≤0.01, Non-parametric Mann-Whitney U-test.

In A549, *PRMT1*, *PRMT4*, *PRMT5* and *PRMT7* expression decreased after exposure to HX (*Figure 20*, 0.551 ± 0.033, 0.557 ± 0.035, 0.515 ± 0.033, 0.527 ± 0.046 after 24 h exposure to HX, respectively). *PRMT2* and *PRMT9* decreased after 24 h of HX but increased to NX level after longer duration of HX

(0.788 ± 0.029, 0.606 ± 0.165, respectively). Interestingly, *PRMT2* mRNA expression was increased after 72 h HX in endothelial cells in contrast to a decreased mRNA expression after 24 h HX in epithelial A549. *PRMT8* expression was not detected, as also seen in endothelial cells. On the contrary to endothelial cells, *PRMT6 and END1* expression were not detected in A549 (data not shown). The expression of *HIF1A* was significantly decreased after exposure to HX to 0.278 ± 0.102 after 24 h HX, 0.531 ± 0.157 after 48 h HX and 0.658 ± 0.079 after 72 h HX compared to NX, as also seen in HPAEC.

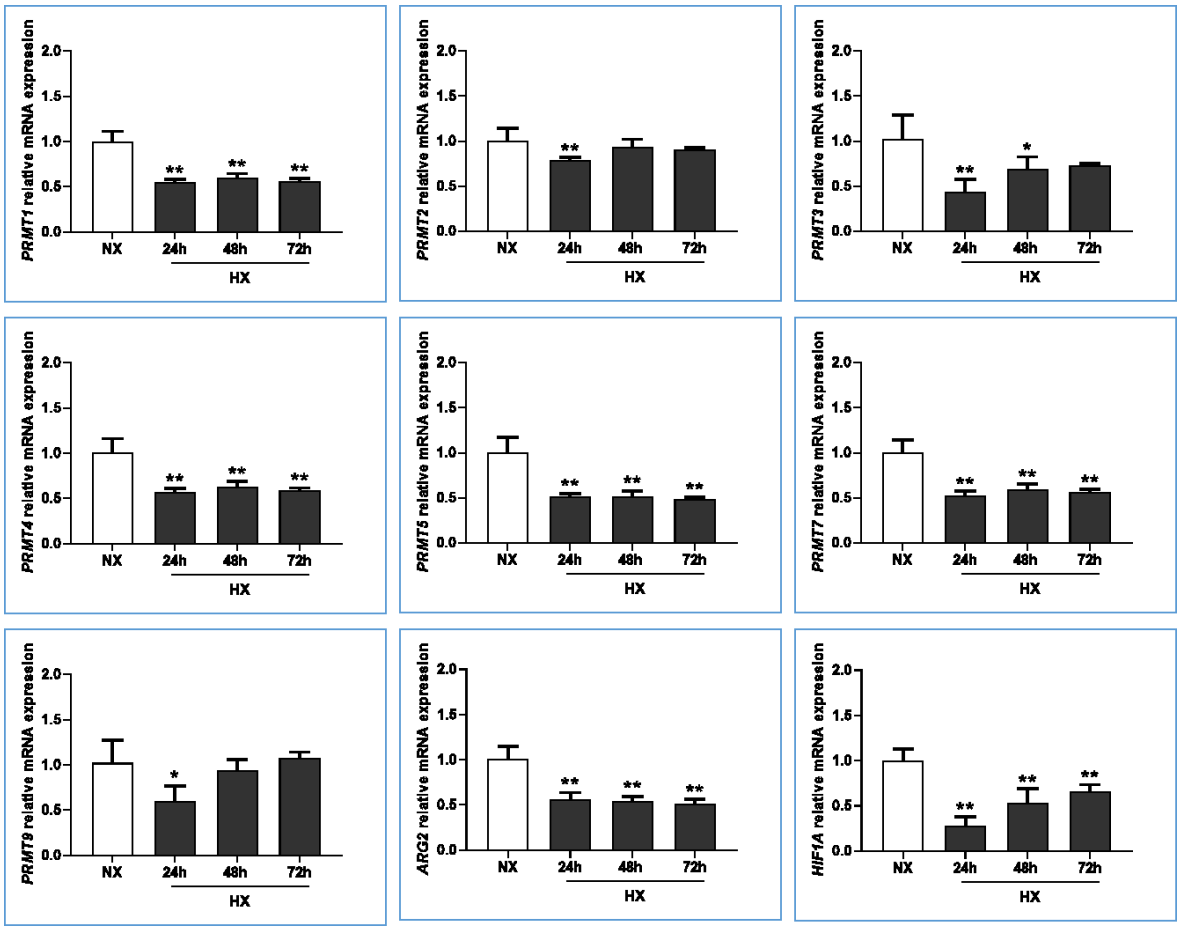

Figure 20: Relative PRMT, ARG2 and HIF1A mRNA expression in A549 after exposure to NX and 24 h, 48 h and 72 h HX. A549 were incubated in NX and 24 h, 48 h and 72 h of HX. Relative mRNA expression was assessed using qRT-PCR and normalised to RPL13A. Expression in control (NX) was set to 1. Bars represent mean ± SD. N=5, *= p≤0.1; **= p≤0.01, Non-parametric Mann-Whitney U-test.

4.1.6 Protein expression in A549 alveolar epithelial cells

Representative Western blots for DDAH1, DDAH2, HIF1A and HIF2A of A549 incubated in HX and NX are shown in *Figure 21*.

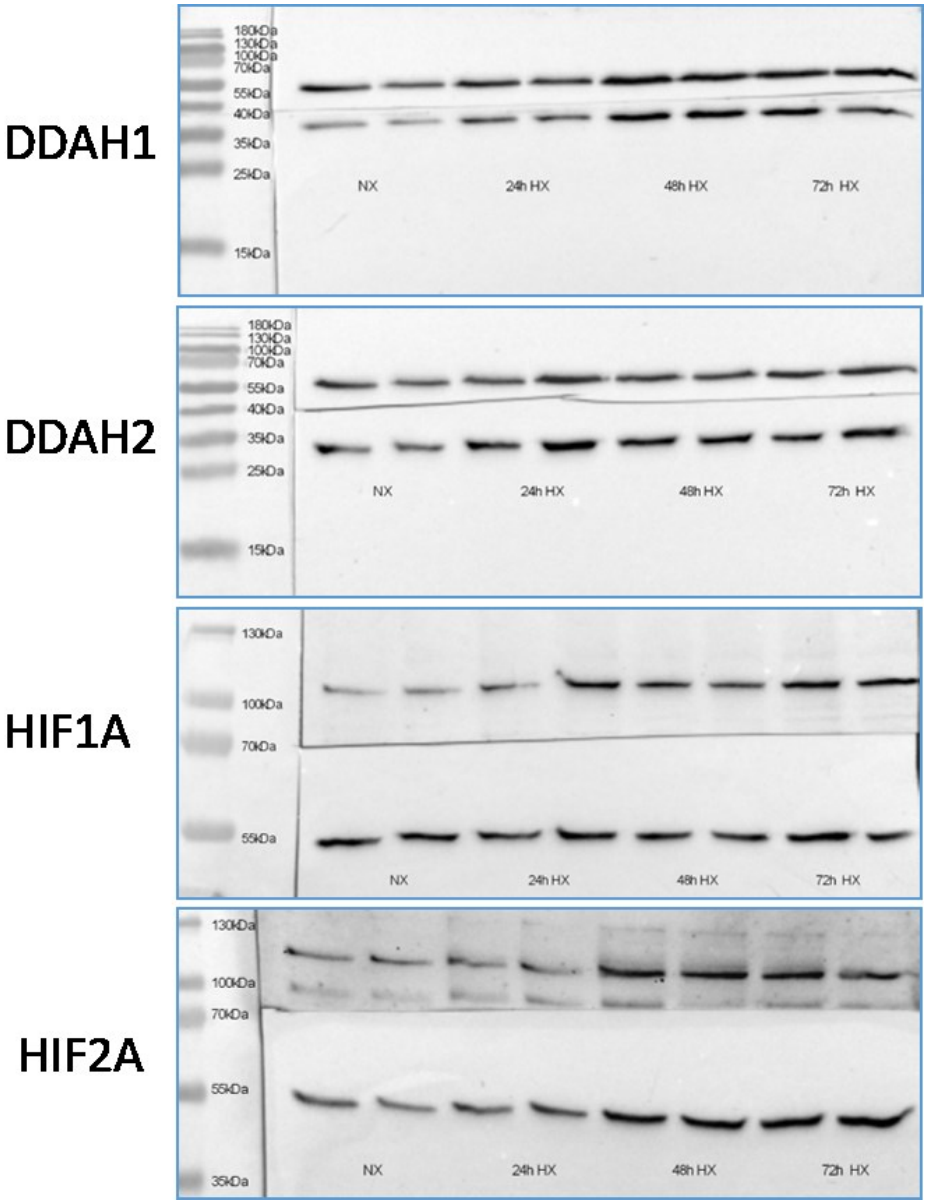

Figure 21: Representative Western Blots of DDAH1, DDAH, HIF1A and HIF2A in A549. Western blots were performed in a Wet Tank Blotting chamber. Left lane contains prestained ladder, in order to verify correct size of detected proteins. DDAH1 and DDAH2 Blots: upper band (ca. 55 kDa) represents TUBB as housekeeping control, lower band the respective target (37 kDa and 30 kDa for DDAH1 and DDAH2, respectively). In HIF1A and HIF2A Western blots, upper band represents the target protein (116kDa), lower band the housekeeping control TUBB. A colorimetric picture showing the ladder was merged with chemi-luminescent pictures of the targets.

In DDAH1 and DDAH2 Western blots, the upper band (55 kDa) represented the TUBB control, the lower band the respective target protein. In HIF and HIF Western blots, the upper band was HIF1A or HIF2A protein (116 kDa and 120 kDa, respectively), the lower band the TUBB control. Ladders and sizes can be seen on the left lane of each blot.

The results of the quantification of protein expression can be seen in *Figure 22*. HX did not affect DDAH1 protein expression but led to an increase in DDAH2 protein expression after 48 h and 72 h of HX (1.679 ± 0.345 and 1.577 ± 0.309, respectively). This is notably, as there was no difference in DDAH2 expression in endothelial cells. HIF1A protein expression was also increased by hypoxia and further increased with ongoing hypoxia (1.553 ± 0.350, 1.767 ± 0.208, 2.039 ± 0.325 after 24 h, 48 h and 72 h of HX, respectively). Interestingly, HIF2A protein expression was no affected by HX.

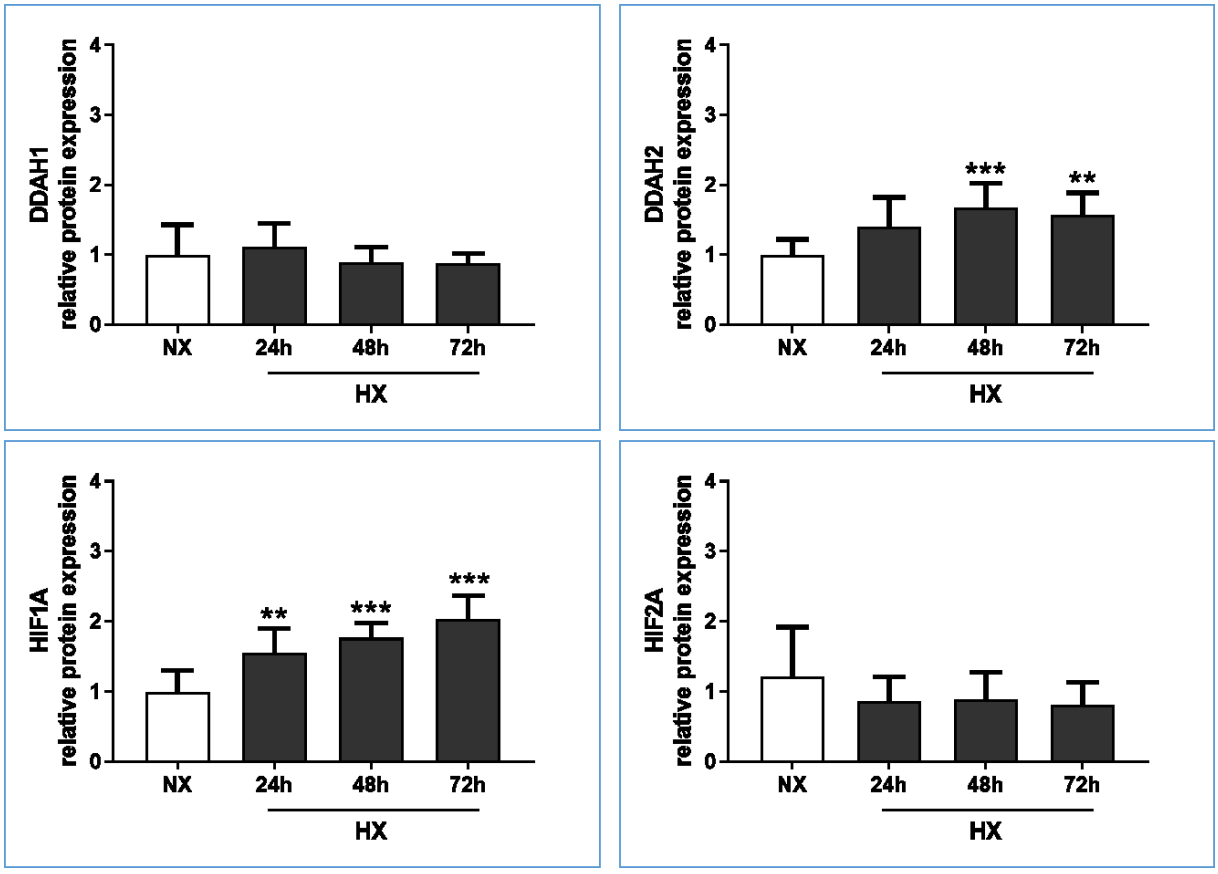

Figure 22: Relative protein expression in A549 in HX compared to NX. SDS-PAGE followed by Western blot were performed for a densiometric quantification of the respective proteins. Volume intensities of target proteins of each sample was normalized to volume intensities of its respective TUBB control. NX protein expression was set to 1. Bars represent mean ± SD. N=8, **= p≤0.01, ***= p≤0.001, Non-parametric Mann-Whitney U-test.

4.1.7 Metabolite profile of A549 alveolar epithelial cells/ADMA release

The results of the metabolite analysis in cells and supernatant medium of A549 incubated in NX and HX can be seen in *Figure 23*. The amount of SDMA in A549 cells decreased after exposure to 72 h of hypoxia (0.003 ± 0.001 µM/g protein compared to 0.004 ± 0.001 µM/g protein after incubation in NX) but increased in supernatant medium (0.051 ± 0.013 µM/g protein after 48 h HX and 0.042 ± 0.020 µM/g protein after 72 h HX compared to 0.021 ± 0.011 µM/g protein after exposure to NX). ADMA concentration in A549 cells was not affected by HX, but its concentration in the supernatant medium increased after exposure to HX (0.083 ± 0.021 µM/g protein after 48 h HX and 0.073 ± 0.030 µM/g protein after 72 h HX), like seen for SDMA concentration. Overall, the ADMA and SDMA concentration in supernatant medium was higher than in cell pellets.

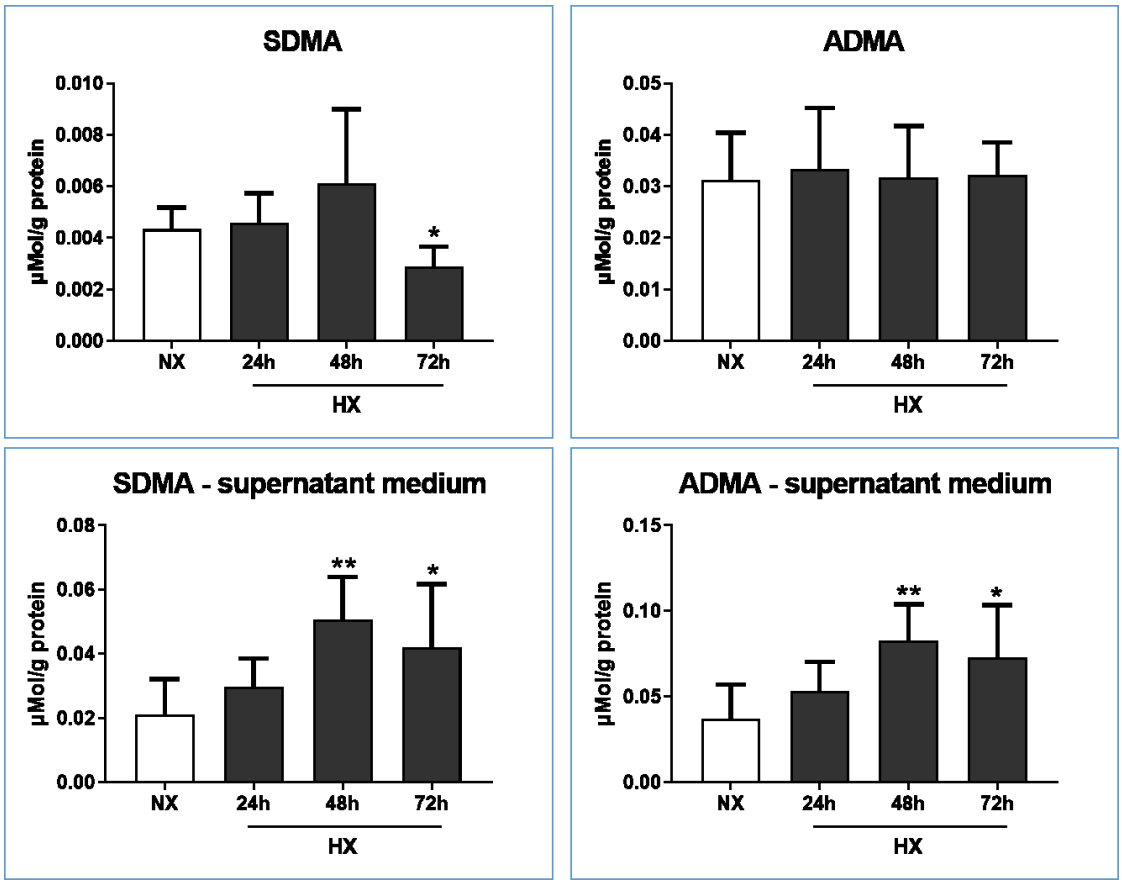

Figure 23: Metabolite profile of epithelial A549 cells after exposure to NX and HX. Medium was collected, cells were harvested and lysed, and protein concentration was measured. SDMA and ADMA concentrations per g protein were measured using LC-MS/MS. Bars represent mean ± SD. N=6, *= p≤0.1; **= p≤0.01, Non-parametric Mann-Whitney U-test.

4.2 Pharmacological inhibition and stabilisation of HIF

4.2.1 Testing of different concentrations of HIF inhibitors and HIF stabiliser

The cell densities of EA.hy926 incubated with different amounts of the HIF inhibitors and the HIF stabiliser as well as cell densities for NX control, HX control and DMSO control are shown in *Table 26*.

Table 26: Tested concentrations of compounds used in EA.hy926 and resulting confluence. EA.hy926 cells were incubated in NX or HX with or without (controls) the respective compounds for 72 h. Confluence was monitored microscopically every 24 h. n=2 dishes per condition were tested.

Compound	Tested concentrations	Confluence after 24 h	Confluence after 48 h	Confluence after 72 h
PT2399	0.2 µM	40 %	70 %	>90 %
	0.02 µM	40 %	80 %	>90 %
	2 µM	40 %	70 %	>90 %
	0.1 µM	40 %	70 %	>90 %
	0.3 µM	40 %	70 %	>90 %
KC7FC	20 µM	10 %	10 %	<10 %
	2 µM	40 %	60 %	>90 %
	100 µM	0	0	0
	10 µM	40 %	60 %	>90 %
	30 µM	0	0	0
DMOG	1 mM	30 %	50 %	60-70 %
	0.1 mM	40 %	70 %	>90 %
	0.5 mM	40 %	70 %	80 %
	1.5 mM	30 %	40 %	60 %
Controls	NX	40 %	70 %	>90 %
	DMSO	40 %	70 %	>90 %
	HX	40 %	60 %	90 %

Incubation of EA.hy926 with any tested concentration of PT2399 did not affect cell growth. Incubation with KC7F2 in concentrations higher than 10 µM led to cell death, whereas incubation with DMOG in concentrations higher as 0.5 mM led to decreased cell growth. Some of the tested conditions led to a morphological change, as shown in *Figure 24*. The incubation with 20 µM KC7F2 for example led to a roundness of cells and cell death. The endothelial cells did not build their typical

cell protrusions. The incubation with 1.5 mM DMOG on the other hand led to a decreased cell growth. Incubation with 10 mM DMOG was not possible, as DMSO concentration would have been too high due to the maximal concentration of 200 mM DMOG in DMSO (5 % final concentration of DMSO).

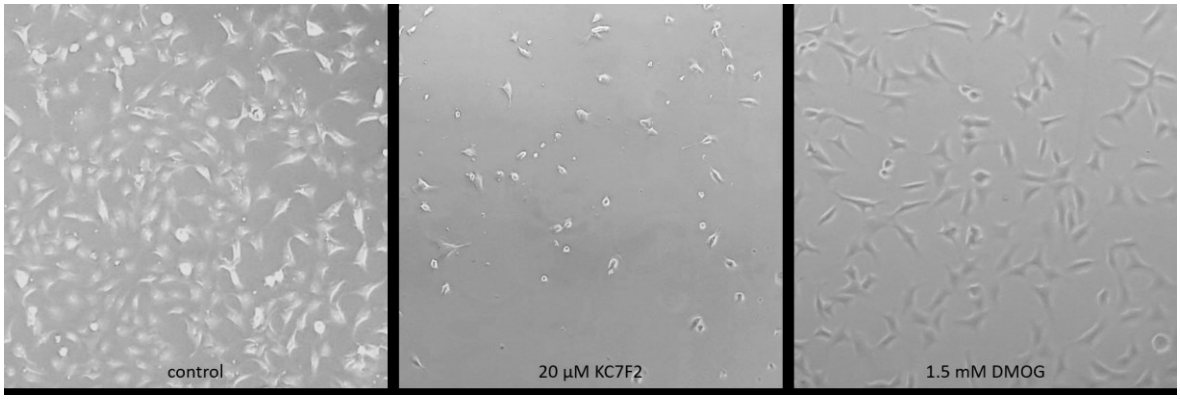

Figure 24: Incubation of EA.hy926 cells with KC7F2 and DMOG compared to incubation without supplement. EA.hy926 cells were incubated in NX (control and DMOG) or HX (KC7F2) for 72 h. Pictures were taken after 48 h incubation.

The cell confluence of HCAEC incubated with adjusted amounts of the HIF inhibitors and the HIF stabiliser as well as cell densities for NX control, HX control and DMSO control are shown in *Table 27*.

Table 27: Tested concentrations in HCAEC and resulting confluence. HCAEC cells were incubated in NX or HX with or without (controls) the respective compounds for 72 h. Confluence was monitored microscopically every 24 h. n=2 samples per condition were tested.

Compound	Tested concentrations	Confluence after 24 h	Confluence after 48 h	Confluence after 72 h
PT2399	0.2 µM	30 %	60 %	90 %
	2 µM	30 %	60 %	90 %
	5 µM	30 %	60 %	80 %
	10 µM	30 %	50 %	80 %
KC7FC	2 µM	30 %	50 %	60-70 %
	5 µM	30 %	50 %	40 %
	10 µM	30 %	20 %	<10 %
	15 µM	20 %	20 %	0 %
DMOG	0.1 mM	30 %	60 %	80 %
	0.5 mM	30 %	50 %	50-60 %
	1 mM	30 %	50 %	50 %
Controls	NX	30 %	50 %	80 %
	DMSO	30 %	50 %	80 %
	HX	30 %	40 %	70 %

In HCAEC, incubation with PT2399 did not affect cell growth. When applied in higher concentrations than 2 µM, incubation with KC7F2 led to decreased cell growth or cell death and incubation with 0.5 mM or 1 mM DMOG resulted in decreased cell growth compared to cells incubated without compound.

Results of *VEGFA* qRT-PCR can be seen in *Figure 25,* however no test for statistical significance was performed as sample size in this pretest was limited (N=2). Incubation with 10 µM PT2399 resulted in the highest decrease of *VEGFA*-expression compared to HX. Incubation with KC7F2 also led to a reduced *VEGFA* mRNA-expression compared to HX, but incubation with 5 µM KC7F2 resulted in poor RNA concentrations which is why only one sample could be used for DNA synthesis. 0.5 mM and 1 mM of the HIF stabiliser DMOG led to an increased *VEGFA* expression compared to NX.

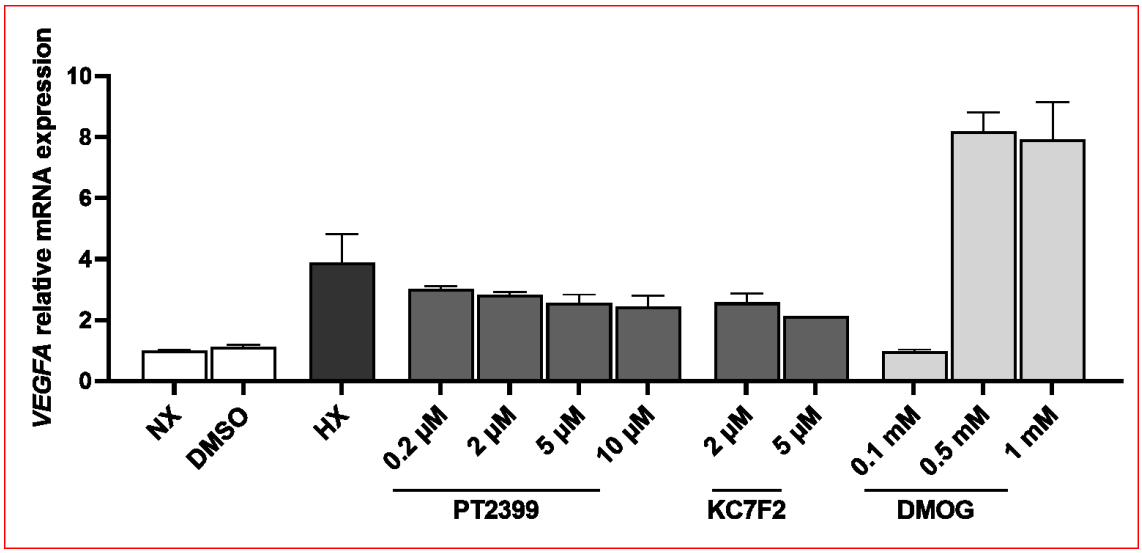

Figure 25: Relative VEGFA mRNA expression in HCAEC incubated with HIF inhibitors and a HIF stabiliser. HCAEC were incubated in NX (NX control, DMSO control, DMOG) or HX (HX control, PT2399, KC7F2) for 72 h. RNA was isolated, relative *VEGFA* mRNA expression was assessed using qRT-PCR and normalized to *RPL13A* to evaluate the effects of HIF inhibitors and HIF stabiliser on HIF target gene expression. Expression in control (NX) was set to 1. Bars represent mean ± SD. Due to low sample size of N=2 no test for statistical significance was performed.

The cell densities of HPAEC incubated with adjusted amounts of the HIF inhibitors and the HIF stabiliser can be seen in *Table 28*.

Table 28: Tested concentrations in HPAEC and resulting confluence. HPAEC cells were incubated in NX or HX with or without (controls) the respective compounds for 72 h. Confluence was monitored microscopically every 24 h. n=2 dishes per condition were tested.

Compound	Tested concentrations	Confluence after 24 h	Confluence after 48 h	Confluence after 72 h
PT2933	2 µM	15 %	30 %	60 %
	5 µM	20 %	30 %	60 %
	10 µM	20 %	30 %	50 %
KC7FC	1 µM	20 %	30 %	60 %
	2 µM	15 %	30 %	50 %
	5 µM	15 %	20 %	20 %
DMOG	0.1 mM	20 %	30 %	50 %
	0.5 mM	20 %	30 %	50 %
	1 mM	20 %	30 %	50 %
Controls	NX	20 %	40 %	70 %
	DMSO	20 %	40 %	60 %
	HX	20 %	30 %	50 %

In HPAEC, an overall lower cell density was observed. Incubation with PT2399 did not affect cell growth. As also seen in HCAEC, concentration of 5 µM KC7F2 led to reduced cell growth, lower concentrations did not show inhibitory effects on cell growth. In contrast to HCAEC, incubation with 0.5 mM or 1 mM DMOG did not affect cell growth of HPAEC more than incubation with 0.1 mM DMOG. Cells incubated with any of the tested concentrations of DMOG showed a small decrease in confluence compared to NX control.

The results of the VEGFA qRT-PCR are shown in *Figure 26*. Interestingly incubation with 10 µM PT2399 did not show a higher decrease of *VEGFA* mRNA-expression compared to HX than 2 µM or 5 µM PT2399. In HCAEC on the contrary, the effect of PT2933 on *VEGFA* mRNA expression increased with higher concentrations of this compound. Incubation with KC7F2 also led to a reduced *VEGFA* mRNA-expression compared to HX, with the highest effect after incubation with 2 µM KC7F2. As seen in HCAEC, 0.5 mM and 1 mM of the HIF stabiliser DMOG led to an increased *VEGFA* expression compared to NX. All in all, the observed effects of the HIF inhibitors and the HIF stabiliser on *VEGFA* mRNA expression in HPAEC were lower than in HCAEC.

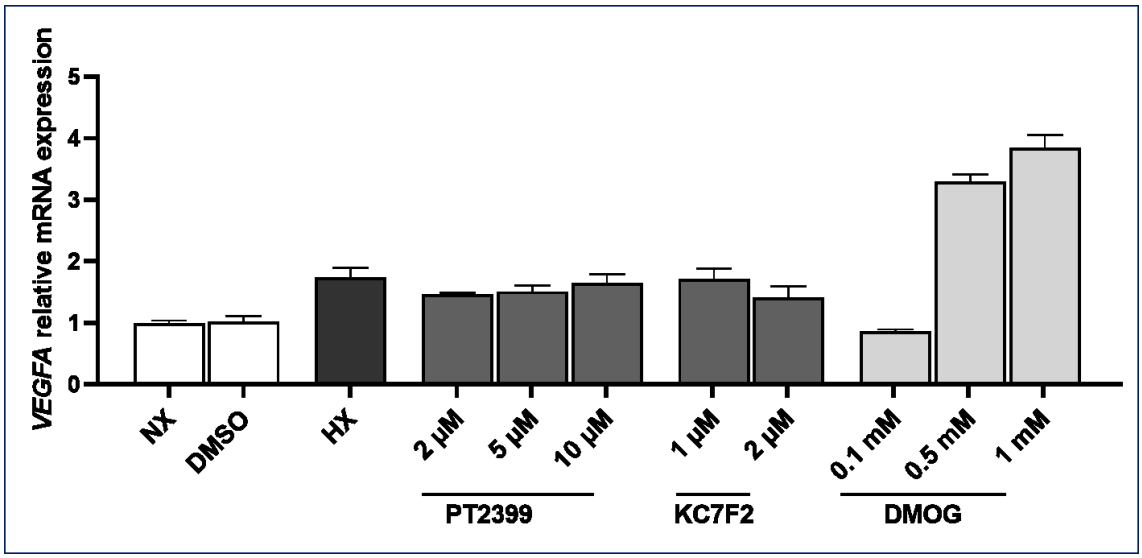

Figure 26: Relative VEGFA mRNA expression in HPAEC incubated with HIF inhibitors and a HIF stabiliser. HPAEC were incubated in NX (NX control, DMSO control, DMOG) or HX (HX control, PT2399, KC7F2) for 72 h. RNA was isolated, relative *VEGFA* mRNA expression was assessed using qRT-PCR and normalized to *RPL13A* to evaluate the effects of HIF inhibitors and HIF stabiliser on HIF target gene expression. Expression in control (NX) was set to 1. Bars represent mean ± SD. Due to low sample size of N=2 no test for statistical significance was performed.

After testing different concentrations of the compounds in primary endothelial cells, A549 epithelial cells were incubated with different concentrations as well. As seen in *Table 29* the cell confluence was not affected by any tested concentration of the different compounds.

Table 29: Tested concentrations in A549 and resulting confluence. A549 cells were incubated in NX or HX with or without (controls) the respective compounds for 72 h. Confluence was monitored microscopically every 24 h. n=2 dishes per condition were tested.

Compound	Tested concentrations	Confluence after 24 h	Confluence after 48 h	Confluence after 72 h
PT2933	2 µM	30 %	70 %	100 %
	10 µM	30 %	70 %	95 %
	20 µM	40 %	70 %	100 %
KC7FC	1 µM	40 %	80 %	100 %
	2 µM	30 %	70 %	95 %
	10 µM	40 %	70 %	95 %
DMOG	0.1 mM	35 %	70 %	100 %
	0.5 mM	40 %	70 %	90 %
	1 mM	40 %	60 %	80 %
Controls	HX	30 %	70 %	100 %
	HX DMSO	30 %	70 %	95 %
	NX	40 %	70 %	100 %
	NX DMSO	40 %	70 %	95 %

As also done for primary endothelial cells, a *VEGFA* qRT-PCR was performed (*Figure 27*). Notably, incubation with PT2399 further increased *VEGFA* mRNA-expression compared to HX and did not show the expected inhibitory effect. This effect increased with higher concentrations of PT2399. Incubation with KC7F2 did not show an effect on *VEGFA* mRNA-expression compared to HX. Incubation with 0.5 mM and 1 mM of the HIF stabiliser DMOG led to an increased *VEGFA* expression compared to NX, as also seen in endothelial cells, whereby the increase in *VEGFA* mRNA expression was lower compared to HCAEC and HPAEC.

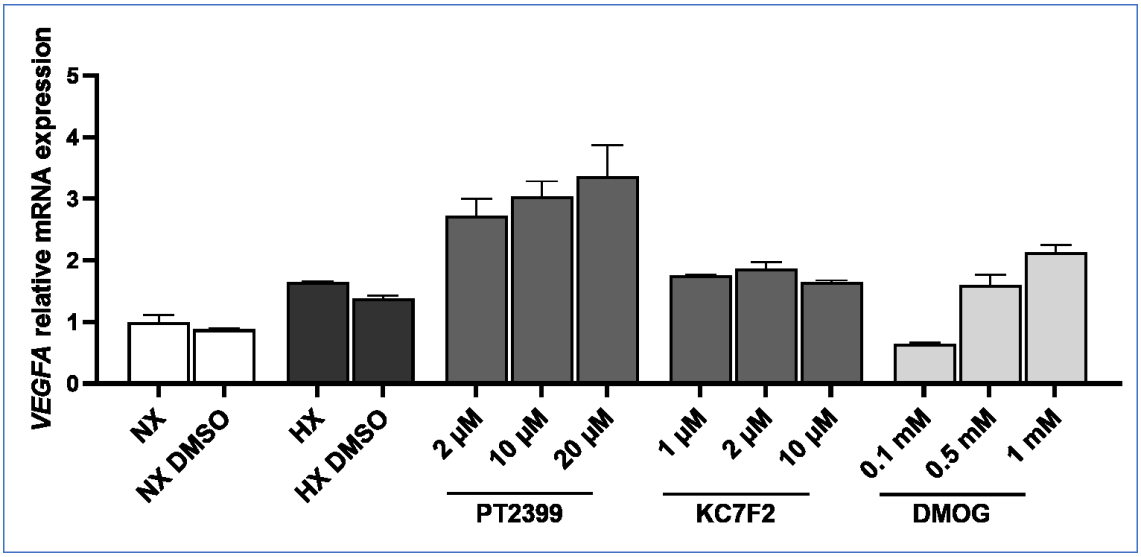

Figure 27: Relative VEGFA mRNA expression in A549 incubated with HIF inhibitors and a HIF stabiliser. A549 were incubated in NX (NX control, DMSO control, DMOG) or HX (HX control, PT2399, KC7F2) for 72 h. RNA was isolated, relative *VEGFA* mRNA expression was assessed using qRT-PCR and normalized to *RPL13A* to evaluate the effects of HIF inhibitors and HIF stabiliser on HIF target gene expression. Expression in control (NX) was set to 1. Bars represent mean ± SD. Due to low sample size of N=2 no test for statistical significance was performed.

4.2.2 Pharmacological HIF inhibition with optimized concentrations

HCAEC. The effect of the compounds used in optimal concentration on mRNA expression of *VEGFA*, *NOS3, DDAH1* and *DDAH2* in HCAEC after 72 h incubation are shown in *Figure 28*.

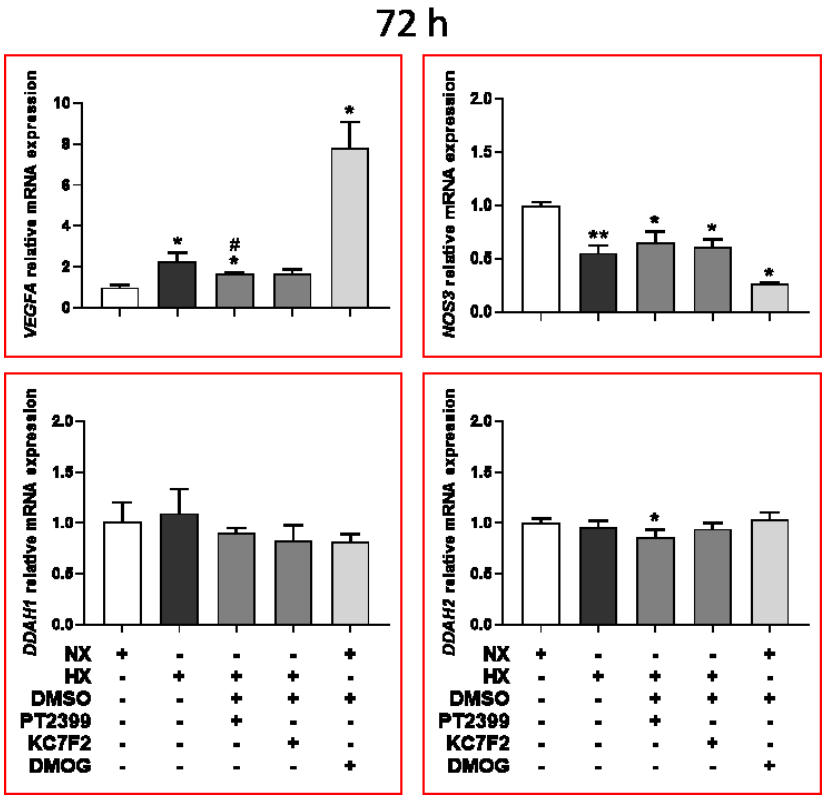

Figure 28: Relative mRNA expression in HCAEC after 72 h incubation with HIF inhibitors and HIF stabiliser. HCAEC were incubated for 72 h in NX (white bar), with HIF stabiliser DMOG in NX (light grey bar, right), in HX (black bar), with HIF1A inhibitor KC7F2 in HX or HIF2A inhibitor PT2399 in HX (both dark grey). Relative mRNA expression was assessed using qRT-PCR. Expression in control (NX) was set to 1. Bars represent mean ± SD. N=4, N=3 for 72 h incubation with KC7F2 after Grubb's test for outliers. *= p≤0.1 compared to NX control; **= p≤0.01 compared to NX control; #= p≤0.1 compared to HX control; ##*= p≤0.01 compared to HX control, Non-parametric Mann-Whitney U-test.

Cells incubated in HX and NX with DMSO control did not show a change in mRNA expression of any of the evaluated targets (data not shown). Notably, one sample of KC7F2 incubation was excluded after identification as outlier using Grubb's test for outliers resulting in a reduced sample size of N=3 for this experimental condition.

VEGFA expression increased more than 2-fold after exposure to HX (2.284 ± 0.408), incubation with HIF stabiliser DMOG led to an approximately 8-fold increase compared to NX control (7.815 ± 1.272). HCAEC incubated with PT2399 showed increased *VEGFA* mRNA expression compared to NX (1.703 ± 0.041), but reduced mRNA expression compared to HX control (p = 0.029). Incubation with KC7F2 did not alter *VEGFA* mRNA expression compared to NX or to HX control. *NOS3* expression was reduced after exposure to HX (0.555 ± 0.070), an effect that was also achieved

by incubation with HIF stabiliser DMOG (0.266 ± 0.012). Incubation with PT2399 and KC7F2 led to a minor decrease in *NOS3* mRNA expression compared to HX control, however this effect was not statistical significant. As previously observed, HX did not affect *DDAH1* mRNA expression in HCAEC. Neither HIF stabilisation in NX using DMOG nor HIF inhibition in HX by PT2399 and KC7F2 resulted in altered *DDAH1* mRNA expression compared to NX or HX control. Unlike previously observed, *DDAH2* mRNA expression was not affected by exposure to HX. Incubation with PT2399 led to a decrease in *DDAH2* expression compared to NX (0.863 ± 0.073). Incubation with KC7F2 and DMOG did not alter *DDAH2* mRNA expression in HCAEC.

HPAEC. As HPAEC showed regulation of *DDAH1* mRNA expression after 24 h HX and *DDAH2* mRNA expression after 72 h (*Figure 11*), cells were incubated for these two periods with HIF inhibitors and HIF stabiliser. The resulting relative mRNA expression can be seen in *Figure 29*. Notably, one sample of 24 h incubation with PT2399 was excluded after identification as outlier using Grubb's test for outliers resulting in a reduced sample size of N=3 for this experimental condition. Incubation with DMSO did not result in alternated mRNA expression of the evaluated target genes, except for *NOS3* whose mRNA expression decreased after 72 h incubation with DMSO in NX compared to NX control (0.919 ± 0.057, p = 0.016 data not shown). Incubation in NX with DMSO for 72 h led to increased *VEGFA* expression compared to NX control (1.237 ± 0.122, p = 0.029).

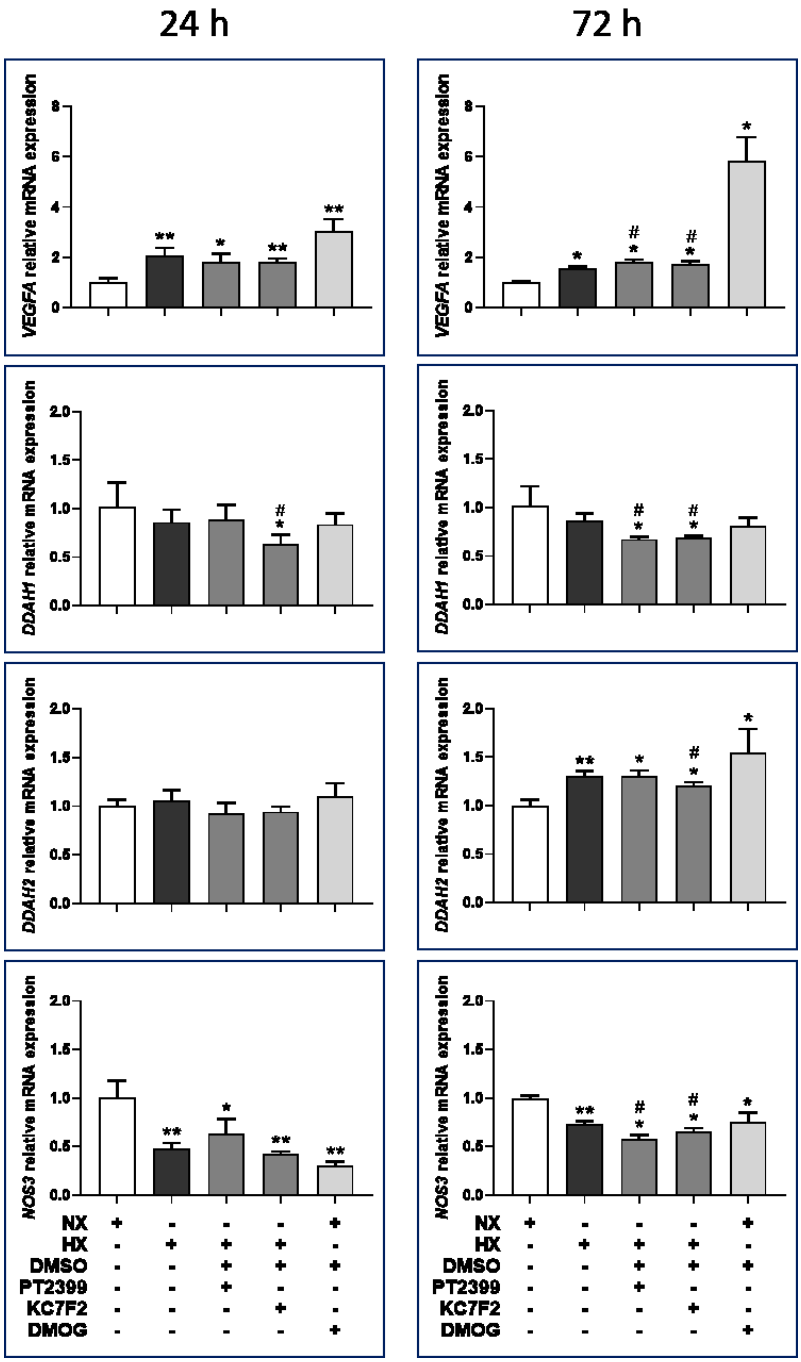

Figure 29: Relative mRNA expression in HPAEC after 24 h and 72 h incubation with HIF inhibitors and HIF stabiliser. HPAEC were incubated for 72 h in NX (white bar), with HIF stabiliser DMOG (light grey bar, right) in NX, in HX (black bar), with HIF1A inhibitor KC7F2 in HX or HIF2A inhibitor PT2399 in HX (both dark grey). Relative mRNA expression was assessed using qRT-PCR. Expression in control (NX) was set to 1. Bars represent mean ± SD. N=4, N=3 for 24 h incubation with PT2399 after Grubb's test for outliers. *= p≤0.1 compared to NX control; **= p≤0.01 compared to NX control; #= p≤0.1 compared to HX control; ##*= p≤0.01 compared to HX control, Non-parametric Mann-Whitney U-test.

After exposure to HX, *VEGFA* mRNA expression in HPAEC increased up to 2.060 ± 0.327 and 1.576 ± 0.046 after 24 h and 72 h ox HX, respectively. Incubation with DMOG led to an even stronger increase in mRNA expression, both after 24 h (3.034 ± 0.483) and 72 h incubation (5.844 ± 0.932). When incubated for 24 h with KC7F2 or PT2399, *VEGFA* mRNA expression did not change compared

to HX control, after incubation for 72 h however, cells incubated with KC7F2 and PT2399 both showed increased *VEGFA* mRNA expression compared to NX and HX control. *DDAH1* mRNA expression in HPAEC was not affected by exposure to HX and incubation with DMOG did not lead to a change in mRNA expression as well. Incubation with HIF inhibitors on the other hand led to a decrease in *DDAH1* mRNA expression. Incubation with KC7F2 decreased mRNA expression to 0.641 ± 0.091 and 0.688 ± 0.151 compared to NX control as well as HX control after 24 h and 72 h of HX, respectively. PT2399 led to a decrease of *DDAH1* expression after 72 h incubation (0.676 ± 0.027) compare to both, NX and HX controls. As previously shown, *DDAH2* mRNA expression was not affected by 24 h HX but increased after exposure to 72 h HX (1.305 ± 0.050). This effect was mimicked by 72 h incubation with HIF stabiliser DMOG in NX (1.549 ± 0.245). Incubation for 24 h with HIF inhibitors and HIF stabiliser did not affect *DDAH2* mRNA expression. Incubation of HPAEC with KC7F2 for 72 h on the other hand led to a significant decrease of *DDAH2* mRNA expression compared to HX control (1.205 ± 0.040, p-value 0.032 vs. HX control). *NOS3* mRNA expression was decreased after 24 h HX (0.477 ± 0.064) and 72 h HX (0.729 ± 0.034) which could also be observed after incubation with DMOG in NX (0.309 ± 0.038 and 0.754 ± 0.096 after 24 h and 72 h HX, respectively). However, incubation with HIF inhibitors could not prevent hypoxic *NOS3* decrease and led to even stronger decrease after incubation for 72 h compared to HX control (0.582 ± 0.042 and 0.656 ± 0.037, p-values 0.016 and 0.032 for incubation with PT2399 and KC7F2 compared to HX control, respectively). Yet, it is important to note that incubation with the NX DMSO control led to a significant difference in *NOS3* mRNA expression compared to NX control (0.912 ± 0.06, p-value 0.016 compared to NX control).

A549. Relative mRNA expression in A549 after 24 h and 72 h incubation with HIF compounds compared to NX control are depicted in Figure 30. *VEGFA* mRNA increased after exposure to HX (1.272 ± 0.181 and 1.528 ± 0.313 after 24 h and 72 h HX, respectively). HIF stabilisation by DMOG incubation led to even higher increase in *VEGFA* mRNA expression than HX (1.508 ± 0.228 and 2.105 ± 0.275, after 24 h and 72 h HX, respectively). *VEGFA* expression was affected by incubation with DMSO, which caused a decrease in mRNA expression of about 15 % in NX compared to NX control (0.869 ± 0.070 vs. 1.003 ± 0.085) and 30 % in HX compared to HX control (1.003 ± 0.063 vs. 1.528 ± 0.313). As seen before, incubation with PT2399 and KC7F2 did not have an impact on *VEGFA* expression, independent on incubation period. Again, *DDAH1* mRNA expression was decreased after 24 h HX (0.555 ± 0.182) and after incubation with DMOG at HX (0.482 ± 0.089) to about half the expression level compared to NX control. Incubation with DMSO at HX led to a further decrease in *DDAH1* mRNA expression after 24 h (0.405 ± 0.035) than HX control. Incubation with HIF inhibitor PT2399 led to a lower reduction in *DDAH1* expression than HX, although the difference between HX control and PT2399 was not significant (p-value 0.08). Incubation with KC7F2 did not restore NX expression level, but *DDAH1* mRNA expression increased to NX level after 72 h incubation under all conditions as previously seen (*Figure 19*). Interestingly, *DDAH2* expression increased after exposure to 24 h (1.251 ± 0.074) as well as 72 h HX (1.143 ± 0.085). This increase was not observed before and could also not be achieved by incubation with DMOG (1.106 ± 0.156 and 1.001 ± 0.074 after 24 h and 72 h incubation, respectively). Incubation with DMSO at NX led to an increased mRNA expression (1.138 ± 0.063) as well (data not shown). In contrast to KC7F2, PT2399 was able to restore NX expression level (1.091 ± 0.109, p-value 0.008 compared to HX control after 24 h and 0.891 ± 0.109, p-value 0.001 compared to HX control after 72 h incubation). *NOS2* expression decreased after 24 h of HX to about half the expression level compared to NX control (0.553 ± 0.222), however its expression level adjusted to approximately NX level after 72 h HX (0.0766 ± 0.246). Both, PT2399 and KC7F2 led to increase in *NOS2* mRNA expression compared to HX control, nevertheless this increase was not statistically significant after 24 h incubation. Incubation with PT2399 for 24 h as well as for 72 h led to great variance in relative *NOS2* mRNA expression. The increase in mRNA expression by PT2399 reached statistical significance compared to HX control after 72 h incubation (1.505 ± 0.729 vs. 0.766 ± 0.246, p-value 0.023). Incubation with DMOG led to a strong decrease in mRNA expression to 0.252 ± 0.119 and 0.348 ± 0.115 of NX expression after 24 h and 72 h HX, respectively.

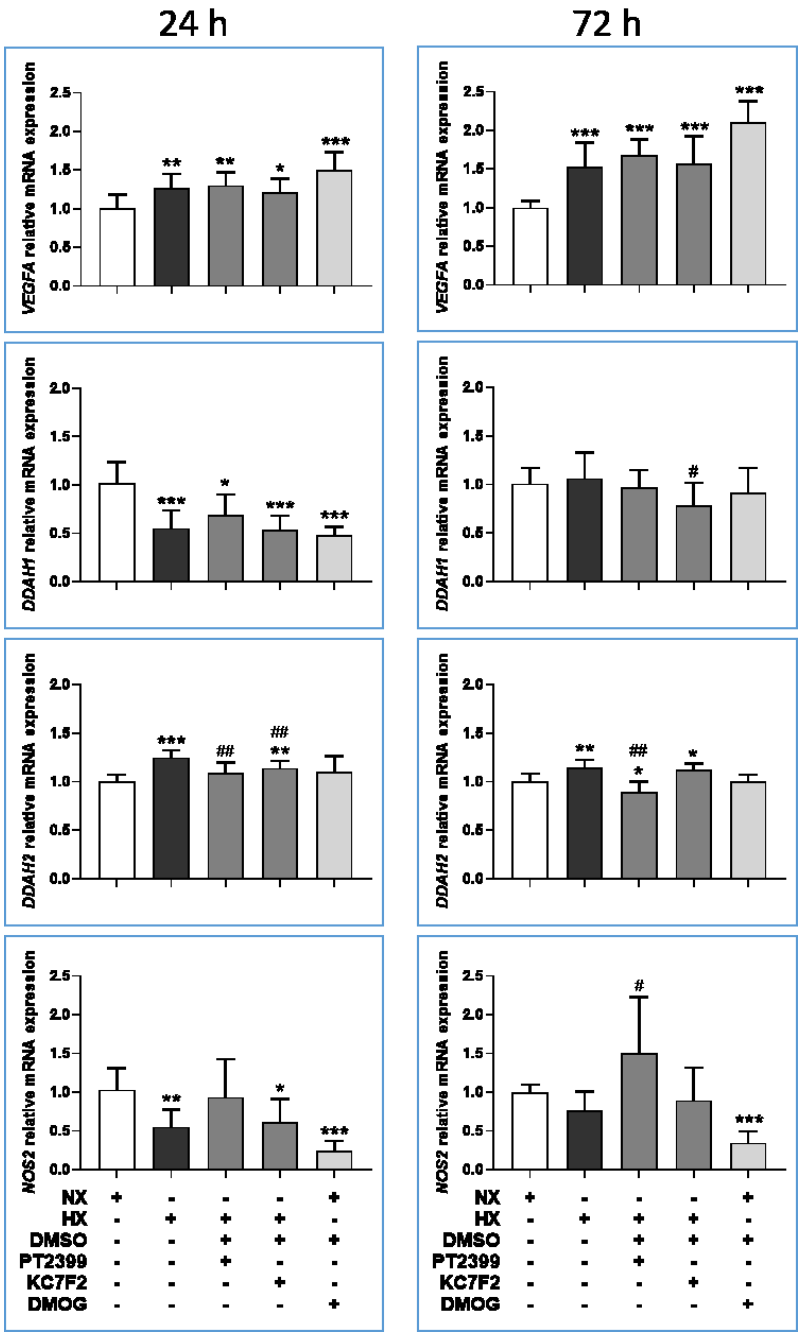

Figure 30: Relative mRNA expression in A549 after 24 h and 72 h incubation with HIF inhibitors and HIF stabiliser. A549 were incubated for 24 h (left) or 72 h (right) in NX (white bar), with HIF stabiliser DMOG (light grey bar, right) in NX, in HX (black bar), with HIF1A inhibitor KC7F2 in HX or HIF2A inhibitor PT2399 in HX (both dark grey). Relative mRNA expression was assessed using qRT-PCR. Expression in control (NX) was set to 1. Bars represent mean ± SD. N=8, *= p≤0.1; **= p≤0.01; #= p≤0.1 compared to HX control; ##= p≤0.01 compared to HX control, Non-parametric Mann-Whitney U-test.

5 Discussion

5.1 Expression stability of putative reference genes in normoxic and hypoxic HCAEC, HPAEC and A549 cells

One approach to gain better insights into complex regulatory mechanisms are gene expression studies. Quantitative real-time polymerase chain reaction (qRT-PCR) is the gold standard for relative quantification of individual transcripts, as this method combines high sensitivity and reproducibility with a simple design and rapid readout [118-121]. In qRT-PCRs, reference genes are used as an internal standard to analyse relative gene expression of any desired target by using the $2^{-\Delta Ct}$ method [117, 122]. This standardisation remains difficult, as results might differ depending on type of RNA isolation, protocol for reverse transcription and the amount of staring material [123]. Although housekeeping genes are presumed to be stably expressed in the cells and / or in the experimental conditions of interest, the expression of commonly used reference genes like *GAPDH* and *ACTB* was shown to vary depending on cell type and experimental conditions [120]. Especially in hypoxic conditions, commonly used housekeeping genes were shown to vary widely [124-127]. Therefore, optimal reference genes need to be determined for a specific experimental setup [128]. The choice of reference genes remains challenging, as it has an impact on reliability of results and thereby on their interpretation [129]. Algorithms like NormFinder and geNorm rank candidate reference genes by stability. However, different methods and algorithms might lead to different rankings [130]. As there is no objective criterion to select the most appropriate gene, it is important to note that the results of these rankings might not necessarily show the “best” gene and therefore it should be considered to perform other analyses, for example calculation of mean Ct, mean SD value after pairwise ΔCt comparison or equivalence tests. For this reason, we combined the results of mean Ct, Ct CV, pairwise ΔCt comparison and the NormFinder algorithm in order to find the steadiest housekeeping gene in HX for a comparison of gene expression in HCAEC, HPAEC and A549 cells.

Klenke et al. suggested to analyse expression levels of putative reference genes from different pathways [128]. We therefore selected genes encoding for rRNA (*18S*), cytoskeleton (*ACTB*), class I major histocompatibility complex (*B2M*), glycolytic pathway (*GAPDH*), protein folding (*PPIA*), ribosomes (*RPLP1* and *RPL13A*), electron transport chain (*SDHA*) and transcription (*TBP*).

In qRT-PCR, Ct values represent the number of PCR cycles at which the fluorescent signal can be detected above the background signal; thus the Ct value inversely correlates with the amount of template mRNA in the respective qRT-PCR reaction. This means that a wide transcription range indicates a generally more variable gene expression. Ct CV values and the resulting mean SD of

pairwise ΔCt comparison can also be used to assess the expression stability of the putative reference genes. The coefficient of variation depicts the percentage ratio of the standard deviation to the arithmetic mean; a low Ct CV indicates therefore a stable gene expression. A low mean SD value after pairwise ΔCt comparison indicates a more stable expression as well [115, 128]. Using the NormFinder algorithm, generated stability values give further insight into gene expression stability. A low stability value reflects hereby a higher gene expression stability. The algorithm can be used with or without prior log transformation. Usually, log transformation is used to deal with skewed data and to reduce variability of data. Nevertheless, if used at all log transformation must be applied with caution, which is why several groups recommend to abandon this method [131]. Although other papers highly recommend using log transformation, we decided not to log transform our data. As recommended by Andersen et al., biological replicates were treated individually and independent treatments which interfere expression variation (in this case incubation period, condition, cell lines) were considered as grouping variables [116].

18S. As seen in *Figure 7* Ct values obtained for *18S* were low compared to the other tested genes indicating that *18S* was the most abundant transcript of these genes. As rRNA makes about 80 % of total RNA, rRNA transcripts tend to be more abundant than mRNA transcripts. Therefore, *18S* transcript levels are considered to be highly abundant in comparison to target mRNA transcript levels, which is why 18S as well as 28S rRNA molecules are usually not used for normalisation of mRNA expression [127]. Even small changes in *18S* gene expression would lead to big differences in target after normalization. Moreover, rRNA and mRNA are transcribed by different polymerases, polymerase I and polymerase II, respectively. Thus, their synthesis is regulated via different pathways [132]. For better comparison, reference genes should be expressed in constant number in all cells and in a similar copy number to the gene of interest. The Ct value of a suitable reference gene should be between cycle 15 and 30, while the SD should not surpass 1.0 [133]. Not only were Ct values of *18S* lower than recommended, but also was the coefficient of variation higher than for any other putative reference gene (*Table 22*). Therefore, *18S* was not the first choice as reference gene for our experimental setting.

ACTB. *ACTB* showed similar Ct values in all cell lines (*Figure 7*) and a relatively low Ct CV, but showed only a moderate mean SD of pairwise comparison of ΔCt values of putative reference genes (*Table* 23). Our analyses showed that *ACTB* was more stable in pulmonary artery endothelial and alveolar epithelial cells than in coronary artery endothelial cells. According to *Table 25*, it was not under the top 3 putative reference genes after all analyses. It was mentioned in several studies that *ACTB* might be differentially expressed after exposure to HX. In HUVEC *ACTB* expression decreased after exposure to hypoxia [134]. Moreover, actin expression was reduced in brain

endothelial cells in HX [135] as well as in bovine and human artery endothelial cells. It appears that ROS affect endothelial cell signalling pathways which may regulate actin cytoskeleton [136]. It was also suggested, that superoxide or ROS may directly affect the cytoskeleton [137]. As ROS increase during HX, *ACTB* appeared not to be a suitable reference gene for our analyses.

B2M. *B2M* showed a high transcription range (*Figure 7*) and a high Ct CV (*Table 24*) when comparing all cell lines. When comparing all cell lines using the pairwise comparison of ΔCt values of putative reference genes *B2M* showed the highest mean SD and therefore the lowest stability in HX according to this analysis. Together with *SDMA*, *B2M* has the lowest mean rank of putative reference genes (*Table 25*), which is why it was excluded as putative reference gene. According to literature high fluctuations in *B2M* expression in MCF-7 and HEK cells after exposure to HX were reported [127], underlining the variance in gene expression levels under hypoxic conditions. Moreover, there is evidence that HX and therefore HIF stabilisation leads to an increase in MHC class I, providing a possible explanation for hypoxic regulation of *B2M* [138].

GAPDH. For *GAPDH*, the pairwise comparison of ΔCt values resulted in high mean SDs. Especially in HCAEC (mean SD 0.460, rank 8) and A549 (mean SD 0.379, rank 9) *GAPDH* showed a lower stability compared to other putative reference genes. When comparing all cell lines, *GAPDH* showed the same tendencies (mean SD 0.617, rank 7). Moreover, *GAPDH* showed a high range in stability values calculated by the NormFinder algorithm (*Figure 8*). For A549, *GAPDH* showed the highest stability value and therefore lowest expression stability under the evaluated conditions. According to literature, *GAPDH* belongs to the least stably expressed genes in human retinal endothelial cells [139], HUVEC [134] and bovine endothelial cells [140] after exposure to HX and its protein levels increase to 3-4-fold in rat alveolar epithelial cells after 18 hours of hypoxia [141]. Published data suggest that *GAPDH* is directly upregulated by an interaction between the hypoxia inducible factors HIF1A and HIF2A through a 5' hypoxic regulatory element [142]. According to our results and literature, *GAPDH* was therefore not a suitable reference gene for our experimental setting.

PPIA. *PPIA* showed a low transcription range (*Figure 7*) and had the lowest Ct CV of all tested putative reference genes and therefore highest stability according to this test when comparing all cell lines. Calculating pairwise comparison of ΔCt values, *PPIA* showed a low mean SD (rank 2), but stability values calculated by the NormFinder algorithm were high, with the second lowest expression stability in A549. In A549, *PPIA* expression appeared to vary, as Ct CV also resulted in a low stability (rank 8). *PPIA* was ranked on rank 1 after calculating the mean rank of all analyses. However, in osteoarthritis chondrocytes *PPIA* expression was increased by hypoxia [143]. *PPIA* was also shown to be a major ROS-induced factor in atherosclerosis [144]. It plays a major role in regulating proliferation, migration and tube formation of pulmonary arterial endothelial cells and

was upregulated and acetylated under HX [145]. Due to the top mean rank, *PPIA* was set on the shortlist of putative reference genes.

RPL13A. *RPL13A* showed a moderate transcription range within the different cell lines and conditions (*Figure 7*) as well as Ct CV when comparing all cell lines together. In A549, *RPL13A* showed the lowest mean SD values after pairwise comparison of ΔCt values, however it showed only average mean SD when comparing all cell lines. Interestingly, all stability values calculated for *RPL13A* by the NormFinder algorithm were likewise low, calculated for each cell line separately as well as calculated for all cell lines together. When calculating the stability value for all cell lines together, *RPL13A* showed the highest expression stability of all tested putative reference genes. Using the NormFinder algorithm, Foldager et al. received smaller stability values for *RPL13A* in chondrocytes, thereby indicating higher stability in comparison to *GAPDH*, *B2M* and *ACTB* [146]. Another group found *RPL13A* to be the optimal reference gene for normalization of target gene expression in human blood before and after exposure to high-altitude and thereby exposure to a reduced amount of oxygen [147]. In this study, *RPL13A* expression in both conditions was more stable than expression of *GAPDH*, *ACTB* and *18S*. These results are in line with our findings using the NormFinder algorithm. Therefore, *RPL13A* was short-listed as putative reference gene.

RPLP1. *RPLP1* showed a moderate transcription range as well as average Ct CV. It was ranked in the middle after calculating mean SD of pairwise comparison of ΔCt values. According to the results of the NormFinder algorithm, stability values of *RPLP1* were also in the middle ranks. When calculating the mean rank after all analyses, *RPLP1* was ranked on rank 4 indicating a rather stable expression. Nevertheless, RPLP1 was not under the top 3 candidate reference genes after calculating the mean rank of putative reference genes for all cell lines (*Table 25*). In rat heart tissue cells, *RPLP1* was the steadiest putative reference gene after 6 h of with the lowest stability value calculated using NormFinder [128]. Several studies used *RPLP1* as reference gene for normalization in endothelial or epithelial cells [148-150], but none of the groups worked with HX or explained their choice of *RPLP1* as reference gene. In EA.hy926 though, *RPLP1* expression decreased after exposure to HX [151].

SDHA. *SDHA* showed a wide transcription range within the different cell lines with a standard deviation of 0.747 (*Figure 7*) and therefore appears to vary highly. With a Ct CV of 4.19 % in A549, *SDHA* showed a low expression stability. Using the pairwise comparison of ΔCt values of putative reference genes, *SDHA* was shown to have the highest mean SD in HPAEC and HCAEC and also appears to have a low expression stability in A549 (rank 7), which makes it an improper reference gene. According to Xiao et al. [147], *SDHA* was a suitable reference gene expression in human blood before and after exposure to high-altitude. Nevertheless, according to our results *SDHA* was not a suitable reference gene for our experimental setting.

TBP. *TBP* showed the lowest expression levels throughout all cell types and one of the lowest Ct CV calculated for all cell lines together as well as the highest expression stability when comparing mean SD of pairwise comparison of ΔCt. According to Ct CV and pairwise comparison of ΔCt, *TBP* appeared therefore to show a low expression variance between different conditions as well as between cell lines and seemed to be an appropriate choice as reference gene. *TBP* was used for gene expression normalization in combination with *18S* in various endothelial cells (e.g. HUVEC, HPAEC, HCAEC) after exposure to NX and HX [152], however there was no explanation for the choice of reference genes. Our results generated by using the NormFinder algorithm however calculated high stability values for *TBP* with a wide range of calculated stability values for the separate cell lines. In HPAEC, TBP received the second highest stability value, in A549 the third highest stability value. According to the NormFinder analysis, *TBP* appears therefore to have a low expression stability in pulmonary cells. As *TBP* was on rank 2 after calculating mean ranks of all analyses, it was set on shortlist as putative reference gene.

5.2 Selection of reference gene for target gene normalisation in HCAEC, HPAEC and A549 cells

To our knowledge, we were the first ones to test for optimal reference genes in pulmonary epithelial and human pulmonary and coronary artery endothelial cells. As we aimed to compare target gene expression between conditions as well as between cell lines, we wanted to use the same reference gene for all three cell lines. Little is known about the expression of the nine candidate genes in hypoxic epithelial and endothelial cells. Most studies used HUVEC, but as reference genes may vary depending on cell line, experimental setting and handling [128, 153], comparing results is difficult.

Interestingly, experiments with HUVEC exposed to oxidative stress found *ACTB* and *GAPDH* to be stably expressed according to NormFinder [118, 154]. Opposite to our results, incubation of HUVEC with $CoCl_2$ mimicking HX resulted in low stability values for *RPL13A* [134]. This clearly illustrates, why testing for a suitable reference gene is indispensable for each experimental setup. As reported by Caradec and colleagues, the best reference gene differs greatly depending on the performed analysis [127]. This might also explain different results received by different groups.

PPIA, *RPL13A* and *TBP* were the top candidate reference genes after calculating the mean rank of all analyses. Each of the putative reference genes received top ranks in some of the performed analyses and was not listed on top of the list using other analyses. We aimed to compare all cell lines using the same reference gene, therefore we decided to use *RPL13A* as reference gene. It showed good results in all performed analyses for all cell lines and the best stability value after

NormFinder analysis of all cell lines together. Moreover, the stability values of *RPL13A* generated by the NormFinder algorithm were similar in all cell lines calculated for each cell line separately. Another reason for the selection of *RPL13A* as reference gene was the ROS-induced increase of *PPIA* [143, 145]. As ROS increases in HX, *PPIA* might therefore also increase in hypoxic endothelial cells. This fact and the low stability values calculated for A549 by the NormFinder algorithm led to the exclusion of *PPIA* as putative reference gene for our experimental setup.

5.2.1 Importance of reference gene selection

To clarify the importance of the choice of reference genes and the resulting impact on relative target gene expression, we normalized *VEGFA* expression to *RPL13A*, *B2M* and *SDHA*. *VEGFA* is a well-known hypoxia regulated gene whose induction by hypoxia is crucial for hypoxia-mediated angiogenesis and hematopoiesis [155, 156]. Several groups reported increased *VEGFA* expression in endothelial cells after exposure to hypoxia [157, 158], the hypoxic increase in mRNA expression is thought to be HIF-mediated [159-161]. As *VEGFA* expression is clearly hypoxia-regulated, we used *VEGFA* mRNA expression to verify hypoxic effects on cells. As seen in *Figure 9, VEGFA* showed an explicit increase in expression after exposure to HX. It is however noteworthy, that the chosen reference gene has a major impact on the calculated mRNA expression of *VEGFA*.

5.3 Hypoxic regulation of the L-arginine-ADMA-NO-pathway in coronary and pulmonary artery endothelial and alveolar epithelial cells

Our study has three major findings:

1. Comparing HPAEC and HCAEC there are no differences in hypoxic regulation of genes and proteins involved in the L-arginine-ADMA-NO pathway.
2. In A549 alveolar epithelial cells, hypoxic regulation of the L-arginine-ADMA-NO pathway shows differences compared to the regulation in hypoxic pulmonary artery endothelial cells.
3. The hypoxic regulation of the L-arginine-ADMA-NO pathway in human coronary and pulmonary artery endothelial cells and in alveolar epithelial cells does not seem to be strictly HIF-dependent.

It is well established that hypoxia leads to coronary vasodilation and pulmonary vasoconstriction. Within the coronary circuit, NO was proven the main regulator of vascular perfusion and therefore a key part in regional adaption of the blood flow [8, 11, 12]. Thus, a possible mechanism leading to the different answers towards hypoxia in coronary and pulmonary circuit is a differential regulation of the L-Arginine-ADMA-NO pathway. NO is generated by NOS out of the semi-essential amino acid L-arginine. ADMA is a competitive inhibitor of NOS, influences NO homeostasis and might thereby indirectly regulate vascular perfusion [49, 55]. ADMA is generated by protein degradation of methylated proteins and is therefore part of physiological protein turnover. Its clearance occurs via degradation by two enzymes of the DDAH family, DDAH1 and DDAH2, indicating a protective role of these proteins against ADMA related diseases [17, 70].

We aimed to compare hypoxic regulation of genes involved in the L-arginine-ADMA-NO pathway between human coronary and pulmonary artery endothelial cells in order to find a putative explanation for the opposing effects of hypoxic coronary vasodilation and hypoxic pulmonary vasoconstriction. As NO is the main regulator in vascular perfusion, a differential regulation of synthesis and homeostasis might explain the different answers towards hypoxia. According to this explanation, one would expect higher NOS3 activity in hypoxic HCAEC and therefore increased amounts of NO that in turn cause vasodilation. In HPAEC on the other hand, one would expect reduced NOS3 activity and reduced amount of NO. NOS regulation however is complex and there are various transcriptional and post-transcriptional factors regulating NOS3 expression and activity. A reduced NOS3 activity might be caused by lower mRNA expression, lower protein amounts,

and/or lower protein activity, whereby protein activity correlates with ADMA concentrations and therefore with DDAH1 and DDAH2 protein expression and activity.

However, according to our results, *NOS3* mRNA expression in both human coronary artery endothelial cells and human pulmonary artery endothelial cells was reduced after exposure to hypoxia and does not show differences between HCAEC and HPAEC. This reduced mRNA expression might appear unexpected in HCAEC, but according to literature, several other groups found decreased *NOS* mRNA expression after exposure to HX as well. In HUVEC, HX seems to inhibit *NOS3* expression via transcriptional as well as posttranscriptional mechanisms [162]. One factor influencing *NOS3* mRNA are cytokines. They were shown to affect the stability of *NOS3* mRNA by a process involving the induction and expression of cytosolic proteins. Those bind to a cytidine-rich region within the 3'-untranslated region (UTR) of the *NOS3* mRNA, thereby probably alter its configuration, and increase its susceptibility for RNase activity thus lowering *NOS3* mRNA levels [163]. As cytokines like interleukin 6 [164] and TNF-alpha [165] increase in cells exposed to HX, this might explain reduced *NOS3* mRNA levels. In bovine aortic endothelial cells incubation with TNF-alpha decreased NOS activity, protein and mRNA expression [166, 167]. Another group found *NOS3* mRNA to be highly stable in normoxic endothelial cells due to the formation heterogeneous nuclear ribonucleoprotein E1 (hnRNP E1)-containing RNP complexes on evolutionary conserved pyrimidine rich sequence elements within the 3'UTR. Under hypoxic conditions however, they observed decreased *NOS3* mRNA, probably caused by a disruption of hnRNP E1/NOS3 3'-UTR interactions via increased AKT-mediated serine phosphorylation [166]. Another mechanism regulating NOS3 activity in hypoxia or under oxidative stress is DNA methylation. In bovine artery endothelial cells, DNA methylation inhibited *NOS3* promoter activity [168], resulting in reduced *NOS3* mRNA. HX and ischemia were also shown to reduce NOS3 expression via posttranscriptional mechanisms that result in *NOS3* transcript destabilisation via miR-200b [169]. These data support our findings of reduced *NOS3* mRNA expression after exposure to HX. Noteworthy, Ct values of *NOS3* qRT-PCRs in HPAEC were lower (2 cycles) compared to HCAEC which might indicate a generally lower *NOS3* mRNA level in HPAEC. However, in our experiments hypoxic regulation of *NOS3* mRNA expression did not differ between pulmonary and coronary endothelium.

NOS3 protein expression on the other hand was shown to increase in hypoxic HCAEC but not in HPAEC. Increased NOS3 protein expression in HCAEC could imply increased NOS3 activity and therefore increased NO causing vasodilation. As we received more faint bands in HCAEC performing a semi dry Western blot, quantification of NOS3 protein expression was difficult, but due to the strictly limited material could not be repeated. The increase of NOS3 protein in HCAEC after exposure to hypoxia but a reduced mRNA expression might be caused by hypoxic mRNA

destabilisation as described above. Another possible explanation is hypoxic protein stabilisation of NOS3. Hypoxia was shown to increase HSP90 binding to NOS3 via PI3K-AKT in porcine coronary artery endothelium [170]. As HSP90 acts as physiological binding partner and regulator of NOS3 and is thought to induce a conformational change or to stabilise the dimeric form of the protein, this might be one explanation for NOS3 protein stabilisation and increased protein activity [24]. The basal expression of several genes crucial for endothelial function (including NOS3) is controlled by DNA methylation and histone posttranslational modifications [171]. Histone post-translational modifications were shown to take part in NOS3 regulation in artery endothelial cells, not only on mRNA expression levels but on protein expression levels as well. Synthetic hypoxia-sensitive miR-21-5p was shown to decreases NOS3 and DDHA1 at both protein and transcript levels. As miR-21 decreased under HX [172], this could be another mechanism stabilising NOS3 protein in HX. In HPAEC however, Pekarova et al. [60] did also not find an effect on NOS3 protein expression after exposure to 48 h HX. Noteworthy, in their experimental setting hypoxia was set to 5 % O_2, which is considered as mild HX [173], compared to our hypoxic environment containing only 1 % O_2. Usually, NOS3 is associated to the membrane [43, 44]. As HX results in increased calcium concentrations and NOS dissociation from the membrane [45], it is possible that in hypoxic HCAEC more calmodulin-bound NOS dissociated into the cytoplasm. When preparing samples for Western blots, we centrifuged samples after cell lysis and discarded cellular debris. Eventually, membrane-bound NOS in HPAEC therefore got lost, while cytoplasmic NOS3 in HCAEC was within the protein containing supernatant and could therefore be detected.

To evaluate putative differences between NO production in HCAEC and HPAEC, assessing NOS3 protein activity is indispensable. Oxidative stress was associated with elevated concentrations of ADMA caused by increases in the activity of PRMTs and decreases in the DDAH-enzymes [69, 174]. Interestingly, we did not observe elevated but rather reduced *PRMT* mRNA expression in both hypoxic HCAEC and HPAEC, nor did we detect increased ADMA concentrations in HCAEC or HPAEC after exposure to HX that might explain a putative reduced NOS activity. A cohort study in human subjects however showed, that single-nucleotide polymorphisms in the gene encoding for *PRMT1* are not associated with elevated blood ADMA [81], suggesting a minor role of *PRMT1* for NO homeostasis. We further evaluated DDAH1 and DDAH2 gene and protein expression to gain deeper insights into a putative NOS inhibition by ADMA. While *DDAH1* mRNA expression showed a notable difference as it decreased in HPAEC after 24 h HX but not in HCAEC, no differences on protein expression level were observed. It is however important to note, that Western blots are a semi-quantitative method [175]. Moreover, the correlation between transcription and translation is not always linear. Increased mRNA expression does not necessarily result in elevated protein levels, as

there are several factors regulating protein synthesis and protein stability. The processes of initiation, elongation and termination are all targets in regulation of protein synthesis [176]. Protein stability controlled by post-translational modifications is another factor regulating protein levels [177]. Therefore, assessing protein activity rather than protein expression could give a better insight into molecular regulation of the L-arginine-ADMA-NO pathway.

However, the decrease in *DDAH1* mRNA was also observed in A549, suggesting that HX might have the same decreasing effect on *DDAH1* mRNA expression in pulmonary endothelial and epithelial cells. As DDAH1 appears to be the main ADMA-degrading enzyme [178, 179], reduced DDAH1 protein activity would lead to an accumulation of ADMA and therefore reduced NOS activity by competitive inhibition of NOS. This accumulation of ADMA could be observed in the supernatant medium of hypoxic A549, underlining this hypothesis. Elevated ADMA concentrations together with reduced DDAH1 expression were also observed in lung tissue of rats exposed to chronic hypoxia [180]. *DDAH2* mRNA expression on the other hand increased in both HCAEC and HPAEC after 72 h of hypoxia, however this increase in mRNA expression did not result in elevated DDAH2 protein expression. It appears therefore that there is no difference in ADMA metabolism between hypoxic HPAEC and HCAEC. In A549 on the contrary, we were able to show increased ADMA and SDMA concentrations after exposure to HX, although DDAH2 protein expression increased in hypoxic conditions. A recently published study suggests, that DDAH2 does not take part in ADMA degradation, which might explain elevated ADMA concentrations despite increased DDAH2 protein expression under hypoxia [178].

Another limiting factor in NO synthesis is the availability of L-arginine as substrate for NOS. Arginase activity might therefore also participate in reduced release of NOS as it uses L-arginine as substrate. Arginase affinity for L-arginine was shown to be lower than NOS3 affinity for L-arginine, however it competes for L-arginine as substrate and regulates its availability. We did not find *ARG1* expression in epithelial or endothelial cells, which is not surprising as this isoform appears to be mainly expressed in liver, macrophages and bone marrow. *ARG2* expression did not differ between the cell lines and appears therefore not to be the main factor regulating the different answers to hypoxia und pulmonary and coronary vasculature. Endothelin is a potent vasoconstrictor [181] and thereby an antagonist of NO. We could however not observe any differences in mRNA expression levels between hypoxic HPAEC and HCAEC that might explain HPV. In A549 cells, no *END1* expression was detected, suggesting *END1* does not play a key part in differential answers towards HX within the pulmonary and coronary circuit. As HIF appears to be involved in hypoxic regulation of gene expression and therefore might play a role in the hypoxic regulation of the L-arginine-ADMA-NO pathway, we examined *HIF1A* mRNA expression. Like also observed by Bartoszewski et al. [152], we

found decreased *HIF1A* mRNA expression levels in HPAEC and HCAEC after exposure to HX. In hypoxic epithelial cells though the observed decrease in *HIF1A* mRNA expression was more pronounced compared to endothelial cells, which could indicate a higher sensitivity to HX. Although HIF1A and HIF2A are mainly degraded in normoxia due to ubiquitination by pVHL, other regulatory pathways have been described, including oxygen independent mechanisms [173, 182, 183]. Thus, the observed stronger decrease of *HIF1A* mRNA expression in A549 does not necessarily indicate higher oxygen sensitivity.

As already mentioned, regulation of NOS3 activity is complex. Besides several other effects, hypoxia reversibly suppresses Na^+/K^+ ATPase activity [1, 4, 5]. The Na^+/K^+ ATPase catalyses the export of Na^+ out of cell and import of K^+ into the cell against the electrochemical gradient via hydrolysis of ATP. If the ion transport is reduced, the intracellular calcium concentration increases, as the transport of calcium depends after antiport principle of the sodium-concentration gradient (Na^+/Ca^{2+} exchanger). Hypoxia also increases the AMP:ATP ratio, induces AMPK via phosphorylation and therefore leads to an increase of intracellular Ca^{2+}. In pulmonary artery smooth muscle cells, HX led to calcium-release, the opening of calcium-permeable non-selective cation-channels, inhibition of voltage-dependent potassium channels, membrane depolarization and calcium influx through voltage-dependent calcium channels [184, 185]. Therefore, HX might lead to an increase in calcium as a cofactor for NOS3, NOS3 translocation from caveolae by binding of calcium-calmodulin.

Another important regulator of NOS3 activity is phosphorylation. It could be interesting to perform Western blots for phosphorylated NOS3 to gain further insight into protein activity. It is important to note though, that depending on the phosphorylation site, NOS3 is either activated or inhibited [186] and phosphorylation is only one of several mechanisms regulating NOS3 activity. Moreover, several kinases phosphorylating NOS3 in response to shear stress [163, 167], and therefor regulation by those kinases does not take place in cell culture models. Oxidative stress was shown to effect NOS3 function through BH_4 bioavailability and uncoupling NOS3 [172], suggesting another regulatory mechanism of NOS3 protein activity.

Taken together, we did not find differences in mRNA expression, protein expression or protein activity of genes involved in the L-arginine-ADMA-NO pathway between hypoxic HCAEC and HPAEC, which could explain the opposing effects of hypoxic coronary vasodilation and hypoxic pulmonary vasoconstriction. According to our results, DDAH1 and DDAH2 protein expression appears not to be affected by hypoxia, neither in HPAEC nor in HCAEC. No differential regulation in DDAH1 and DDAH2 protein expression between hypoxic HPAEC and HCAEC was observed. We did find increased ADMA concentrations in hypoxic epithelial A549 as well as decreased *DDAH1* mRNA

expression though. As alveolar epithelial cells are the first cell layer in contact with inhaled air, we therefore suggest an oxygen-sensing role for pulmonary epithelial cells and a cellular cross talk between pulmonary epithelial and endothelial cells, which causes HPV.

5.4 Effects of HIF inhibition and HIF stabilisation on gene expression of genes involved in the L-arginine-ADMA-NO pathway in HCAEC, HPAEC and A549 cells

Within the coronary system, hypoxic gene regulation appears to be HIF-regulated; the underlying mechanisms leading to hypoxic pulmonary vasoconstriction however remain elusive. To investigate whether the hypoxic regulation of gene and protein expression of genes involved in the L-arginine-ADMA-NO-pathway is HIF-dependent, the three cell lines were incubated with two HIF inhibitors and a HIF stabiliser. HIF inhibitors were applied to cells incubated in HX, trying to achieve NX expression levels of genes of the ADMA-NO-pathway; the stabiliser to cells incubated in NX, aiming to achieve HX expression levels. Drug-like chemicals as PT2399 were shown to directly bind to the HIF2A PAS B domain and thereby prevent HIF2A from binding to the β-subunit. As this binding is crucial for HIF transcriptional activity, PT2399 was used to decreases transcription of HIF2A target-genes. In renal cell carcinomas, incubation with 1 µM as well as 10 µM PT2399 minimally affected calcium channel, potassium channel, bradykinin and *VEGFA* [112, 187]. KC7F2 is a cell-permeable symmetrical cystamine compound that selectively suppresses cellular HIF1A protein synthesis. It does not affect the transcription of *HIF1A* mRNA but results in decreased transcriptions of HIF1A-dependent genes by inhibition of HIF1a protein synthesis at the translation level. KC7F2 specifically targets the mTOR complex 1 pathway, which leads to the inhibition of protein synthesis [113]. The HIF stabiliser DMOG is a cell-permeable 2-oxoglutarate analogue that acts as a competitive inhibitor against all oxoglutarate-dependent dioxygenases, including PHDs and FIH and was thereby shown to stabilise HIF1A as well as HIF2A [188].

Due to observed cytotoxicity of the tested concentrations of the HIF inhibitors and the HIF stabiliser in EA.hy926 cells, concentrations for incubation with primary cell lines HCAEC and HPAEC were adjusted. In HUVEC, one group [189] used 10 µM KC7F2 for HIF inhibition. As we observed strong growth inhibitory/cytotoxic effects using higher concentrations than 2 µM KC7F2 in HCAEC and HPAEC primary cells, we could not use higher concentrations of the compound. DMOG used in higher concentrations that 0.5 mM did not further affect VEGFA mRNA expression. We therefore decided to use 0.5 mM DMOG as final concentration for incubation in order to keep DMSO concentration as low as possible to avoid any side effects.

As *VEGFA* is a target of both HIF1A and HIF2A [173], it is possible that the inhibition of one of the two isoforms was not sufficient, giving a putative explanation for the observed low effects on

VEGFA mRNA expression compared to HIF stabilisation using DMOG which stabilises both isoforms. Besides some common target genes, HIF1A and HIF2A are altogether non-redundant and have different target genes and mechanisms of regulation [173], suggesting that inhibition of one of the two isoforms should affect gene expression of respective target genes.

According to the results of our experiments with HIF inhibitory and a HIF stabilising compounds, expression of *DDAH1* and *DDAH2* in HCAEC appear not to be HIF-regulated. *VEGFA* mRNA expression on the other hand showed a strong increase after incubation at NX with the HIF stabiliser DMOG as well as a significant decrease towards the HX control when incubated wit PT2399, indicating a HIF2A dependent regulation of *VEGFA* mRNA expression. *NOS3* expression in HCAEC decreased after incubation at NX with the HIF stabiliser DMOG, however incubation at HX with neither HIF1A inhibitor KC7F2 nor HIF2A inhibitor PT2399 was sufficient to restore NX expression levels. These results indicate a not strictly HIF-dependent regulation of *NOS3* mRNA expression in HCAEC. In HPAEC, increased *VEGFA* mRNA expression and the decreased *NOS3* mRNA expression were also achieved by HIF stabilisation in NX with DMOG. However, inhibition of HIF1A or HIF2A did not lead to adjustment to NX expression level. DDAH1 mRNA expression was also not affected by incubation with HIF inhibitors nor the stabiliser, suggesting that regulation of gene expression of the L-arginine-ADMA-NO pathway is not HIF-dependent in HPAEC, except of *DDAH2* regulation. Notably, *DDAH2* increased after exposure to HX as well as after incubation with DMOG and incubation with KC7F2 led to a significant reduction of *DDAH2* mRNA expression compared to HX control. These results imply a HIF1A-dependent regulation of *DDAH2* expression in HPAEC. In A549, results of HIF inhibition and HIF stabilisation are ambiguous. While HIF stabilisation with DMOG leads to the same effect on mRNA expression of *VEGFA*, *DDAH1* and *NOS2* like observed in HX, it does not affect DDAH2 mRNA expression. HIF inhibition however did not affect *VEGFA*, *DDAH1* and *NOS2* mRNA expression, but resulted in significantly different *DDAH2* mRNA expression compared to HX control. These results do also not point towards a clearly HIF-regulated hypoxic gene expression of genes of the L-arginine-ADMA-NO pathway.

Overall, we were able to show that hypoxic regulation of gene expression of genes of the L-arginine-ADMA-NO pathway within pulmonary artery endothelial cells and alveolar epithelial cells is not strictly HIF-dependent. The responsible transcription factors regulating hypoxic gene expression need to be determined in future studies.

5.5 Future experiments – Outlook

We were able to show that gene expression of genes involved in the L-arginine-ADMA-NO pathway in hypoxic HCAEC and HPAEC is regulated the same way. mRNA expression and protein expression of the L-arginine-ADMA-NO pathway did not show any differences between hypoxic HCAEC and HPAEC. We were also able to show that ADMA concentrations in those cells did not increase after exposure to HX. However, there are several other mechanisms regulating protein activity of NOS, DDAH1 and DDAH2. We are therefore currently working on the establishment of an assay for the fluorimetric determination of extracellular NO using 4,5-diaminofluorescein (DAF-2) in order to compare NO concentrations in normoxic and hypoxic HCAEC and HPAEC, as well as in A549 cells in order to gain a deeper insight into NOS activity. We are further aiming to establish an LC-MS/MS based activity assay for DDAH and NOS proteins using different isotope-labelled metabolites. Using isotope labelled L-arginine and citrulline as well as differently labelled ADMA and citrulline we want to compare NOS and DDAH protein activity, respectively.

We were also able to show that hypoxic gene expression of *DDAH1*, *DDAH2* and *NOS3* in HCAEC, HPAEC and alveolar epithelial A549 cells is not strictly HIF-regulated. According to literature, NOS3, DDAH1 and DDAH2 are regulated by a variety of transcription factors. The NOS3 promoter was shown to exhibit homologies to binding sites for transcription factors like SP1, SP3, YY1, STAT3 and NF-κB [190, 191]. DDAH activity was shown to be positively regulated by pyrrolidine dithiocarbamate, an antagonist of NF-κB, suggesting NF-κB as putative transcription factor regulating DDAH expression [73]. In a future experiment, we want to take a closer look on putative transcription factors regulating hypoxic gene expression in HPAEC and alveolar epithelial A549 cells. Therefore, we plan to perform RNA sequencing in order to find hypoxic regulated gene clusters with common transcription factor binding sites.

6 References

1. Umbrello M, Dyson A, Feelisch M, Singer M. The key role of nitric oxide in hypoxia: hypoxic vasodilation and energy supply-demand matching. Antioxid Redox Signal. 2013;19(14):1690-710.

2. Bunn HF, Poyton RO. Oxygen sensing and molecular adaptation to hypoxia. Physiol Rev. 1996;76(3):839-85.

3. Rolfe DF, Brown GC. Cellular energy utilization and molecular origin of standard metabolic rate in mammals. Physiol Rev. 1997;77(3):731-58.

4. Klausen T, Olsen NV, Poulsen TD, Richalet JP, Pedersen BK. Hypoxemia increases serum interleukin-6 in humans. Eur J Appl Physiol Occup Physiol. 1997;76(5):480-2.

5. Wheaton WW, Chandel NS. Hypoxia. 2. Hypoxia regulates cellular metabolism. Am J Physiol Cell Physiol. 2011;300(3):C385-93.

6. MacIntyre NR. Tissue hypoxia: implications for the respiratory clinician. Respir Care. 2014;59(10):1590-6.

7. Boutilier RG. Mechanisms of cell survival in hypoxia and hypothermia. J Exp Biol. 2001;204(Pt 18):3171-81.

8. Lopez-Barneo J, Pardal R, Ortega-Saenz P. Cellular mechanism of oxygen sensing. Annu Rev Physiol. 2001;63:259-87.

9. Sommer N, Dietrich A, Schermuly RT, Ghofrani HA, Gudermann T, Schulz R, et al. Regulation of hypoxic pulmonary vasoconstriction: basic mechanisms. Eur Respir J. 2008;32(6):1639-51.

10. Euler USv, Liljestrand G. Observations on the Pulmonary Arterial Blood Pressure in the Cat. Acta Physiologica Scandinavica. 1946;12(4):301-20.

11. Boger RH, Bode-Boger SM, Thiele W, Creutzig A, Alexander K, Frolich JC. Restoring vascular nitric oxide formation by L-arginine improves the symptoms of intermittent claudication in patients with peripheral arterial occlusive disease. J Am Coll Cardiol. 1998;32(5):1336-44.

12. Osterziel KJ, Bode-Boger SM, Strohm O, Ellmer AE, Bit-Avragim N, Hanlein D, et al. Role of nitric oxide in the vasodilator effect of recombinant human growth hormone in patients with dilated cardiomyopathy. Cardiovasc Res. 2000;45(2):447-53.

13. Moncada S, Palmer RM, Higgs EA. Nitric oxide: physiology, pathophysiology, and pharmacology. Pharmacol Rev. 1991;43(2):109-42.

14. Boger RH. Asymmetric dimethylarginine (ADMA) modulates endothelial function--therapeutic implications. Vasc Med. 2003;8(3):149-51.

15. Feletou M, Vanhoutte PM. Endothelial dysfunction: a multifaceted disorder (The Wiggers Award Lecture). Am J Physiol Heart Circ Physiol. 2006;291(3):H985-1002.

16. Zhao YY, Zhao YD, Mirza MK, Huang JH, Potula HH, Vogel SM, et al. Persistent eNOS activation secondary to caveolin-1 deficiency induces pulmonary hypertension in mice and humans through PKG nitration. J Clin Invest. 2009;119(7):2009-18.

17. Hulin JA, Gubareva EA, Jarzebska N, Rodionov RN, Mangoni AA, Tommasi S. Inhibition of Dimethylarginine Dimethylaminohydrolase (DDAH) Enzymes as an Emerging Therapeutic Strategy to Target Angiogenesis and Vasculogenic Mimicry in Cancer. Front Oncol. 2019;9:1455.

18. Mayer B, Hemmens B. Biosynthesis and action of nitric oxide in mammalian cells. Trends Biochem Sci. 1997;22(12):477-81.

19. Kilbourn RG, Szabo C, Traber DL. Beneficial versus detrimental effects of nitric oxide synthase inhibitors in circulatory shock: lessons learned from experimental and clinical studies. Shock. 1997;7(4):235-46.

20. Ignarro LJ. Haem-dependent activation of cytosolic guanylate cyclase by nitric oxide: a widespread signal transduction mechanism. Biochem Soc Trans. 1992;20(2):465-9.

21. Hu LS, George J, Wang JH. Current concepts on the role of nitric oxide in portal hypertension. World J Gastroenterol. 2013;19(11):1707-17.

22. Boulanger C, Luscher TF. Release of endothelin from the porcine aorta. Inhibition by endothelium-derived nitric oxide. J Clin Invest. 1990;85(2):587-90.

23. Wang W, Diamond SL. Does elevated nitric oxide production enhance the release of prostacyclin from shear stressed aortic endothelial cells? Biochem Biophys Res Commun. 1997;233(3):748-51.

24. Garcia-Cardena G, Fan R, Shah V, Sorrentino R, Cirino G, Papapetropoulos A, et al. Dynamic activation of endothelial nitric oxide synthase by Hsp90. Nature. 1998;392(6678):821-4.

25. Liu J, Garcia-Cardena G, Sessa WC. Biosynthesis and palmitoylation of endothelial nitric oxide synthase: mutagenesis of palmitoylation sites, cysteines-15 and/or -26, argues against depalmitoylation-induced translocation of the enzyme. Biochemistry. 1995;34(38):12333-40.

26. Pollock JS, Nakane M, Buttery LD, Martinez A, Springall D, Polak JM, et al. Characterization and localization of endothelial nitric oxide synthase using specific monoclonal antibodies. Am J Physiol. 1993;265(5 Pt 1):C1379-87.

27. Alderton WK, Cooper CE, Knowles RG. Nitric oxide synthases: structure, function and inhibition. Biochem J. 2001;357(Pt 3):593-615.

28. Hemmens B, Mayer B. Enzymology of nitric oxide synthases. Methods Mol Biol. 1998;100:1-32.

29. Andrew PJ, Mayer B. Enzymatic function of nitric oxide synthases. Cardiovasc Res. 1999;43(3):521-31.

30. Sennequier N, Stuehr DJ. Analysis of substrate-induced electronic, catalytic, and structural changes in inducible NO synthase. Biochemistry. 1996;35(18):5883-92.

31. Fulton D, Gratton JP, McCabe TJ, Fontana J, Fujio Y, Walsh K, et al. Regulation of endothelium-derived nitric oxide production by the protein kinase Akt. Nature. 1999;399(6736):597-601.

32. Triggle CR, Samuel SM, Ravishankar S, Marei I, Arunachalam G, Ding H. The endothelium: influencing vascular smooth muscle in many ways. Can J Physiol Pharmacol. 2012;90(6):713-38.

33. Hannemann J, Boger R. Dysregulation of the Nitric Oxide/Dimethylarginine Pathway in Hypoxic Pulmonary Vasoconstriction-Molecular Mechanisms and Clinical Significance. Front Med (Lausanne). 2022;9:835481.

34. Papapetropoulos A, Rudic RD, Sessa WC. Molecular control of nitric oxide synthases in the cardiovascular system. Cardiovasc Res. 1999;43(3):509-20.

35. Wu G, Morris SM, Jr. Arginine metabolism: nitric oxide and beyond. Biochem J. 1998;336 (Pt 1):1-17.

36. Bredt DS, Ferris CD, Snyder SH. Nitric oxide synthase regulatory sites. Phosphorylation by cyclic AMP-dependent protein kinase, protein kinase C, and calcium/calmodulin protein kinase; identification of flavin and calmodulin binding sites. J Biol Chem. 1992;267(16):10976-81.

37. Nakane M, Mitchell J, Forstermann U, Murad F. Phosphorylation by calcium calmodulin-dependent protein kinase II and protein kinase C modulates the activity of nitric oxide synthase. Biochem Biophys Res Commun. 1991;180(3):1396-402.

38. Cooke JP. The pivotal role of nitric oxide for vascular health. Can J Cardiol. 2004;20 Suppl B:7B-15B.

39. Cooke JP, Dzau VJ. Nitric oxide synthase: role in the genesis of vascular disease. Annu Rev Med. 1997;48:489-509.

40. Boger RH, Bode-Boger SM, Frolich JC. The L-arginine-nitric oxide pathway: role in atherosclerosis and therapeutic implications. Atherosclerosis. 1996;127(1):1-11.

41. Craici IM, Wagner SJ, Weissgerber TL, Grande JP, Garovic VD. Advances in the pathophysiology of pre-eclampsia and related podocyte injury. Kidney Int. 2014;86(2):275-85.

42. Lewis NCS, Bain AR, Wildfong KW, Green DJ, Ainslie PN. Acute hypoxaemia and vascular function in healthy humans. Exp Physiol. 2017;102(12):1635-46.

43. Michel JB, Feron O, Sacks D, Michel T. Reciprocal regulation of endothelial nitric-oxide synthase by Ca2+-calmodulin and caveolin. J Biol Chem. 1997;272(25):15583-6.

44. Prabhakar P, Thatte HS, Goetz RM, Cho MR, Golan DE, Michel T. Receptor-regulated translocation of endothelial nitric-oxide synthase. J Biol Chem. 1998;273(42):27383-8.

45. Sessa WC. eNOS at a glance. J Cell Sci. 2004;117(Pt 12):2427-9.

46. Zhao CX, Xu X, Cui Y, Wang P, Wei X, Yang S, et al. Increased endothelial nitric-oxide synthase expression reduces hypertension and hyperinsulinemia in fructose-treated rats. J Pharmacol Exp Ther. 2009;328(2):610-20.

47. Fulton MD, Brown T, Zheng YG. The Biological Axis of Protein Arginine Methylation and Asymmetric Dimethylarginine. Int J Mol Sci. 2019;20(13).

48. Fleming I, Fisslthaler B, Dimmeler S, Kemp BE, Busse R. Phosphorylation of Thr(495) regulates Ca(2+)/calmodulin-dependent endothelial nitric oxide synthase activity. Circ Res. 2001;88(11):E68-75.

49. Boger RH. The emerging role of asymmetric dimethylarginine as a novel cardiovascular risk factor. Cardiovasc Res. 2003;59(4):824-33.

50. Bode-Boger SM, Scalera F, Kielstein JT, Martens-Lobenhoffer J, Breithardt G, Fobker M, et al. Symmetrical dimethylarginine: a new combined parameter for renal function and extent of coronary artery disease. J Am Soc Nephrol. 2006;17(4):1128-34.

51. Strobel J, Mieth M, Endress B, Auge D, Konig J, Fromm MF, et al. Interaction of the cardiovascular risk marker asymmetric dimethylarginine (ADMA) with the human cationic amino acid transporter 1 (CAT1). J Mol Cell Cardiol. 2012;53(3):392-400.

52. Boger RH. Asymmetric dimethylarginine (ADMA): a novel risk marker in cardiovascular medicine and beyond. Ann Med. 2006;38(2):126-36.

53. Boger RH, Sullivan LM, Schwedhelm E, Wang TJ, Maas R, Benjamin EJ, et al. Plasma asymmetric dimethylarginine and incidence of cardiovascular disease and death in the community. Circulation. 2009;119(12):1592-600.

54. Nicholson TB, Chen T, Richard S. The physiological and pathophysiological role of PRMT1-mediated protein arginine methylation. Pharmacol Res. 2009;60(6):466-74.

55. Herrmann F, Pably P, Eckerich C, Bedford MT, Fackelmayer FO. Human protein arginine methyltransferases in vivo--distinct properties of eight canonical members of the PRMT family. J Cell Sci. 2009;122(Pt 5):667-77.

56. Bedford MT, Clarke SG. Protein arginine methylation in mammals: who, what, and why. Mol Cell. 2009;33(1):1-13.

57. Zakrzewicz D, Zakrzewicz A, Preissner KT, Markart P, Wygrecka M. Protein Arginine Methyltransferases (PRMTs): promising targets for the treatment of pulmonary disorders. Int J Mol Sci. 2012;13(10):12383-400.

58. Wei H-H, Fan X-J, Hu Y, Tian X-X, Guo M, Fang Z-Y, et al. 2020.

59. Tang J, Frankel A, Cook RJ, Kim S, Paik WK, Williams KR, et al. PRMT1 is the predominant type I protein arginine methyltransferase in mammalian cells. J Biol Chem. 2000;275(11):7723-30.

60. Pekarova M, Koudelka A, Kolarova H, Ambrozova G, Klinke A, Cerna A, et al. Asymmetric dimethyl arginine induces pulmonary vascular dysfunction via activation of signal transducer and activator of transcription 3 and stabilization of hypoxia-inducible factor 1-alpha. Vascul Pharmacol. 2015;73:138-48.

61. Wang Z, Yang B, Chen X, Zhou Q, Li H, Chen S, et al. Nobiletin Regulates ROS/ADMA/DDAHII/eNOS/NO Pathway and Alleviates Vascular Endothelium Injury by Iron Overload. Biol Trace Elem Res. 2020;198(1):87-97.

62. Iannone L, Zhao L, Dubois O, Duluc L, Rhodes CJ, Wharton J, et al. miR-21/DDAH1 pathway regulates pulmonary vascular responses to hypoxia. Biochem J. 2014;462(1):103-12.

63. Anderssohn M, Maass LM, Diemert A, Luneburg N, Atzler D, Hecher K, et al. Severely decreased activity of placental dimethylarginine dimethylaminohydrolase in pre-eclampsia. Eur J Obstet Gynecol Reprod Biol. 2012;161(2):152-6.

64. Usui M, Matsuoka H, Miyazaki H, Ueda S, Okuda S, Imaizumi T. Increased endogenous nitric oxide synthase inhibitor in patients with congestive heart failure. Life Sci. 1998;62(26):2425-30.

65. Boger RH, Bode-Boger SM, Tsao PS, Lin PS, Chan JR, Cooke JP. An endogenous inhibitor of nitric oxide synthase regulates endothelial adhesiveness for monocytes. J Am Coll Cardiol. 2000;36(7):2287-95.

66. Boger RH. The pharmacodynamics of L-arginine. Altern Ther Health Med. 2014;20(3):48-54.

67. Boger RH, Bode-Boger SM, Brandes RP, Phivthong-ngam L, Bohme M, Nafe R, et al. Dietary L-arginine reduces the progression of atherosclerosis in cholesterol-fed rabbits: comparison with lovastatin. Circulation. 1997;96(4):1282-90.

68. Rodionov RN, Murry DJ, Vaulman SF, Stevens JW, Lentz SR. Human alanine-glyoxylate aminotransferase 2 lowers asymmetric dimethylarginine and protects from inhibition of nitric oxide production. J Biol Chem. 2010;285(8):5385-91.

69. Teerlink T. ADMA metabolism and clearance. Vasc Med. 2005;10 Suppl 1:S73-81.

70. Leiper JM, Santa Maria J, Chubb A, MacAllister RJ, Charles IG, Whitley GS, et al. Identification of two human dimethylarginine dimethylaminohydrolases with distinct tissue distributions and homology with microbial arginine deiminases. Biochem J. 1999;343 Pt 1:209-14.

71. Wang D, Gill PS, Chabrashvili T, Onozato ML, Raggio J, Mendonca M, et al. Isoform-specific regulation by N(G),N(G)-dimethylarginine dimethylaminohydrolase of rat serum asymmetric dimethylarginine and vascular endothelium-derived relaxing factor/NO. Circ Res. 2007;101(6):627-35.

72. Schwedhelm E, Xanthakis V, Maas R, Sullivan LM, Schulze F, Riederer U, et al. Asymmetric dimethylarginine reference intervals determined with liquid chromatography-tandem mass spectrometry: results from the Framingham offspring cohort. Clin Chem. 2009;55(8):1539-45.

73. Palm F, Onozato ML, Luo Z, Wilcox CS. Dimethylarginine dimethylaminohydrolase (DDAH): expression, regulation, and function in the cardiovascular and renal systems. Am J Physiol Heart Circ Physiol. 2007;293(6):H3227-45.

74. Knipp M, Charnock JM, Garner CD, Vasak M. Structural and functional characterization of the Zn(II) site in dimethylargininase-1 (DDAH-1) from bovine brain. Zn(II) release activates DDAH-1. J Biol Chem. 2001;276(44):40449-56.

75. Frey D, Braun O, Briand C, Vasak M, Grutter MG. Structure of the mammalian NOS regulator dimethylarginine dimethylaminohydrolase: A basis for the design of specific inhibitors. Structure. 2006;14(5):901-11.

76. Holden DP, Cartwright JE, Nussey SS, Whitley GS. Estrogen stimulates dimethylarginine dimethylaminohydrolase activity and the metabolism of asymmetric dimethylarginine. Circulation. 2003;108(13):1575-80.

77. Eid HM, Lyberg T, Arnesen H, Seljeflot I. Insulin and adiponectin inhibit the TNFalpha-induced ADMA accumulation in human endothelial cells: the role of DDAH. Atherosclerosis. 2007;194(2):e1-8.

78. Tan B, Jiang DJ, Huang H, Jia SJ, Jiang JL, Hu CP, et al. Taurine protects against low-density lipoprotein-induced endothelial dysfunction by the DDAH/ADMA pathway. Vascul Pharmacol. 2007;46(5):338-45.

79. Ito A, Tsao PS, Adimoolam S, Kimoto M, Ogawa T, Cooke JP. Novel mechanism for endothelial dysfunction: dysregulation of dimethylarginine dimethylaminohydrolase. Circulation. 1999;99(24):3092-5.

80. Lin KY, Ito A, Asagami T, Tsao PS, Adimoolam S, Kimoto M, et al. Impaired nitric oxide synthase pathway in diabetes mellitus: role of asymmetric dimethylarginine and dimethylarginine dimethylaminohydrolase. Circulation. 2002;106(8):987-92.

81. Hannemann J, Zummack J, Hillig J, Rendant-Gantzberg L, Boger R. Association of Variability in the DDAH1, DDAH2, AGXT2 and PRMT1 Genes with Circulating ADMA Concentration in Human Whole Blood. J Clin Med. 2022;11(4).

82. Leiper J, Nandi M, Torondel B, Murray-Rust J, Malaki M, O'Hara B, et al. Disruption of methylarginine metabolism impairs vascular homeostasis. Nat Med. 2007;13(2):198-203.

83. Ghebremariam YT, Erlanson DA, Cooke JP. A novel and potent inhibitor of dimethylarginine dimethylaminohydrolase: a modulator of cardiovascular nitric oxide. J Pharmacol Exp Ther. 2014;348(1):69-76.

84. Hasegawa K, Wakino S, Tatematsu S, Yoshioka K, Homma K, Sugano N, et al. Role of asymmetric dimethylarginine in vascular injury in transgenic mice overexpressing dimethylarginie dimethylaminohydrolase 2. Circ Res. 2007;101(2):e2-10.

85. Dayoub H, Achan V, Adimoolam S, Jacobi J, Stuehlinger MC, Wang BY, et al. Dimethylarginine dimethylaminohydrolase regulates nitric oxide synthesis: genetic and physiological evidence. Circulation. 2003;108(24):3042-7.

86. Pullamsetti SS, Savai R, Schaefer MB, Wilhelm J, Ghofrani HA, Weissmann N, et al. cAMP phosphodiesterase inhibitors increases nitric oxide production by modulating dimethylarginine dimethylaminohydrolases. Circulation. 2011;123(11):1194-204.

87. Gac P, Poreba M, Jurdziak M, Trzmielewska E, Goclawska K, Derkacz A, et al. Cardiovascular risk factors and the concentration of asymmetric dimethylarginine. Adv Clin Exp Med. 2020;29(1):63-70.

88. Murphy RB, Tommasi S, Lewis BC, Mangoni AA. Inhibitors of the Hydrolytic Enzyme Dimethylarginine Dimethylaminohydrolase (DDAH): Discovery, Synthesis and Development. Molecules. 2016;21(5).

89. Valkonen VP, Tuomainen TP, Laaksonen R. DDAH gene and cardiovascular risk. Vasc Med. 2005;10 Suppl 1:S45-8.

90. Chandel NS, Schumacker PT. Cellular oxygen sensing by mitochondria: old questions, new insight. J Appl Physiol (1985). 2000;88(5):1880-9.

91. Kemp PJ. Detecting acute changes in oxygen: will the real sensor please stand up? Exp Physiol. 2006;91(5):829-34.

92. Guzy RD, Schumacker PT. Oxygen sensing by mitochondria at complex III: the paradox of increased reactive oxygen species during hypoxia. Exp Physiol. 2006;91(5):807-19.

93. Johnson RS. Scientific Background - How cells sense and adapt to oxygen availability: The Nobel Assembly at Karolinska Institutet; 2019 [07.07.2023]. Available from: https://www.nobelprize.org/uploads/2019/10/advanced-medicineprize2019.pdf.

94. Semenza GL. HIF-1: mediator of physiological and pathophysiological responses to hypoxia. J Appl Physiol (1985). 2000;88(4):1474-80.

95. Pugh CW, Ratcliffe PJ. Regulation of angiogenesis by hypoxia: role of the HIF system. Nat Med. 2003;9(6):677-84.

96. Brunelle JK, Bell EL, Quesada NM, Vercauteren K, Tiranti V, Zeviani M, et al. Oxygen sensing requires mitochondrial ROS but not oxidative phosphorylation. Cell Metab. 2005;1(6):409-14.

97. Maxwell PH, Wiesener MS, Chang GW, Clifford SC, Vaux EC, Cockman ME, et al. The tumour suppressor protein VHL targets hypoxia-inducible factors for oxygen-dependent proteolysis. Nature. 1999;399(6733):271-5.

98. Iommarini L, Porcelli AM, Gasparre G, Kurelac I. Non-Canonical Mechanisms Regulating Hypoxia-Inducible Factor 1 Alpha in Cancer. Front Oncol. 2017;7:286.

99. Wenger RH, Stiehl DP, Camenisch G. Integration of oxygen signaling at the consensus HRE. Sci STKE. 2005;2005(306):re12.

100. Lee P, Chandel NS, Simon MC. Cellular adaptation to hypoxia through hypoxia inducible factors and beyond. Nat Rev Mol Cell Biol. 2020;21(5):268-83.

101. RKI. [14.07.2023]. Available from: https://www.rki.de/EN/Content/Health_Monitoring/Main_Topics/Chronic_Disease/Cardiovascular_Disease/cardiovascular_disease_node.html.

102. WHO. [14.07.23]. Available from: https://www.who.int/health-topics/cardiovascular-diseases#tab=tab_1.

103. Hultgren HN. High altitude pulmonary edema: hemodynamic aspects. Int J Sports Med. 1997;18(1):20-5.

104. Boger R, Hannemann J. Dual role of the L-arginine-ADMA-NO pathway in systemic hypoxic vasodilation and pulmonary hypoxic vasoconstriction. Pulm Circ. 2020;10(2):2045894020918850.

105. Pullamsetti S, Kiss L, Ghofrani HA, Voswinckel R, Haredza P, Klepetko W, et al. Increased levels and reduced catabolism of asymmetric and symmetric dimethylarginines in pulmonary hypertension. FASEB J. 2005;19(9):1175-7.

106. Luneburg N, Siques P, Brito J, Arriaza K, Pena E, Klose H, et al. Long-Term Chronic Intermittent Hypobaric Hypoxia in Rats Causes an Imbalance in the Asymmetric Dimethylarginine/Nitric Oxide Pathway and ROS Activity: A Possible Synergistic Mechanism for Altitude Pulmonary Hypertension? Pulm Med. 2016;2016:6578578.

107. Luneburg N, Siques P, Brito J, De La Cruz JJ, Leon-Velarde F, Hannemann J, et al. Long-Term Intermittent Exposure to High Altitude Elevates Asymmetric Dimethylarginine in First Exposed Young Adults. High Alt Med Biol. 2017;18(3):226-33.

108. Brito J, Siques P, Lopez R, Romero R, Leon-Velarde F, Flores K, et al. Long-Term Intermittent Work at High Altitude: Right Heart Functional and Morphological Status and Associated Cardiometabolic Factors. Front Physiol. 2018;9:248.

109. Siques P, Brito J, Schwedhelm E, Pena E, Leon-Velarde F, De La Cruz JJ, et al. Asymmetric Dimethylarginine at Sea Level Is a Predictive Marker of Hypoxic Pulmonary Arterial Hypertension at High Altitude. Front Physiol. 2019;10:651.

110. Hannemann J, Balfanz P, Schwedhelm E, Hartmann B, Ule J, Muller-Wieland D, et al. Elevated serum SDMA and ADMA at hospital admission predict in-hospital mortality of COVID-19 patients. Sci Rep. 2021;11(1):9895.

111. PromoCell. [14.07.2023]. Available from: https://promocell.com/wp-content/uploads/product-information/manual/C-12221.pdf.

112. Cho H, Du X, Rizzi JP, Liberzon E, Chakraborty AA, Gao W, et al. On-target efficacy of a HIF-2alpha antagonist in preclinical kidney cancer models. Nature. 2016;539(7627):107-11.

113. Narita T, Yin S, Gelin CF, Moreno CS, Yepes M, Nicolaou KC, et al. Identification of a novel small molecule HIF-1alpha translation inhibitor. Clin Cancer Res. 2009;15(19):6128-36.

114. Weidemann A, Breyer J, Rehm M, Eckardt KU, Daniel C, Cicha I, et al. HIF-1alpha activation results in actin cytoskeleton reorganization and modulation of Rac-1 signaling in endothelial cells. Cell Commun Signal. 2013;11:80.

115. Silver N, Best S, Jiang J, Thein SL. Selection of housekeeping genes for gene expression studies in human reticulocytes using real-time PCR. BMC Mol Biol. 2006;7:33.

116. Andersen CL, Jensen JL, Orntoft TF. Normalization of real-time quantitative reverse transcription-PCR data: a model-based variance estimation approach to identify genes suited for normalization, applied to bladder and colon cancer data sets. Cancer Res. 2004;64(15):5245-50.

117. Schmittgen TD, Livak KJ. Analyzing real-time PCR data by the comparative C(T) method. Nat Protoc. 2008;3(6):1101-8.

118. Saiki RK, Gelfand DH, Stoffel S, Scharf SJ, Higuchi R, Horn GT, et al. Primer-directed enzymatic amplification of DNA with a thermostable DNA polymerase. Science. 1988;239(4839):487-91.

119. Wong ML, Medrano JF. Real-time PCR for mRNA quantitation. Biotechniques. 2005;39(1):75-85.

120. Schmittgen TD, Zakrajsek BA, Mills AG, Gorn V, Singer MJ, Reed MW. Quantitative reverse transcription-polymerase chain reaction to study mRNA decay: comparison of endpoint and real-time methods. Anal Biochem. 2000;285(2):194-204.

121. Wang T, Brown MJ. mRNA quantification by real time TaqMan polymerase chain reaction: validation and comparison with RNase protection. Anal Biochem. 1999;269(1):198-201.

122. Huggett J, Dheda K, Bustin S, Zumla A. Real-time RT-PCR normalisation; strategies and considerations. Genes Immun. 2005;6(4):279-84.

123. Dheda K, Huggett JF, Chang JS, Kim LU, Bustin SA, Johnson MA, et al. The implications of using an inappropriate reference gene for real-time reverse transcription PCR data normalization. Anal Biochem. 2005;344(1):141-3.

124. Zhong H, Simons JW. Direct comparison of GAPDH, beta-actin, cyclophilin, and 28S rRNA as internal standards for quantifying RNA levels under hypoxia. Biochem Biophys Res Commun. 1999;259(3):523-6.

125. Graven KK, Zimmerman LH, Dickson EW, Weinhouse GL, Farber HW. Endothelial cell hypoxia associated proteins are cell and stress specific. J Cell Physiol. 1993;157(3):544-54.

126. Graven KK, Yu Q, Pan D, Roncarati JS, Farber HW. Identification of an oxygen responsive enhancer element in the glyceraldehyde-3-phosphate dehydrogenase gene. Biochim Biophys Acta. 1999;1447(2-3):208-18.

127. Caradec J, Sirab N, Keumeugni C, Moutereau S, Chimingqi M, Matar C, et al. 'Desperate house genes': the dramatic example of hypoxia. Br J Cancer. 2010;102(6):1037-43.

128. Klenke S, Renckhoff K, Engler A, Peters J, Frey UH. Easy-to-use strategy for reference gene selection in quantitative real-time PCR experiments. Naunyn Schmiedebergs Arch Pharmacol. 2016;389(12):1353-66.

129. Bas A, Forsberg G, Hammarstrom S, Hammarstrom ML. Utility of the housekeeping genes 18S rRNA, beta-actin and glyceraldehyde-3-phosphate-dehydrogenase for normalization in real-time quantitative reverse transcriptase-polymerase chain reaction analysis of gene expression in human T lymphocytes. Scand J Immunol. 2004;59(6):566-73.

130. Curis E, Nepost C, Grillault Laroche D, Courtin C, Laplanche JL, Etain B, et al. Selecting reference genes in RT-qPCR based on equivalence tests: a network based approach. Sci Rep. 2019;9(1):16231.

131. Feng C, Wang H, Lu N, Chen T, He H, Lu Y, et al. Log-transformation and its implications for data analysis. Shanghai Arch Psychiatry. 2014;26(2):105-9.

132. Chapman JR, Waldenstrom J. With Reference to Reference Genes: A Systematic Review of Endogenous Controls in Gene Expression Studies. PLoS One. 2015;10(11):e0141853.

133. Van Acker SI, Van Acker ZP, Haagdorens M, Pintelon I, Koppen C, Zakaria N. Selecting Appropriate Reference Genes for Quantitative Real-Time Polymerase Chain Reaction Studies in Isolated and Cultured Ocular Surface Epithelia. Sci Rep. 2019;9(1):19631.

134. Bakhashab S, Lary S, Ahmed F, Schulten HJ, Bashir A, Ahmed FW, et al. Reference genes for expression studies in hypoxia and hyperglycemia models in human umbilical vein endothelial cells. G3 (Bethesda). 2014;4(11):2159-65.

135. Brown RC, Davis TP. Hypoxia/aglycemia alters expression of occludin and actin in brain endothelial cells. Biochem Biophys Res Commun. 2005;327(4):1114-23.

136. Crawford LE, Milliken EE, Irani K, Zweier JL, Becker LC, Johnson TM, et al. Superoxide-mediated actin response in post-hypoxic endothelial cells. J Biol Chem. 1996;271(43):26863-7.

137. Chai YC, Ashraf SS, Rokutan K, Johnston RB, Jr., Thomas JA. S-thiolation of individual human neutrophil proteins including actin by stimulation of the respiratory burst: evidence against a role for glutathione disulfide. Arch Biochem Biophys. 1994;310(1):273-81.

138. Greijer AE, van der Groep P, Kemming D, Shvarts A, Semenza GL, Meijer GA, et al. Up-regulation of gene expression by hypoxia is mediated predominantly by hypoxia-inducible factor 1 (HIF-1). J Pathol. 2005;206(3):291-304.

139. Xie J, Liu X, Li Y, Liu Y, Su G. Validation of RT-qPCR reference genes and determination of Robo4 expression levels in human retinal endothelial cells under hypoxia and/or hyperglycemia. Gene. 2016;585(1):135-42.

140. Graven KK, Troxler RF, Kornfeld H, Panchenko MV, Farber HW. Regulation of endothelial cell glyceraldehyde-3-phosphate dehydrogenase expression by hypoxia. J Biol Chem. 1994;269(39):24446-53.

141. Escoubet B, Planes C, Clerici C. Hypoxia increases glyceraldehyde-3-phosphate dehydrogenase transcription in rat alveolar epithelial cells. Biochem Biophys Res Commun. 1999;266(1):156-61.

142. Graven KK, Bellur D, Klahn BD, Lowrey SL, Amberger E. HIF-2alpha regulates glyceraldehyde-3-phosphate dehydrogenase expression in endothelial cells. Biochim Biophys Acta. 2003;1626(1-3):10-8.

143. Ruiz-Romero C, Calamia V, Rocha B, Mateos J, Fernandez-Puente P, Blanco FJ. Hypoxia conditions differentially modulate human normal and osteoarthritic chondrocyte proteomes. J Proteome Res. 2010;9(6):3035-45.

144. Cheng F, Yuan W, Cao M, Chen R, Wu X, Yan J. Cyclophilin A Protects Cardiomyocytes against Hypoxia/Reoxygenation-Induced Apoptosis via the AKT/Nox2 Pathway. Oxid Med Cell Longev. 2019;2019:2717986.

145. Mao M, Yu X, Ge X, Gu R, Li Q, Song S, et al. Acetylated cyclophilin A is a major mediator in hypoxia-induced autophagy and pulmonary vascular angiogenesis. J Hypertens. 2017;35(4):798-809.

146. Foldager CB, Munir S, Ulrik-Vinther M, Soballe K, Bunger C, Lind M. Validation of suitable house keeping genes for hypoxia-cultured human chondrocytes. BMC Mol Biol. 2009;10:94.

147. Xiao J, Li X, Liu J, Fan X, Lei H, Li C. Identification of reference genes in blood before and after entering the plateau for SYBR green RT-qPCR studies. PeerJ. 2017;5:e3726.

148. Poirier B, Briand V, Kadereit D, Schafer M, Wohlfart P, Philippo MC, et al. A G protein-biased S1P(1) agonist, SAR247799, protects endothelial cells without affecting lymphocyte numbers. Sci Signal. 2020;13(634).

149. Eswaramoorthy SD, Dhiman N, Korra G, Oranges CM, Schaefer DJ, Rath SN, et al. Isogenic-induced endothelial cells enhance osteogenic differentiation of mesenchymal stem cells on silk fibroin scaffold. Regen Med. 2019;14(7):647-61.

150. Wassmer CH, Lebreton F, Bellofatto K, Perez L, Cottet-Dumoulin D, Andres A, et al. Bio-Engineering of Pre-Vascularized Islet Organoids for the Treatment of Type 1 Diabetes. Transpl Int. 2021;35:10214.

151. Liang GP, Su YY, Chen J, Yang ZC, Liu YS, Luo XD. Analysis of the early adaptive response of endothelial cells to hypoxia via a long serial analysis of gene expression. Biochem Biophys Res Commun. 2009;384(4):415-9.

152. Bartoszewski R, Moszynska A, Serocki M, Cabaj A, Polten A, Ochocka R, et al. Primary endothelial cell-specific regulation of hypoxia-inducible factor (HIF)-1 and HIF-2 and their target gene expression profiles during hypoxia. FASEB J. 2019;33(7):7929-41.

153. Bustin SA, Benes V, Garson JA, Hellemans J, Huggett J, Kubista M, et al. The MIQE guidelines: minimum information for publication of quantitative real-time PCR experiments. Clin Chem. 2009;55(4):611-22.

154. Li T, Diao H, Zhao L, Xing Y, Zhang J, Liu N, et al. Identification of suitable reference genes for real-time quantitative PCR analysis of hydrogen peroxide-treated human umbilical vein endothelial cells. BMC Mol Biol. 2017;18(1):10.

155. Shweiki D, Itin A, Soffer D, Keshet E. Vascular endothelial growth factor induced by hypoxia may mediate hypoxia-initiated angiogenesis. Nature. 1992;359(6398):843-5.

156. Park JE, Keller GA, Ferrara N. The vascular endothelial growth factor (VEGF) isoforms: differential deposition into the subepithelial extracellular matrix and bioactivity of extracellular matrix-bound VEGF. Mol Biol Cell. 1993;4(12):1317-26.

157. Liu Y, Cox SR, Morita T, Kourembanas S. Hypoxia regulates vascular endothelial growth factor gene expression in endothelial cells. Identification of a 5' enhancer. Circ Res. 1995;77(3):638-43.

158. Namiki A, Brogi E, Kearney M, Kim EA, Wu T, Couffinhal T, et al. Hypoxia induces vascular endothelial growth factor in cultured human endothelial cells. J Biol Chem. 1995;270(52):31189-95.

159. Semenza GL. Angiogenesis in ischemic and neoplastic disorders. Annu Rev Med. 2003;54:17-28.

160. Zimna A, Kurpisz M. Hypoxia-Inducible Factor-1 in Physiological and Pathophysiological Angiogenesis: Applications and Therapies. Biomed Res Int. 2015;2015:549412.

161. Forsythe JA, Jiang BH, Iyer NV, Agani F, Leung SW, Koos RD, et al. Activation of vascular endothelial growth factor gene transcription by hypoxia-inducible factor 1. Mol Cell Biol. 1996;16(9):4604-13.

162. McQuillan LP, Leung GK, Marsden PA, Kostyk SK, Kourembanas S. Hypoxia inhibits expression of eNOS via transcriptional and posttranscriptional mechanisms. Am J Physiol. 1994;267(5 Pt 2):H1921-7.

163. Fleming I, Busse R. Molecular mechanisms involved in the regulation of the endothelial nitric oxide synthase. Am J Physiol Regul Integr Comp Physiol. 2003;284(1):R1-12.

164. Yan SF, Tritto I, Pinsky D, Liao H, Huang J, Fuller G, et al. Induction of interleukin 6 (IL-6) by hypoxia in vascular cells. Central role of the binding site for nuclear factor-IL-6. J Biol Chem. 1995;270(19):11463-71.

165. Mendes RT, Nguyen D, Stephens D, Pamuk F, Fernandes D, Hasturk H, et al. Hypoxia-induced endothelial cell responses - possible roles during periodontal disease. Clin Exp Dent Res. 2018;4(6):241-8.

166. Ho JJ, Robb GB, Tai SC, Turgeon PJ, Mawji IA, Man HS, et al. Active stabilization of human endothelial nitric oxide synthase mRNA by hnRNP E1 protects against antisense RNA and microRNAs. Mol Cell Biol. 2013;33(10):2029-46.

167. Forstermann U, Li H. Therapeutic effect of enhancing endothelial nitric oxide synthase (eNOS) expression and preventing eNOS uncoupling. Br J Pharmacol. 2011;164(2):213-23.

168. Chan Y, Fish JE, D'Abreo C, Lin S, Robb GB, Teichert AM, et al. The cell-specific expression of endothelial nitric-oxide synthase: a role for DNA methylation. J Biol Chem. 2004;279(33):35087-100.

169. Janaszak-Jasiecka A, Siekierzycka A, Bartoszewska S, Serocki M, Dobrucki LW, Collawn JF, et al. eNOS expression and NO release during hypoxia is inhibited by miR-200b in human endothelial cells. Angiogenesis. 2018;21(4):711-24.

170. Chen JX, Meyrick B. Hypoxia increases Hsp90 binding to eNOS via PI3K-Akt in porcine coronary artery endothelium. Lab Invest. 2004;84(2):182-90.

171. Krause BJ, Costello PM, Munoz-Urrutia E, Lillycrop KA, Hanson MA, Casanello P. Role of DNA methyltransferase 1 on the altered eNOS expression in human umbilical endothelium from intrauterine growth restricted fetuses. Epigenetics. 2013;8(9):944-52.

172. Penaloza E, Soto-Carrasco G, Krause BJ. MiR-21-5p directly contributes to regulating eNOS expression in human artery endothelial cells under normoxia and hypoxia. Biochem Pharmacol. 2020;182:114288.

173. Koh MY, Powis G. Passing the baton: the HIF switch. Trends Biochem Sci. 2012;37(9):364-72.

174. Forstermann U, Sessa WC. Nitric oxide synthases: regulation and function. Eur Heart J. 2012;33(7):829-37, 37a-37d.

175. Mahmood T, Yang PC. Western blot: technique, theory, and trouble shooting. N Am J Med Sci. 2012;4(9):429-34.

176. Hershey JW, Sonenberg N, Mathews MB. Principles of translational control: an overview. Cold Spring Harb Perspect Biol. 2012;4(12).

177. Lee JM, Hammaren HM, Savitski MM, Baek SH. Control of protein stability by post-translational modifications. Nat Commun. 2023;14(1):201.

178. Ragavan VN, Nair PC, Jarzebska N, Angom RS, Ruta L, Bianconi E, et al. A multicentric consortium study demonstrates that dimethylarginine dimethylaminohydrolase 2 is not a dimethylarginine dimethylaminohydrolase. Nat Commun. 2023;14(1):3392.

179. Leiper J, Murray-Rust J, McDonald N, Vallance P. S-nitrosylation of dimethylarginine dimethylaminohydrolase regulates enzyme activity: further interactions between nitric oxide synthase and dimethylarginine dimethylaminohydrolase. Proc Natl Acad Sci U S A. 2002;99(21):13527-32.

180. Millatt LJ, Whitley GS, Li D, Leiper JM, Siragy HM, Carey RM, et al. Evidence for dysregulation of dimethylarginine dimethylaminohydrolase I in chronic hypoxia-induced pulmonary hypertension. Circulation. 2003;108(12):1493-8.

181. Yanagisawa M, Kurihara H, Kimura S, Tomobe Y, Kobayashi M, Mitsui Y, et al. A novel potent vasoconstrictor peptide produced by vascular endothelial cells. Nature. 1988;332(6163):411-5.

182. Liu YV, Semenza GL. RACK1 vs. HSP90: competition for HIF-1 alpha degradation vs. stabilization. Cell Cycle. 2007;6(6):656-9.

183. Ravi R, Mookerjee B, Bhujwalla ZM, Sutter CH, Artemov D, Zeng Q, et al. Regulation of tumor angiogenesis by p53-induced degradation of hypoxia-inducible factor 1alpha. Genes Dev. 2000;14(1):34-44.

184. Sweeney M, Yuan JX. Hypoxic pulmonary vasoconstriction: role of voltage-gated potassium channels. Respir Res. 2000;1(1):40-8.

185. Lin MJ, Leung GP, Zhang WM, Yang XR, Yip KP, Tse CM, et al. Chronic hypoxia-induced upregulation of store-operated and receptor-operated Ca2+ channels in pulmonary arterial smooth muscle cells: a novel mechanism of hypoxic pulmonary hypertension. Circ Res. 2004;95(5):496-505.

186. Rafikov R, Fonseca FV, Kumar S, Pardo D, Darragh C, Elms S, et al. eNOS activation and NO function: structural motifs responsible for the posttranslational control of endothelial nitric oxide synthase activity. J Endocrinol. 2011;210(3):271-84.

187. Scheuermann TH, Tomchick DR, Machius M, Guo Y, Bruick RK, Gardner KH. Artificial ligand binding within the HIF2alpha PAS-B domain of the HIF2 transcription factor. Proc Natl Acad Sci U S A. 2009;106(2):450-5.

188. Jaakkola P, Mole DR, Tian YM, Wilson MI, Gielbert J, Gaskell SJ, et al. Targeting of HIF-alpha to the von Hippel-Lindau ubiquitylation complex by O2-regulated prolyl hydroxylation. Science. 2001;292(5516):468-72.

189. Tang X, Cui K, Lu X, Wu P, Yu S, Yang B, et al. A Novel Hypoxia-inducible Factor 1alpha Inhibitor KC7F2 Attenuates Oxygen-induced Retinal Neovascularization. Invest Ophthalmol Vis Sci. 2022;63(6):13.

190. Li H, Wallerath T, Forstermann U. Physiological mechanisms regulating the expression of endothelial-type NO synthase. Nitric Oxide. 2002;7(2):132-47.

191. Searles CD. Transcriptional and posttranscriptional regulation of endothelial nitric oxide synthase expression. Am J Physiol Cell Physiol. 2006;291(5):C803-16.

7 Supplementary data

Supplementary table 1: Summary of results of of pairwise comparison of ΔCt values, Ct CV and NormFinder analysis. Pairwise comparison of ΔCt values, Ct CV and NormFinder analysis were performed in order to find the most suitable reference gene. Mean SD values were calculated using the pairwise ΔCt comparison and ranked from low SDs to high SDs. The analysis was performed for each cell line separately as well as for all cell lines together. Ct CV were calculated for each cell line separately as well as for all cell lines together and ranked from low to high. Stability values gained for gene expression of putative reference genes were obtained using the NormFinder algorithm an ranked from low (highest stability) to high stability values (lowest stability).

	HCAEC			**HPAEC**			**A549**			**All**		
Ranking	**ΔCt**	**Ct CV**	**Norm Finder**	**ΔCt**	**Ct CV**	**Norm Finder**	**ΔCt**	**Ct CV**	**Norm Finder**	**ΔCt**	**Ct CV**	**Norm Finder**
1	*TBP*	*TBP*	*RPLP1*	*PPIA*	*SDHA*	*PPIA*	*RPL13A*	*RPL13A*	*ACTB*	*TBP*	*PPIA*	*RPL13A*
2	*RPLP1*	*PPIA*	*PPIA*	*B2M*	*ACTB*	*18S*	*ACTB*	*SDHA*	*RPL13A*	*PPIA*	*TBP*	*18S*
3	*PPIA*	*RPL13A*	*ACTB*	*18S*	*B2M*	*ACTB*	*B2M*	*RPLP1*	*RPLP1*	*18S*	*ACTB*	*ACTB*
4	*RPL13A*	*RPLP1*	*RPL13A*	*ACTB*	*TBP*	*B2M*	*TBP*	*GAPDH*	*B2M*	*RPLP1*	*RPLP1*	*RPLP1*
5	*ACTB*	*B2M*	*18S*	*RPLP1*	*GAPDH*	*RPL13A*	*RPLP1*	*TBP*	*18S*	*RPL13A*	*RPL13A*	*PPIA*
6	*18S*	*ACTB*	*TBP*	*GAPDH*	*PPIA*	*GAPDH*	*18S*	*ACTB*	*SDHA*	*ACTB*	*GAPDH*	*TBP*
7	*B2M*	*GAPDH*	*B2M*	*TBP*	*RPL13A*	*RPLP1*	*SDHA*	*B2M*	*TBP*	*GAPDH*	*SDHA*	*B2M*
8	*GAPDH*	*SDHA*	*GAPDH*	*RPL13A*	*RPLP1*	*TBP*	*PPIA*	*PPIA*	*PPIA*	*SDHA*	*B2M*	*GAPDH*
9	*SDHA*	*18S*	*SDHA*	*SDHA*	*18S*	*SDHA*	*GAPDH*	*18S*	*GAPDH*	*B2M*	*18S*	*SDHA*

8 Eidesstattliche Versicherung - Declaration on oath

Hiermit erkläre ich an Eides statt, dass ich die vorliegende Dissertationsschrift selbst verfasst und keine anderen als die angegebenen Quellen und Hilfsmittel benutzt habe.

I hereby declare, on oath, that I have written the present dissertation by my own and have not used other than the acknowledged resources and aids.

Hamburg, den 12.12.2023

Unterschrift

9 Acknowledgment

Mein herzlicher Dank gilt Prof. Dr. Rainer H. Böger und PD Dr. Juliane Hannemann für die einmalige Möglichkeit, meine Promotion am Institut für Klinische Pharmakologie und Toxikologie in der AG Hannemann zu absolvieren. Vielen Dank für das spannende Thema, die fachlichen Diskussionen und die Möglichkeit, das Projekt auf internationalen Konferenzen vorstellen zu dürfen. Dank Euch konnte ich in den letzten Jahren sowohl beruflich als auch persönlich wachsen.

Großer Dank gilt Herrn Prof. Dr. Dr. Andreas H. Guse für die Betreuung meiner Promotion, die Funktion als Gutachter sowie die Mitgliedschaft in meiner Prüfungskommission.

Vielen Dank an Frau Prof. Dr. Julia Kehr und Herrn Prof. Dr. Wolfgang Streit, die sich ebenfalls bereit erklärt haben, meiner Prüfungskommission beizuwohnen.

Vielen lieben Dank an die gesamte AG Hannemann für die tolle gemeinsame Zeit und die kollegiale Zusammenarbeit. Danke an Mariola Kastner, Fiona Kleinsang, Yoana Mileva, Antonia Röglin, Heike Stang und Daniel Stuht. Besonderer Dank gilt Mariola Kastner und Fiona Kleinsang für die tatkräftige Unterstützung in den letzten Jahren.

Ich danke meinen Freunden, egal ob neu oder alt, für ihr Verständnis, die immer offenen Ohren und die vielen unvergesslichen Momente. Vielen Dank für die Ablenkung und den Zuspruch, wann immer es nötig war. Meinen Dank an Lea Altendorf, durch die unsere TV-Abende noch unvergesslicher und zum wöchentlichen Höhepunkt wurden. Besonderer Dank an Heike Stang, die von Arbeitskollegin zur Freundin wurde. Ich kann mir keine bessere Büronachbarin vorstellen und bin unendlich dankbar für die gemeinsame Zeit, die Auslandsreisen und Feierabendstunden. Ohne dich wären die letzten Jahre sehr viel weniger schön gewesen! Vielen Dank an Dr. Arne Krüger, durch den die Zeit in Brasilien und in Hamburg zu einem Abenteuer wurde, das ich nicht missen möchte. Danke für die aufbauenden Worte und den Glauben an mich, besonders in der letzten Phase meiner Doktorarbeit.

Persönlicher Dank gilt meiner Familie. Ich danke meinen Eltern Anke und Frank Schmidt-Hutten für ihre Unterstützung und ihre stete Zuversicht. Danke, dass ihr mir alle Möglichkeiten der Welt geboten und immer an mich geglaubt habt. Danke an meine Geschwister Hanna und Jan, die mir immer den Rücken frei gehalten haben und mir eine große Stütze in unruhigen Zeiten waren. Mein größter Dank gilt meinen Großeltern Eveline und Reiner Nabor und Gisela Schmidt-Hutten für ihre Unterstützung bei der Verwirklichung meiner Träume. Ohne Euch wäre meine Reise so nicht möglich gewesen. Vielen Dank!